BUOYANCY EFFECTS ON HEAT, MASS AND MOMENTUM TRANSFER DURING THE MELTING OF A HORIZONTAL ICE SHEET ABOVE FRESH OR SALINE WATER FLOWING AT LAMINAR REYNOLDS NUMBERS

PRADEEP KUMAR SRIVASTAVA


CENTRE FOR NFLD. STUDIES
OCT 5 1981
MEMORIAL UNIVERSITY
OF NEWFOUNDLAND

NOTICE

The quality of this microfiche is heavily dependent upon the quality of the original thesis submitted for microfilming. Every effort has been made to ensure the highest quality of reproduction possible.

If pages are missing, contact the university which granted the degree.

Some pages may have indistinct print especially if the original pages were typed with a poor typewriter ribbon or if the university sent us a poor photocopy.

Previously copyrighted materials (journal articles, published tests, etc.) are not filmed.

Reproduction in full or in part of this film is governed by the Canadian Copyright Act, R.S.C. 1970, c. C-30. Please read the authorization forms which accompany this thesis.

AVIS

La qualité de cette microfiche dépend grandement de la qualité de la thèse soumise au microfilmage. Nous avons tout fait pour assurer une qualité supérieure de reproduction.

S'il manque des pages, veuillez communiquer avec l'université qui a conféré le grade.

La qualité d'impression de certaines pages peut laisser à désirer, surtout si les pages originales ont été dactylographiées à l'aide d'un ruban usé ou si l'université nous a fait parvenir une photocopie de mauvaise qualité.

Les documents qui font déjà l'objet d'un droit d'auteur (articles de revue, examens publiés, etc.) ne sont pas microfilmés.

La reproduction, même partielle, de ce microfilm est soumise à la Loi canadienne sur le droit d'auteur, SRC 1970, c. C-30. Veuillez prendre connaissance des formules d'autorisation qui accompagnent cette thèse.

THIS DISSERTATION
HAS BEEN MICROFILMED
EXACTLY AS RECEIVED

LA THÈSE A ÉTÉ
MICROFILMÉE TELLE QUE
NOUS L'AVONS REÇUE

BUOYANCY EFFECTS ON HEAT, MASS AND MOMENTUM TRANSFER DURING THE MELTING OF A HORIZONTAL ICE SHEET ABOVE FRESH OR SALINE WATER FLOWING AT LAMINAR REYNOLDS NUMBERS

by

Pradeep Kumar Srivastava
B.Tech. (Mech.) Banaras Hindu University, 1976

A Thesis submitted in partial fulfillment of the
requirements for the degree of
Master of Engineering

Faculty of Engineering and Applied Science
Memorial University of Newfoundland

December 1979

St. John's Newfoundland

Canada

ABSTRACT

A finite difference steady state two-dimensional analysis is made for the combined convection heat, mass and momentum transfer phenomena for pure or saline ($S_\infty = 5^0/oo$ and $35^0/oo$) water flowing at laminar Reynolds numbers below a semi-infinite horizontal melting sheet of pure ice. All fluid properties, except density in the body forces terms of the momentum equation, are assumed to be constant.

For the fresh water case, a 51 by 21 grid is used for the computer analysis and downstream boundary conditions are applied at a distance of 1.731 m from the leading edge. For $S_\infty = 5^0/oo$ and $35^0/oo$ 52 by 52 and 68 by 65 grids are used respectively and downstream boundary conditions are applied at a distance of 1.021 m. The results of the analysis are presented for free stream velocities of 0.025, 0.02, 0.015 and 0.01 m/s and free stream temperatures ranging from 2^0C to 20^0C. Results obtained with the present analysis are compared with the forced convection case.

For fresh water, the streamlines resulting from the present analysis are closer to the ice sheet than is found for forced convection, but the heat transfer to the ice sheet is lowered. For saline water, the streamlines are shifted further away from the ice sheet for combined convection than for forced convection and the local heat transfer rates are lowered. The solution method is not convergent for conditions when the buoyancy terms become large.

ACKNOWLEDGEMENTS

I wish to express my sincere gratitude to Professor Norman W. Wilson for his guidance as a thesis supervisor, and to Dr. Frederick A. Aldrich, Dean of Graduate Studies, for financial support throughout the research period.

The computer facilities of the Faculty of Engineering and Applied Science, Memorial University of Newfoundland, were employed for the computer work. Thanks are due to Miss Donna Parsons for her help especially in interpreting many error messages during the computation work. I would like to extend my appreciation to Mrs. Dallas Strange for her efforts in typing the manuscript.

Special words of thanks to my parents for sending me to Canada for higher studies.

TABLE OF CONTENTS

LIST OF TABLES

LIST OF FIGURES

TERMINOLOGY

c_p = Specific heat, J/kg^oc

D = Mass diffusion coefficient for salt, m^2/s

g = Acceleration due to gravity, m/s^2

I = Number of grids in X-direction

J = Number of grids in Y-direction

h = Heat transfer coefficient

k = Thermal conductivity, W/m^oC

L = Latent heat of fusion of ice, J/kg

Nu = Local Nusselt number, $\frac{hx}{k}$

Pr = Prandtl number, $\frac{\mu c_p}{k}$

Re = Reynolds number, $\frac{U_\infty x}{\nu}$

S = Local salinity of fluid, $^o/oo$ (ppt.) or g/kg.

Sc = Schmidt number, $\mu/\rho D$

S_∞ = Free stream salinity

S_w = Wall salinity

T = Local temperature of fluid, ^oC

T_∞ = Free stream temperature

T_w = Wall temperature

U_∞ = Free stream velocity, m/s

V_w = Melt velocity

u,v = Velocities in X and Y-directions

x,y = Cartesian coordinates

α_T, β_T, σ_o, σ_T = Coefficients in determining density of sea water (see equations 8,9,19,11).

μ = Dynamic viscosity, kg/m.s

ν = Kinematic viscosity

ρ = Local density of fluid, kg/m^3

ψ = Stream function, kg/m.s

ω = Vorticity, S^{-1}

INTRODUCTION

If warm fresh or saline water flows at laminar Reynolds numbers below a horizontal ice sheet, convective conditions prevail for heat, mass and momentum transfer and a change of phase can occur at the solid-liquid interface. If the conduction of heat out of the water and through the ice is sufficiently large, freezing occurs at the interface. Conversely, if the conduction of heat into the ice is small, the heat transfer from the water to the ice will result in melting at the solid-liquid interface. In this case, if the free stream temperature and salinity are sufficiently low and the free stream water velocity is sufficiently high, the resulting forced convection conditions lend themselves to solution by boundary layer methods. Because the density of water depends on its temperature and salinity, density gradients will exist but the resulting buoyancy terms will be negligible in comparison to the convective and dissipative terms in the equation of motion. Increasing either the free stream temperature or salinity, will increase the density gradients, and this may result in significant buoyancy effects. Similarly, lowering of the free stream velocity can make the buoyancy effects more predominant. In these cases boundary layer methods may not be sufficient for analysis of the melting characteristics.

The heat transfer processes near a melting flat surface has been investigated analytically in the past for forced convection laminar flow by Yen and Tien [1], and the mass transfer effects of pure

ice melting into saline water have been included in studies by Pozvonkov [2] and by Griffin [3,4,5]. Yen and Tien studied the case where melting and freezing are involved, and that work is of considerable interest from practical as well as theoretical viewpoints. In studying the above problem, the classical treatment of convective heat transfer between a solid boundary and a fluid in relative motion was used only as an approximation. This is due to the fact that the melting (or freezing) which takes place at the boundary creates a finite interfacial velocity. It is well known from studies of boundary layer control by Schlicting [6] and of mass transfer by Bird et al. [7] that the presence of such an interfacial velocity can greatly influence the transfer rates. Yen and Tien considered the case of pure water flowing over a melting ice sheet. They employed an extension of the Leveque solution to the melting process. The work of Pozvonkov et al. represents a more refined application of the integral method as originally developed for melting of vertical ice sheets by Merk [8]. Griffin [3] determined the velocity, temperature and concentration distributions near a horizontal melting surface of glacial or pure ice in saline water for laminar flow conditions using integral techniques. He applied an energy balance to the transfer process that occurs during the melting of an ice sheet in saline water, and estimated the rate of melting and the relative thicknesses of the momentum, temperature and salinity boundary layers for forced convection conditions. His analysis also accounts for the subcooling of the solid below the melting temperature and the effect of this subcooling on the heat and mass transfer rates. Griffin's solution assumes that

the momentum, temperature and salinity boundary layer thicknesses are given by relations derived for the pure water case by Pozvonkov et al.

It was described clearly by Long [9] and Turner [10] that when cross stream buoyancy exists in a fluid flowing near a horizontal solid boundary, the streamlines in the fluid can take on a wave like pattern. Robertson, Seinfeld and Leal [11] investigated the problem of simultaneous forced and free convection flow of a Newtonian fluid past a hot or cold horizontal flat plate by means of numerical solutions of two dimensional equations of motion and energy subject to the Boussinesq approximation. They found that the buoyancy effects induced by a hot or cold body can cause considerable deviation from the basic forced convection flow which would exist if the body and free stream fluid were at the same temperature. Sparrow and Minkowyz [12] have shown that the cross stream buoyancy induced body force acts effectively to produce a streamwise pressure gradient in the fluid adjacent to the plate surface. This pressure gradient is favourable, in the usual boundary layer sense, when the plate is hot, and adverse when the plate is cold. Leal and Acravos [13] obtained numerical solutions to the two-dimensional Navier Stokes and energy equations for flow past a flat plate.

Meroney and Yamada [14] investigated both experimentally and numerically the perturbations of a horizontal flow of air by a heated boundary which may represent a heated island or an urban region. They used a set of two-dimensional, time dependent and non-linear equations to solve the above problem. Their experimental and analytical results agreed quantitatively. Among other things, their results clearly establish the presence of stable recirculating zones and "lee

waves" in the air flow on the downstream side of an island heated at a constant temperature. In their analysis, the region of interest extends far downstream from the heated island which is finite in length. This permits the application of suitable closure boundary conditions in a region where the flow field is no longer appreciably affected by the presence of the island. This is also the case in the references [11] and [13].

From the above review of the available literature, the work done in the past can be summarized as follows:

(1) The prediction of heat, mass and momentum transfer during the laminar forced convection melting of an ice sheet in saline water has been studied before, but only forced convection solutions exist.

(2) Cross stream buoyancy effects for flows over non-melting surfaces have been studied as is represented in references [9, 10, 11, 12, 13 and 14]. In each case, stable solutions were found for flows over horizontal surfaces of finite length.

The objectives of the present study can now be broadly defined. Firstly, the buoyancy terms should be included in an analysis of the steady flow of fresh or saline water below a melting horizontal ice sheet, and the effects of the buoyancy terms should be investigated. Since the buoyancy forces act across the direction of the free stream flow, boundary layer methods may not be sufficient; therefore, a two-dimensional analysis, such as that described in general by Gosman et al. [15], is necessary. This analysis should be made to describe the flow of fresh or saline water below the leading portion of a long horizontal ice sheet, because of its applicability to the cases of ice covered rivers or oceans which occur in nature.

ANALYSIS

The basic problem of ice melting into saline water is formulated by considering the two-dimensional equations of motion, energy and mass diffusion. In order to reduce the problem to a steady state, the coordinate system is attached in the manner of Roberts [16] to the ice-water interface which is assumed to move towards the water at the melt velocity as shown in figure 1. All fluid properties except density are assumed to be constant and are evaluated at the free stream conditions and the flow is considered to be incompressible.

The governing equations of momentum, energy and mass for two-dimensional incompressible flow, when body forces are present, are as follows:

For Vorticity, ω

$$\frac{\partial}{\partial x}\left\{\omega \frac{\partial \psi}{\partial y}\right\} - \frac{\partial}{\partial y}\left\{\omega \frac{\partial \psi}{\partial x}\right\} - \frac{\partial}{\partial x}\left\{\mu \frac{\partial \omega}{\partial x}\right\} - \frac{\partial}{\partial y}\left\{\mu \frac{\partial u}{\partial y}\right\}$$

$$- \tfrac{1}{2}\left\{\frac{\partial \rho}{\partial y} \frac{\partial}{\partial x}(u^2+v^2) - \frac{\partial \rho}{\partial x} \frac{\partial (u^2+v^2)}{\partial y}\right\} - g \frac{\partial \rho}{\partial x} = 0 \qquad \ldots(1)$$

For Stream function, Ψ

$$- \frac{\partial}{\partial x}\left\{\frac{1}{\rho} \frac{\partial \psi}{\partial x}\right\} - \frac{\partial}{\partial y}\left\{\frac{1}{\rho} \frac{\partial \psi}{\partial y}\right\} - \omega = 0 \qquad \ldots(2)$$

For Energy

$$\frac{\partial}{\partial x}\left\{T \frac{\partial \psi}{\partial y}\right\} - \frac{\partial}{\partial y}\left\{T \frac{\partial \psi}{\partial x}\right\} - \frac{\partial}{\partial x}\left\{\frac{k}{\rho c_p} \frac{\partial T}{\partial x}\right\} - \frac{\partial}{\partial y}\left\{\frac{k}{\rho c_p} \frac{\partial T}{\partial y}\right\} = 0 \qquad \ldots(3)$$

For Salinity, S

$$\frac{\partial}{\partial x}\{S\frac{\partial \psi}{\partial y}\} - \frac{\partial}{\partial y}\{S\frac{\partial \psi}{\partial y}\} - \frac{\partial}{\partial x}\{\rho D\frac{\partial S}{\partial x}\} - \frac{\partial}{\partial y}\{\rho D\frac{\partial S}{\partial y}\} = 0 \quad \ldots (4)$$

In the above equations u and v represent the velocity vector components in the coordinate X and Y-directions respectively, T represents the local temperature and S represents the local salinity in parts per thousand. The fluid properties are density, ρ, dynamic viscosity, μ, thermal conductivity, k, specific heat, c_p, and mass diffusion coefficient, D.

To aid in solving these equations it is noted that vorticity and stream functions are defined by the following two equations:

$$\omega = \frac{\partial v}{\partial x} - \frac{\partial u}{\partial y} \quad \ldots (5)$$

$$\rho u = \frac{\partial \psi}{\partial y} \quad \text{and} \quad \rho v = -\frac{\partial \psi}{\partial x} \quad \ldots (6)$$

Equations (1) to (4) may be written in the following form as in Gosman et al. [15]

$$a_\phi \frac{\partial}{\partial x}\{\phi\frac{\partial \psi}{\partial y}\} - a_\phi \frac{\partial}{\partial y}\{\phi\frac{\partial \psi}{\partial x}\} - \frac{\partial}{\partial x}\{b_\phi \frac{\partial}{\partial x}(c_\phi \phi)\}$$

$$- \frac{\partial}{\partial y}\{b_\phi \frac{\partial}{\partial y}(c_\phi \phi)\} + d_\phi = 0 \quad \ldots (7)$$

where the newly introduced symbols are identified in table 1.

An equation must be chosen to describe the density of sea water in terms of salinity and temperature. In the present analysis,

density was calculated as suggested in references [17] and [18]. Thus, the following sets of equations were used:

$$\sigma_o = -0.093 + 0.8149\,S - 0.000482\,S^2 + 0.0000068\,S^3 \quad (8)$$

$$\alpha_T = \frac{T}{1000}(4.7867 - 0.098185\,T + 0.0010843\,T^2) \quad (9)$$

$$\beta_T = \frac{T}{10^6}(18.03 - 0.8164\,T + 0.01667\,T^2) \quad (10)$$

$$\sigma_T = (\sigma_o + 0.1324)\{1-\alpha_T+\beta_T(\sigma_o-0.1324)\} - \frac{(T+283)(T-3.98)^2}{(T+67.26)503.57} \quad (11)$$

Therefore, the density, $\rho = \sigma_T + 1000.0 \quad kg/m^3$ (12)

Boundary conditions are chosen to be consistent with flow of a warm salty stream below an ice sheet. At the upstream end, velocity, temperature and salinity are assumed to be uniform. Thus at $x = 0$,

$$u = U_\infty, \quad T = T_\infty, \quad S = S_\infty$$

$$\psi = \rho U_\infty y \quad \text{and} \quad \omega = 0.$$

At large distances from the water-ice interface, the fluid is assumed to be unaffected by the presence of the interface. Therefore, for large values of y, $u = U_\infty$, $T = T_\infty$ and $S = S_\infty$. Thus, $\frac{\partial \psi}{\partial y} = \rho U_\infty$ and $\omega = 0$.

The boundary conditions at the melt interface are more involved in comparison to the above. Griffin [5] described an equilibrium condition at the interface whereby the melting temperature is depressed by the presence of dissolved species. The relationship employed here is that recommended by Neuman and Pierson [17] for salt water, namely

$$T_w(x) = 0.003 - 0.0527\, S_w - 0.00004\, S_w^2 \qquad (13)$$

The no-slip boundary condition is assumed with u = 0, but the normal component of velocity, V_w, is not known a-priori. It may be determined by considering an energy balance at the melt interface. If conduction of heat into the ice is assumed to be negligible, then the heat transferred from the water at y = 0 results in melting of the ice. Thus

$$V_w(x) = \frac{k}{\rho L} \frac{\partial T}{\partial y}\bigg|_{y=0} \qquad (14)$$

where L is the latent heat of fusion of the ice. The steady state wall salinity, S_w, at the ice surface can be evaluated by equating the convection of salt away from the ice by the melt water to the molecular diffusion of salt towards the ice. Thus

$$S_w(x) = \frac{D}{V_w} \frac{\partial S}{\partial y}\bigg|_{y=0} \qquad (15)$$

Equations (13), (14) and (15) are interrelated and must be solved iteratively. The melt velocity, V_w, may be utilized in order to evaluate the stream function distribution, ψ_w, along the wall. Hence

$$\psi_w(x) = -\rho \int_0^x V_w dx \qquad (16)$$

From this it follows that the wall vorticity may be evaluated by applying equation (2). If the analysis were based upon boundary layer equations, the boundary conditions described so far would be sufficient to describe the flow near the leading edge of the plate. That is, boundary conditions would then need to be specified only at the leading edge, near the ice surface and far removed from the ice surface. However, if a fully two-dimensional solution is to be found,

boundary conditions must also be specified at the downstream end. This in turn requires that the flow geometry be carefully specified.

Obviously, whatever method is to be used to solve equations (1) to (16), a solution can be expected only for finite values of the x-coordinate. In the present analysis a finite leading portion of a long horizontal ice sheet has been considered. It is assumed that the ice sheet is much longer than the leading portion over which a solution will be found. This implies that the length of the region of interest of the plate may be arbitrarily chosen, provided the gradients of the various variables in the X-direction are very small or predictable. Then the closure boundary conditions for these variables can be set using extrapolation methods from the interior of the region of interest. As is described later, two test programs were run, one with the assumption that at the downstream end the gradients of all variables equalled zero and the other with linear extrapolation of these variables being assumed. The solutions obtained in both cases were identical with only minor variations at the downstream end of the region of interest. Therefore, for simplicity in the present work the zero gradient downstream boundary condition was employed. Thus at $x = x_L$

$$\frac{\partial \omega}{\partial x} = 0$$

$$\frac{\partial \psi}{\partial x} = 0$$

$$\frac{\partial T}{\partial x} = 0.$$

$$\frac{\partial S}{\partial x} = 0$$

For the present work, the boundary conditions discussed above and summarized in figure 1 provides sufficient information to solve the equations (1), (2), (3), (4) and (11). Because of their complexity, direct analytical solution of the equations, is not possible and the application of numerical methods is necessary. In broad terms, a numerical solution can be obtained by approximating the differential equations either by finite difference or by finite element techniques and solving the resulting set of approximate equations. In both techniques the region of interest is discretized and the equations are integrated by approximate methods over small discrete areas. This results, in the case of finite element analysis, in sets of simultaneous linear equations, normally in the form of banded matrices, which can be solved on a digital computer using appropriate matrix techniques. This technique requires large amounts of computer storage if very small finite elements are employed. In the case of finite difference techniques, iterative methods have been devised with lower storage requirements. Because of the availability of a PDP-11/60 computer with a 64 K memory but free computer time, finite difference techniques were chosen for the present work.

Basically, the finite difference scheme developed by Gosman et al. [15] was employed with the incorporation of Spalding's [19] modifications as discussed by Runchal [20]. In the scheme of Gosman et al., all terms in equations (1) to (4) are approximated by central differences, with the exception of the convection terms for which "upwind" differences are used to achieve numerical stability. Spalding's modifications, which are described in detail in Appendix A,

consist of utilizing central differences for the convection terms if their contributions are less than those of the diffusion terms. If the magnitude of the convection terms exceeds that of the diffusion terms, the diffusion terms are neglected and the convection terms are expressed as "upwind" differences. Runchal has shown Spalding's finite difference scheme to be preferable for both accuracy and convergence in simple cases.

The basic computer program given in reference [15] could have been employed in the present work with appropriate modification to incorporate the boundary conditions. However, this program was written in a general form to permit calculations for a wide range of problems for laminar or turbulent flows using Cartesian or polar cylindrical coordinates. If applied to the present case without substantial modification, the program will repeatedly calculate many parameters during each iteration even though the values will not change from iteration to iteration. In view of this, the program was modified substantially for the present work to feature storage of the bulk of the intermediate parameters and dependent variables on a disk with a minimum number of variables being stored in the computer memory at any time. A suitable scheme was incorporated to transfer information between the computer memory and the disk. The net result was that a large number of grid lines could be considered with a limit being imposed by the capacity of the disk rather than by the size of the computer memory. The above approach had been tested against that of reference [15] and yielded identical solutions for flow in a circular pipe.

An initialization program (see Appendix B) was run first by specifying the values of U_∞, T_∞, and S_∞ to create a working data file on the disk. Using this data file, the program (see Appendix C) for the forced convection case was run until it had converged. Then using the resulting data file, the program of Appendix D was run, to include buoyancy terms, until it had converged. In both the cases a convergence criterion of 0.001 was used. In arriving at a solution the nodel ω, ψ, T and S values vary from one cycle of iteration to another. The solution was considered converged when the calculated values of ω, ψ, T and S changed by less than 0.001 of the reference values. For stream function reference value was that farthest from the plate at the upstream end. For vorticity, a reference value was chosen arbitrarily as -2 and for temperature and salinity, the free stream values are employed. Typically, an average run of the combined convection program required about 3 to 10 hours on the PDP-11/60 time sharing computer. The total number of iterations and time requirement mainly depend upon the number of grid lines used in the program. While this much computer time seems excessive by the standards of a large computer facility, it should be recognized that the computations were performed on a mini computer without a high speed processor. Of the various facilities available for this work, the "hands on" control over the programs and plotting facility more than offset the disadvantages of large execution times.

RESULTS AND DISCUSSIONS

The successful solution of partial differential equations by finite difference methods depends upon the approximations which are made in developing the finite difference equations, the choice of a suitable grid and the judicious application of boundary conditions. The finite difference scheme employed here, as has been described previously was chosen for its stability, applicability to a non-uniform grid, and economy in storage requirements.

For the fresh water case, all salinity equations in the analysis were ignored and the melt interface temperature, T_w, was set to zero. Early runs of the computer program with the different Y-direction grids shown in table 2(A) were compared by drawing contour maps of iso-streamlines for U_{oo} = 0.04 m/s and T_{oo} = 20°C. The resulting contour maps could then be directly compared by noting the respective postions of the streamlines. Grid 1 and grid 2 of table 2(A) both describe a portion of the flow field for $0 \leq y \leq .0933$m with grid 2 consisting of a finer grid spacing. Since the resulting streamlines for grid 1 were indistinguishable from those for grid 2, it was concluded that the grid distribution of grid 1 is sufficiently fine. Grid 3 of table 2(A) is identical to grid 2 for $y \leq 0.0933$ but it extends to y = 0.270m. Since for $y \leq$ 0.093m the streamline distributions for grid 3 were indistinguishable from those for grid 2, it was established that the free stream boundary conditions can be applied at y = 0.0933m without effecting the solution for $y \leq 0.0933$m. Therefore, the 21 node Y-direction grid was chosen for the fresh water case, and used for all other runs described below for S = 0°/oo.

A similar technique was employed to investigate the effect of changing the X-direction grid spacing and of changing the location of

application and type of downstream boundary conditions. The location of application of the downstream boundary condition was changed in running the program for the 51 node and the 36 node X-direction grids of table 2(B). These two grids are identical up to x = 1.1723 m, and identical solutions were obtained for values of x in the range $0 \leq x \leq 1.1723$. Thus the solution was shown to be independent of the location of the downstream boundary conditions. The program was then run for the 76 node grid also shown in table 2(B), and the solution so obtained was in full agreement with that from the 51 node grid. This procedure, thus, vindicated the spacing used in the 51 node grid. Finally, the program was modified to incorporate a linear extrapolation for ω, ψ, T, S and ρ at the downstream end for the 51 by 21 node grid. The results so obtained were indistinguishable from the previous results in which the zero gradient boundary condition had been used.

In the above calculations, two methods were used to arrive at solutions. In the first method the program was run until it had converged to a solution for the forced convection case, and this solution was then used as a starting point for the combined convection case which was run until it had converged. In the second method, the forced convection program was run for only 5 iterations and these intermediate results were used as a starting point for the combined convection program. This was then run until it had converged to a solution. For both methods, the results were found to be identical to three significant figures. The only difference was that in the first method a 0.0001 value was necessary for the convergence criteria in order to prevent the program from stopping abnormally early. With the second method,

a 0.001 value was sufficient. This procedure established that the solutions obtained from the numerical approximations were clearly independent of the path taken to arrive at the solutions.

Numerical results were then obtained using the 51 by 21 node grid for free stream velocities ranging from 0.025 to 0.01 m/s over a plate length of 1.731 m for fresh water, while the temperature of the free stream was varied between $2^{o}C$ and $20^{o}C$. The property values used in the above calculations were those corresponding to the free stream conditions, with values of viscosity, thermal conductivity and coefficient of mass diffusion taken from reference [22].

To permit an assessment of the accuracy of the solution and to have a basis for evaluating the effect of buoyancy, solutions were initially obtained for the case of forced convection with melting, which involved a repetition of the work described in reference [21].

At a free stream velocity of 0.025 m/s combined convection solutions were obtained at different free stream temperatures $2^{o}C \leq T_{\infty} \leq 20^{o}C$. Figure 3(b) shows that the stream line patterns for $T_{\infty} = 2^{o}C$ are identical to the corresponding forced convection solution of figure 3(a) up to $x \approx 0.02$ m. Further downstream, the stream lines for the combined convection case lie closer to the ice surface than the corresponding stream lines for the forced convection case. Figure 4(a) shows that for $U_{\infty} = 0.025$ m/s and $T_{\infty} = 20^{o}C$, the stream lines follow a regular pattern for the forced convection with melting case. With the stream function set at zero at the leading edge of the melting surface, negative stream function values originate at increasing distances along the ice surface. For equal increments in

stream function, the longitudinal distance between the successive increments is ever increasing. This corresponds to a high melting rate near the leading edge and a reduction in melting rate further along the plate. When the buoyancy terms are included for the same free stream conditions, the stream lines shown in figure 4(b) have shapes similar to the previous case only at the upstream end. Near the ice sheet, the stream lines are much more closely spaced than in the forced convection case.

The u components of velocity were determined by using $u = \frac{1}{\rho} \frac{\partial \psi}{\partial y}$ for various values of x along the sheet. In most cases velocity profiles near the leading edge were identical with a laminar forced convection solution. Further downstream, the longitudinal velocities near the ice sheet were substantially greater for combined convection than for forced convection. A typical case is shown in figures 5(a) and 5(b) for $T_\infty = 20^oC$, $U_\infty = 0.025$ m/s. Since the velocity near the wall is higher, the wall shear stress is also higher for combined convection than for forced convection since the wall shear stress, τ_w, is equal to $\mu \frac{\partial u}{\partial y}\Big|_{y=0}$. Figure 6(a) shows that the temperatures near the ice sheet for a combined convection case are lower than those obtained for a corresponding forced convection solution shown in figure 6(b). Since the rate of heat transfer from the fluid to the ice is given by $- k \frac{\partial T}{\partial y}\Big|_{y=0}$ the decreased near wall temperature gradients for the combined convection case indicates a reduction in the heat transfer rates when compared to the forced convection case. This is summarized in figure 7 in which the local Nusselt numbers are shown as functions of the local Reynolds numbers for the two cases.

Over most of the Reynolds number range, the local Nusselt number for combined convection is approximately 25% lower than that for forced convection.

Since the solutions discussed so far have differed only by the inclusion of the density gradient terms in the vorticity equation, the effect of these terms is clearly evident. When the density gradient terms are included, the local wall shear stresses are increased, and the local heat transfer rates are decreased. The Reynolds analogy, however, would indicate that if the local wall shear stresses increase then the local heat transfer rates should increase proportionately. The contradiction of the present results with the Reynolds analogy is understandable upon consideration of the mechanism by which the density gradient affect the solution of the vorticity equation.

In the region near the melt interface the no slip boundary condition at the wall results generally in viscous generation of clockwise or negative vorticity in the fluid. Just downstream from the leading edge, the flow field, therefore, assumes a simultaneous growth of momentum and thermal boundary layers characteristic of a forced convection flow. As a result negative values exist for the downstream density gradients, $\frac{\partial \rho}{\partial x}$, near the wall as can be seen in figures 8(a) and 8(b). This results in a clockwise rotational tendency within the fluid which reinforces the negative vorticity originating with the viscous shear stress, and results in steeper velocity gradients near the ice surface. The resulting increased convection parallel and perpendicular to the wall produces lower temperature gradients, which lowers the rate of heat transfer from

the fluid to the ice surface. Since the rate of heat transfer is lower, then the melting rate will also be lower, and the conflict with the Reynolds analogy which was mentioned before is resolved. Further away from the wall, positive values exist for the density gradients as shown in figure 8(a). This positive density gradients results in an anticlockwise rotational tendency which tends to offset the weakened viscous vorticity production. This results in flatter velocity profiles away from the ice sheet than are produced if the density gradient terms are neglected.

Figures 9(a) and 9(b) show that for forced convection or combined convection, as the Reynolds number increases along the plate, the Nusselt number also increases. In both the cases at a particular value of Reynolds number, if the free stream temperature increases, the Nusselt number decreases. For the combined convection case, it is seen from figure 9(b) that when $Re \geq 2500$ there is little change in the local Nusselt number at various temperatures.

At free stream velocities of 0.02 and 0.015 m/s and free stream temperatures $2^{o}C \leq T_{\infty} \leq 20^{o}C$, similar solutions were successfully obtained. The results were similar to the above and are summarized in figures 10 and 11 for combined convection. The free stream velocity was then further lowered to 0.01 m/s and the program was run at different free stream temperatures varying from $2^{o}C$ to $15^{o}C$. Up to $T_{\infty} = 10^{o}C$, the solutions were as stable as those mentioned above requiring typically 405 iterations. At $T_{\infty} = 13.45^{o}C$ a combined convection solution was obtained after 1152 iterations, but there was no converged solution at $T_{\infty} = 13.5^{o}C$. Various degrees of

relaxation parameters were employed to get a converged solution at this temperature but all were unsuccessful. Forced convection solutions were stable up to $T_\infty = 20^oC$. The combined convection results were studied carefully at $T_\infty = 15^oC$. Figure 12(a) was produced by running the program until it had converged to a solution for forced convection. Using this as a starting point, the program was then run for 600 iterations resulting in figure 12(b). This solution was then used as a starting point for a total of 3000 iterations and stream lines were observed at every 100 iterations. Typical stream line patterns are presented in 12(c), 12(d), 12(e) and 12(f). These patterns indicate that the flow is abruptly downward at the leading edge of the ice sheet and downstream from here the flow turns towards the ice sheet once again. Enclosed within this region is a recirculating eddy. Further downstream, the flow is more closely parallel to the ice sheet with relatively small wave-like disturbances. Inspection of these figures show that the streamline patterns change from iteration to iteration, but the recirculating eddy formed near the leading edge after 700 iterations was repeated again after 1525 iterations with an extra recirculation cell further downstream.

The above tendency could be attributed to a numerical instability in the finite difference method, or to the application of a steady state solution to a transient problem. The exact cause could not be clearly established but the effect of $\frac{\partial \rho}{\partial x}$ on the oscillating solutions could be examined.

The effect of $\frac{\partial \rho}{\partial x}$ was studied at every 100^{th} iteration up to 3000 iterations. It was found that at any value of x, $\frac{\partial \rho}{\partial x}$ changes

abruptly its rotational tendency and amplitude from within 100 iterations. For example, figure 13 shows that after 700 iterations, near the ice surface at x = 0.2054 m the negative density gradient produces clockwise rotational tendency which results in a steeper velocity gradient than for purely viscous flow. Further away from the wall $\frac{\partial \rho}{\partial x}$ changes its rotational tendency to anticlockwise which results in a lower velocity gradient. At far distances from the wall $\frac{\partial \rho}{\partial x}$ again changes its rotational tendency to clockwise which reinforce steeper velocity gradients once again. It is seen that positive density gradient is stronger than either of the negative density gradients. This abrupt behaviour of $\frac{\partial \rho}{\partial x}$ could be attributed to the formation of buoyancy cells at the lower horizontal velocity, or simply to a numerical instability in the finite difference approximations. Further work is clearly needed for full investigation.

The results presented so far for the fresh water case are satisfactory to permit extension of the analysis to the saline water cases. Thus the salinity equations were taken into consideration and the melt interface temperature was calculated by using equation (13). For a free stream salinity of $5^{0}/oo$, X and Y-direction grids were established in the same manner as for the fresh water case by using different grids with the nodal values given in tables 3(A) and 3(B). The results obtained with 44, 52 and 56 Y-direction grid and 51 and 76 X-direction grids were identical. In these cases the downstream boundary conditions were applied at x = 1.731 m. One program was run with the 52 by 52 node grid and downstream boundary conditions were applied at x = 1.021 m. The results thus obtained were identical with the previous case. So for simplicity and to reduce execution time the 52 by 52 node grid was chosen and downstream boundary conditions

were applied at x = 1.021 m for the analysis of saline water case when $S_\infty = 5^o/oo$.

Solutions were then obtained successfully at different free stream velocities and at different free stream temperatures. In all cases the streamlines for the forced convection case lie closer to the ice surface than the corresponding streamlines for combined convection. A typical streamline pattern is shown in figure 14 at $U_\infty = 0.025$ m/s and $T_\infty = 20^oC$. This trend is opposite to that found for the fresh water case, because the negative density gradient near the wall is stronger than that in the fresh water case, as can be seen in figure 15. This higher negative $\frac{\partial \rho}{\partial x}$ produces strong clockwise rotation within the fluid which results in the flow being deflected away from the ice surface in the case of combined convection.

Figures 16, 17 and 18 show that Nusselt number as a function of Reynolds number were obtained from solutions at free stream velocities of 0.025, 0.02 and 0.015 m/s and at free stream temperatures $2^oC \leq T_\infty \leq 20^oC$, were similar to the fresh water case.

For a free stream velocity of 0.01 m/s, solutions were obtained successfully up to $T_\infty \leq 17.85^oC$. At $T_\infty = 17.9^oC$ a converged solution could not be obtained. For the fresh water case, solutions were stable only up to $T_\infty \leq 13.45^oC$. This increase in the temperature at which solutions became unstable could be attributed to the salinity boundary layer and the resulting high negative density gradient near the ice surface. The unstable combined convection results were studied carefully at $T_\infty = 18^oC$ in a similar manner to that used for fresh water when $U_\infty = 0.01$ m/s and $T_\infty = 15^oC$. It was observed that it had a

behaviour similar to that for fresh water, namely that the streamline patterns change from iteration to iteration with recirculating cells. This shows the instability in the solution.

Velocity profiles for $S_\infty = 5^o/oo$ are steeper for forced convection than for combined convection. For fresh water the velocity profiles for combined convection are steeper than for forced convection. This opposite trend results from the stronger clockwise rotation produced by $\frac{\partial \rho}{\partial x}$ within the fluid for saline water. A typical velocity profile for both the cases are shown in figures 19(a) and 19(b) at $U_\infty = 0.025$ m/s and $T_\infty = 20^oC$.

The temperature profiles for $S_\infty = 5^o/oo$ had patterns similar to those for fresh water. Typical temperature profiles are shown in figures 20(a) and 20(b) for $U_\infty = 0.025$ m/s and $T_\infty = 20^oC$.

Salinity profiles for $S_\infty = 5^o/oo$ are steeper near the ice surface for combined convection than for forced convection. For combined convection lower temperature reduces the melting rate. Since the melting rate is lower, then the salinity concentration will be higher near the ice surface. Typical salinity profiles are shown in figures 21(a) and 21(b). It can be observed by comparing figure 21(a) to figures 19(a) and 20(a) that the concentration boundary layer is thinner than the momentum and thermal boundary layers. The salinity profile is more rounded for low Reynolds numbers than for high Reynolds numbers. It indicates a very definite dependence of the salinity profile on local Reynolds numbers. For the salinity case, the Schmidt number $\mu/\rho D$, for salt diffusing in water is much greater than one. Thus the value of ρD is small in comparison with that of the viscosity, μ. Therefore it is clear from equation (4) that the salinity profile

is much more strongly influenced by streamwise and cross-stream convection than either the velocity or the temperature profile. Therefore melting at the interface influences the salinity profile much more than it affects the velocity and temperature profiles.

If the free stream velocity is kept constant, as T_∞ is increased, the wall salinity decreases. A typical example is shown in figures 22(a) and 22(b) for both combined and forced convection cases respectively. Very close to the leading edge the local wall salinity distributions portray a forced convection characteristic. For combined convection at the leading edge the local wall salinity is zero corresponding to a large melting rate. S_w then rises abruptly to a local maximum and then falls off further downstream and increases again with increasing distance along the ice surface.

Since the salinity of most oceans lie around $35^0/oo$, it is necessary to study the case of $S_\infty = 35^0/oo$. When the salinity was changed, the X and Y-direction grids were re-established in the same manner as for the previous cases when $S_\infty = 0^0/oo$ and $5^0/oo$ by using the different grids of tables 4(A) and 4(B). The results thus obtained with 65, 68, 70 Y-direction and 68, 77 X-direction node grids were identical. In these cases the downstream boundary conditions were applied at x = 1.021 m. The location of application of downstream boundary condition was vindicated by running a program in which the downstream boundary conditions were applied at x = 0.662 m. The results obtained in both cases were identical. Therefore for the analysis of $S_\infty = 35^0/oo$, the 68 by 65 node grid was used and downstream boundary conditions were applied at x = 1.021 m.

Solutions were then obtained successfully at U_∞ = 0.025 m/s and at various free stream temperatures ranging from 2^0C to 20^0C. As was the case for $S_\infty = 5^0/oo$ the streamlines for the forced convection case lie closer to the ice surface than the corresponding streamlines for combined convection. A typical streamline pattern is shown in figure 23 at U_∞ = 0.025 m/s and $T_\infty = 20^0$C. The Nusselt number is shown as a function of Reynolds number for U_∞ = 0.025 m/s and $2^0\text{C} \leq T_\infty \leq 20^0\text{C}$ in figure 24. These results are similar to those for $S_\infty = 0^0/oo$ and $5^0/oo$.

The free stream velocity was then lowered to 0.02 m/s and the solutions were obtained successfully up to $T_\infty \leq 4.85^0$C. At $T_\infty = 4.9^0$C, a converged solution could not be obtained. The unstable combined convection result were studied carefully at $T_\infty = 4.9^0$C in the same manner to that used for cases when $S_\infty = 0^0/oo$ and $5^0/oo$ and similar conclusions can be drawn.

Velocity, temperature and salinity profiles at various conditions had a pattern similar to the case when $S_\infty = 5^0/oo$. Typical profiles are shown in figures 25(a), 25(b), 26(a), 26(b), 27(a) and 27(b) at U_∞ = 0.025 m/s and $T_\infty = 20^0$C.

Figures 28(a) and 28(b) show that the wall salinity for combined convection has the same pattern as in the case when $S_\infty = 5^0/oo$, namely as the free stream temperature increases, S_w decreases.

Finally, for the conditions where a converged solution could not be obtained, further investigations are required.

CONCLUSIONS

(1) A two-dimensional finite difference technique has been developed for predicting the laminar steady state combined convection heat, mass and momentum transfer to a flow of fresh or saline water below a horizontal pure ice sheet.

(2) For different values of free stream salinities, different numbers of grid lines were needed for solution. As the salinity increases, the number of grid lines also increases. The grid used for the analysis of $S_\infty = 35^0/oo$ would be appropriate for the analysis when $S_\infty \leq 35^0/oo$ but would require longer calculation times.

(3) A converged solution could not be obtained for the following cases:

For $S_\infty = 0^0/oo$, when $U_\infty = 0.01$ m/s, $T_\infty > 13.45^0$C

For $S_\infty = 5^0/oo$ when $U_\infty = 0.01$ m/s, $T_\infty > 17.85^0$C

For $S_\infty = 35^0/oo$ when $U_\infty = 0.02$ m/s, $T_\infty > 4.85^0$C.

(4) In the case of fresh water, the near wall velocity profiles were steeper for combined convection than for forced convection. The opposite trend was observed in saline water cases.

(5) The temperature profiles had similar patterns in all cases, i.e., the temperature near the ice surface were lower for combined convection than for forced convection.

(6) In all cases, the local Nusselt number is lower for combined convection than for forced convection for the same value of Reynolds number.

(7) At any particular velocity, as the free stream temperature is increased, the local wall salinity is decreased.

(8) The density gradient term becomes stronger within the fluid as the free stream salinity is increased.

(9) Further work is needed in the cases where convergence could not be obtained.

REFERENCES

[1] Yen, Y.C. and Tien, C. "Laminar Heat Transfer over a melting plate, the modified Leveque problem." Journal of Geophysical Research, Vol. 68, No. 12, 1963, pp. 3673-3678.

[2] Pozvonkov, F.M., Shurgalzkii, E.F. and Axelrod, L.S. "Heat Transfer at a melting flat surface under conditions of forced convections and laminar boundary layer." International Journal of Heat and Mass Transfer, Vol. 13, 1970, pp. 957-962.

[3] Griffin, O.M. "Heat, mass and momentum transfer during the melting of glacial ice in sea water." Journal of Heat Transfer, Trans. ASME, Series C, Vol. 95, 1973, pp. 317-323.

[4] Griffin, O.M. "An integral method of solution for combined heat and mass transfer problems with phase transformation." Proceedings Fifth International Heat Transfer Conference (Tokyo), Vol. 1, 1974, pp. 211-215.

[5] Griffin, O.M. "A note concerning the transport processes near melting glacial ice in sea water." Journal of Heat Transfer, Trans. ASME, Series C, Vol. 97, 1975, pp. 624-626.

[6] Schilicting, H. "Boundary Layer Theory," Pergamon Press, London, 1955.

[7] Bird, R.B., Stewart, W.E., and Lightfoot, E.N. "Transport Phenomena," John Wiley & Sons, New York, 1960.

[8] Merk, H.J. "The Influence of Melting and Anomalous Expansion on the Thermal Convection in Laminar Boundary Layers." Appl. Scient. Res., Vol. 4, 1953, pp. 435-452.

[9] Long, R.R. "Some Aspects of the Flow of Stratified Fluids, I. A Theoretical Investigation," Tellus, Vol. 5, 1953, pp. 42-57.

[10] Turner, J.S. "Buoyancy Effects in Fluids," Cambridge University Press, New York, 1973, p. 37.

[11] Robertson, G.E., Seinfeld, J.H., and Leal, L.G. "Combined Forced and Free Convection Flow Past a Horizontal Flat Plate." A.I.Ch.E. Journal, Vol. 19, No. 5, 1973, pp. 998-1008.

[12] Sparrow, E.M. and Minowyez, W.J. "Buoyancy effects on horizontal boundary layer flow and Heat Transfer." International Journal of Heat and Mass Transfer, Vol. 5, 1962, p. 505.

[13] Leal, L.G., and Acrivos, A. "Structure of Steady Closed Streamline flows within a boundary layer." The Physics of Fluids Supplement II, 12, 1969, pp. II-105 to 113.

[14] Meroney, R.N. and Yamada, T. "Wind Tunnel and Numerical Experiments at Two-Dimensional Stratified Airflow over a Heated Island," Environmental and Geophysical Heat Transfer, ASME Publication HTD-Vol. 4, 1971, pp. 31-40.

[15] Gosman, A.D., Pun, W.M. Runchal, A.K., Spalding, D.B., and Wolfshtein, M. "Heat and Mass Transfer in Recirculating Flows," Academic Press, London and New York, 1969.

[16] Roberts, A.L. "On the Melting of a Semi-Infinite Body Placed in a Warm Stream of Air." Journal of Fluid Mechanics, Vol. 4, 1958, pp. 505-528.

[17] Neuman, G. and Pierson, W.J. "Principles of Physical Oceanography," Prentice-Hall, Englewood Cliffs, N.J., 1966, pp. 41-43.

[18] "Tables for Sea Water Density," U.S. Navy Hydrographic Office, Washington, H.O. Pub. No. 615, 1952, p. vii.

[19] Spalding, D.B. "A Novel finite difference formulation for differential Expressions involving both first and second derivatives." Int. Journal of Numerical Methods in Engineering, Vol. 4, pp. 551-559, 1972.

[20] Runchal, A.K. "Convergence and Accuracy of Three Finite Difference Schemes for a Two-Dimensional Conduction and Convection Problem." International Journal of Numerical Methods in Engineering, Vol. 4, 1972, pp. 541-550.

[21] Wilson, N.W., and Sarma, T.S. "Prediction of heat, mass and momentum transfer during laminar forced convective melting of ice in saline water." ICSI/AIDJEX Symposium on sea ice - processes and models, Seattle, 6-9, September 1977.

[22] Richardson, J.L., Bergstrainsson, P., Getz, R.J., Peters, D.L., and Sprague, R.W. "Sea Water Mass Diffusion Co-efficient Studies," Philco Aeronutronic Div. Pub., No. U-0321, W.O. 2053, 1964, Office of Naval Res. Contract No. Norn-4061(00).

[23] Pohlhasuen, E. Angew, Z. Math. Mech. Vo., 1921, p. 115.

TABLE 1

Equation Number	ϕ	a_ϕ	b_ϕ	c_ϕ	d_ϕ
1	ω	1	1	μ	$-\frac{1}{2}\left(\frac{\partial \rho}{\partial y}\frac{\partial}{\partial x}(u^2+v^2)\right.$ $\left.-\frac{\partial \rho}{\partial x}\frac{\partial}{\partial y}(u^2+v^2)\right]$ $-g\frac{d\rho}{dx}$
2	ψ	0	$1/\rho$	1	$-\omega$
3	T	1	$k/\rho C_p$	1	0
4	S	1	ρD	1	0

TABLE 2(A)

Y-Direction Grid Spacings for $S_{\infty} = 0^{o}/oo$

Index	All Grids	Grid 1	Grid 2	Grid 3
	X(m)	Y(m)	Y(m)	Y(m)
1	0.000	0.0000	0.0000	0.0000
2	0.00953	0.0005	0.0004	0.0004
3	0.0212	0.0011	0.0008	0.0008
4	0.0353	0.00182	0.0012	0.0012
5	0.0526	0.00268	0.0016	0.0016
6	0.0738	0.00372	0.002	0.002
7	0.0995	0.00496	0.0025	0.0025
8	0.1310	0.00646	0.003	0.0030
9	0.1690	0.00825	0.0035	0.0035
10	0.2054	0.0104	0.004	0.004
11	0.2426	0.0130	0.0045	0.0045
12	0.2798	0.0161	0.0050	0.0050
13	0.3169	0.0198	0.0056	0.0056
14	0.3541	0.0242	0.0063	0.0063
15	0.3913	0.0296	0.007	0.0070
16	0.4285	0.0360	0.0075	0.0075
17	0.4657	0.0437	0.0085	0.0085
18	0.5029	0.0530	0.00925	0.00925
19	0.5401	0.0641	0.0100	0.0100
20	0.5772	0.0774	0.0110	0.01100
21	0.6144	0.0933	0.0125	0.01250
22	0.6516	-	0.0140	0.0140
23	0.6888	-	0.0160	0.0160
24	0.7260	-	0.0180	0.018
25	0.7632	-	0.02	0.020
26	0.8004	-	0.025	0.025
27	0.8376	-	0.03	0.030
28	0.8748	-	0.035	0.035
29	0.9120	-	0.040	0.040
30	0.9492	-	0.0475	0.0475
31	0.9863	-	0.055	0.055
32	1.0235	-	0.065	0.065
33	1.0607	-	0.0774	0.0774
34	1.0979	-	0.0933	0.0933
35	1.1351	-	-	0.1000
36	1.1723	-	-	0.1200
37	1.2102	-	-	0.1300
38	1.2474	-	-	0.1400
39	1.2846	-	-	0.1500
40	1.3218	-	-	0.1600

TABLE 2(A) (Continued)

Index	All Grids X(m)	Grid 1 Y(m)	Grid 2 Y(m)	Grid 3 Y(m)
41	1.3590	-	-	0.1700
42	1.396	-	-	0.1800
43	1.433	-	-	0.1900
44	1.470	-	-	0.2000
45	1.508	-	-	0.2100
46	1.545	-	-	0.2200
47	1.582	-	-	0.2300
48	1.619	-	-	0.2400
49	1.657	-	-	0.2500
50	1.694	-	-	0.2600
51	1.731	-	-	0.2700

TABLE 2(B)

X-direction Grid Spacings for $S_\infty = 0^o/oo$

Index	All Grids Y(m)	Grid 1 X(m)	Grid 2 X(m)	Grid 3 X(m)
1	0.000	0.000	0.0000	0.000
2	0.0005	0.00953	0.00953	0.005
3	0.0011	0.0212	0.02120	0.0125
4	0.00182	0.0353	0.0353	0.02217
5	0.00268	0.0526	0.0526	0.03417
6	0.00372	0.0738	0.0738	0.04917
7	0.00496	0.0995	0.0995	0.06717
8	0.00646	0.1310	0.1310	0.088767
9	0.00825	0.1690	0.1690	0.11067
10	0.0104	0.2054	0.2054	0.13467
11	0.0130	0.2426	0.2426	0.15867
12	0.0161	0.2798	0.2798	0.18267
13	0.0198	0.3169	0.3169	0.20667
14	0.0242	0.3541	0.3541	0.23067
15	0.0296	0.3913	0.3913	0.25467
16	0.0360	0.4285	0.4285	0.27867
17	0.0437	0.4657	0.4657	0.30267
18	0.0530	0.5029	0.5029	0.32667
19	0.0641	0.5401	0.5401	0.35067
20	0.0774	0.5772	0.5772	0.37467
21	0.0933	0.6144	0.6144	0.39867
22	-	0.6516	0.6516	0.42267
23	-	0.6888	0.6888	0.44667
24	-	0.7260	0.7260	0.47067
25	-	0.7632	0.7632	0.49467
26	-	0.8004	0.8004	0.51867
27	-	0.8376	0.8376	0.54267
28	-	0.8748	0.8748	0.56667
29	-	0.9120	0.9120	0.59067
30	-	0.9492	0.9492	0.61467
31	-	0.9863	0.9863	0.63867
32	-	1.0235	1.0235	0.66267
33	-	1.0607	1.0607	0.68667
34	-	1.0979	1.0979	0.71067
35	-	1.1351	1.1351	0.73467
36	-	1.1723	1.1723	0.75867
37	-	1.2102	-	0.78267
38	-	1.2474	-	0.80667
39	-	1.2846	-	0.83067
40	-	1.3218	-	0.85467

TABLE 2(B) (Continued)

Index	All Grids Y(m)	Grid 1 X(m)	Grid 2 X(m)	Grid 3 X(m)
41	-	1.3590	-	0.87867
42	-	1.3960	-	0.90267
43	-	1.433	-	0.92667
44	-	1.470	-	0.95067
45	-	1.508	-	0.97467
46	-	1.545	-	0.99867
47	-	1.582	-	1.02267
48	-	1.619	-	1.04667
49	-	1.657	-	1.07067
50	-	1.694	-	1.09467
51	-	1.731	-	1.11867
52	-	-	-	1.14267
53	-	-	-	1.16667
54	-	-	-	1.19067
55	-	-	-	1.21467
56	-	-	-	1.23867
57	-	-	-	1.26267
58	-	-	-	1.28662
59	-	-	-	1.31067
60	-	-	-	1.33467
61	-	-	-	1.35867
62	-	-	-	1.38267
63	-	-	-	1.40667
64	-	-	-	1.43067
65	-	-	-	1.45467
66	-	-	-	1.47867
67	-	-	-	1.50267
68	-	-	-	1.52667
69	-	-	-	1.55067
70	-	-	-	1.57467
71	-	-	-	1.60067
72	-	-	-	1.62667
73	-	-	-	1.65267
74	-	-	-	1.67867
75	-	-	-	1.70467
76	-	-	-	1.731

TABLE 3(A)

Y-direction Grid Spacing for $S_\infty = 5^o/oo$

	All Grids	Grid 1	Grid 2	Grid 3	Grid 4	Grid 5
Index	X(m)	Y(m)	Y(m)	Y(m)	Y(m)	Y(m)
1	0.000	0.0000	0.0000	0.0000	0.00000	0.00000
2	0.00953	0.00050	0.0004	0.0003	0.0003	0.0003
3	0.0212	0.00110	0.0008	0.0006	0.0006	0.0006
4	0.0353	0.00182	0.0012	0.0009	0.0009	0.0009
5	0.0526	0.00268	0.0017	0.00125	0.00125	0.00125
6	0.0738	0.00372	0.0022	0.0016	0.0016	0.00160
7	0.0995	0.00496	0.0027	0.00195	0.00195	0.00195
8	0.1310	0.00646	0.0033	0.00235	0.00235	0.00235
9	0.1690	0.00825	0.0039	0.00275	0.00275	0.00275
10	0.2054	0.0104	0.0045	0.00315	0.00315	0.00315
11	0.2426	0.0130	0.0053	0.00360	0.00360	0.00360
12	0.2798	0.0161	0.0061	0.00405	0.00405	0.00405
13	0.3169	0.0198	0.0070	0.00455	0.00450	0.00450
14	0.3541	0.0242	0.0079	0.00505	0.0050	0.00500
15	0.3913	0.0296	0.0089	0.00560	0.0055	0.0055
16	0.4285	0.0360	0.0099	0.00615	0.0060	0.0060
17	0.4657	0.0437	0.0119	0.00675	0.00655	0.00655
18	0.5029	0.0530	0.0139	0.00735	0.0071	0.00710
19	0.5401	0.0641	0.0164	0.00800	0.00765	0.00765
20	0.5772	0.0774	0.0189	0.00865	0.00825	0.00825
21	0.6144	0.0933	0.0219	0.00935	0.00885	0.00885
22	0.6516	-	0.0254	0.01005	0.00950	0.00945
23	0.6888	-	0.0294	0.01080	0.01015	0.01010
24	0.7260	-	0.0344	0.01155	0.01085	0.01075
25	0.7632	-	0.0394	0.01235	0.01155	0.01140
26	0.8004	-	0.0444	0.01315	0.01230	0.01210
27	0.8376	-	0.0504	0.01400	0.01305	0.01280
28	0.8748	-	0.0564	0.01485	0.01385	0.01355
29	0.9120	-	0.0634	0.01575	0.01465	0.01430
30	0.9492	-	0.0704	0.01665	0.0155	0.01510
31	0.9863	-	0.0774	0.01765	0.0164	0.01590
32	1.0235	-	0.0849	0.01865	0.0173	0.01675
33	1.0607	-	0.0933	0.02065	0.0183	0.01760
34	1.0979	-	-	0.02265	0.0193	0.01850
35	1.1351	-	-	0.02565	0.0203	0.0194
36	1.1723	-	-	0.02865	0.0223	0.02040
37	1.2102	-	-	0.03265	0.0243	0.02140
38	1.2474	-	-	0.03665	0.0263	0.02290
39	1.2846	-	-	0.04165	0.0293	0.02440
40	1.3218	-	-	0.04815	0.0323	0.02640

TABLE 3(A) (Continued)

Index	All Grids X(m)	Grid 1 Y(m)	Grid 2 Y(m)	Grid 3 Y(m)	Grid 4 Y(m)	Grid 5 Y(m)
41	1.359	-	-	0.05615	0.0353	0.0284
42	1.396	-	-	0.06565	0.0393	0.0309
43	1.433	-	-	0.07865	0.0433	0.0334
44	1.470	-	-	0.0933	0.0473	0.0364
45	1.508	-	-	-	0.0513	0.0394
46	1.545	-	-	-	0.0563	0.0429
47	1.582	-	-	-	0.0613	0.0464
48	1.619	-	-	-	0.0663	0.0504
49	1.657	-	-	-	0.0723	0.0544
50	1.694	-	-	-	0.0783	0.0589
51	1.731	-	-	-	0.0853	0.0639
52	-	-	-	-	0.0933	0.0684
53	-	-	-	-	-	0.0734
54	-	-	-	-	-	0.0794
55	-	-	-	-	-	0.0859
56	-	-	-	-	-	0.0933

TABLE 3(B)

X-direction Grid Spacing for $S_\infty = 5^0/oo$

Index	All Grids Y(m)	Grid 1 X(m)	Grid 2 X(m)
1	0.0000	0.0000	0.0000
2	0.0003	0.005	0.005
3	0.0006	0.0125	0.0125
4	0.0009	0.02217	0.02217
5	0.00125	0.03417	0.03417
6	0.00160	0.04917	0.04917
7	0.00195	0.06717	0.06717
8	0.00235	0.088767	0.088767
9	0.00275	0.11067	0.10900
10	0.00315	0.13467	0.130
11	0.00360	0.15867	0.151
12	0.00405	0.18267	0.172
13	0.00450	0.20667	0.193
14	0.00500	0.23067	0.214
15	0.00550	0.25467	0.235
16	0.00600	0.27867	0.256
17	0.00655	0.30267	0.277
18	0.00710	0.32667	0.298
19	0.00765	0.35067	0.319
20	0.00825	0.37467	0.340
21	0.00885	0.39867	0.361
22	0.00950	0.42267	0.382
23	0.01015	0.44667	0.403
24	0.01085	0.47067	0.424
25	0.01155	0.49467	0.445
26	0.01230	0.51867	0.466
27	0.01305	0.54267	0.487
28	0.01385	0.56667	0.508
29	0.01465	0.59067	0.529
30	0.01550	0.61467	0.550
31	0.0164	0.63867	0.571
32	0.0173	0.66267	0.592
33	0.0183	0.68667	0.613
34	0.0193	0.71067	0.634
35	0.0203	0.73467	0.655
36	0.0223	0.75867	0.676
37	0.0243	0.78267	0.697
38	0.0263	0.80667	0.718
39	0.0293	0.83067	0.739
40	0.0323	0.85467	0.760

TABLE 3(B) (Continued)

Index	All Grids	Grid 1	Grid 2
	Y(m)	X(m)	X(m)
41	0.0353	0.87867	0.781
42	0.0393	0.90267	0.802
43	0.0433	0.92667	0.823
44	0.0473	0.95067	0.845
45	0.0513	0.97467	0.867
46	0.0563	0.99867	0.889
47	0.0613	1.02267	0.911
48	0.0663	1.04667	0.933
49	0.0723	1.07067	0.955
50	0.0783	1.09467	0.977
51	0.0853	1.11867	1.000
52	0.0933	1.14267	1.021
53	-	1.16667	-
54	-	1.19067	-
55	-	1.21467	-
56	-	1.23867	-
57	-	1.26267	-
58	-	1.28667	-
59	-	1.31067	-
60	-	1.33467	-
61	-	1.35867	-
62	-	1.38267	-
63	-	1.40667	-
64	-	1.43067	-
65	-	1.45467	-
66	-	1.47867	-
67	-	1.50267	-
68	-	1.52667	-
69	-	1.55067	-
70	-	1.57467	-
71	-	1.60067	-
72	-	1.62667	-
73	-	1.65267	-
74	-	1.67867	-
75	-	1.70467	-
76	-	1.731	-

TABLE 4(A)

Y-direction Grid Spacings for $S_\infty = 35^0/oo$

Index	All Grids X(m)	Grid 1 Y(m)	Grid 2 Y(m)	Grid 3 Y(m)	Grid 4 Y(m)
1	0.000	0.0000	0.0000	0.000	0.0000
2	0.005	0.0003	0.0025	0.00025	0.00025
3	0.0125	0.0006	0.0005	0.0005	0.0005
4	0.02217	0.0009	0.00075	0.00075	0.00075
5	0.03417	0.00125	0.00105	0.00105	0.00105
6	0.04917	0.00160	0.00135	0.00135	0.00135
7	0.06717	0.00195	0.00165	0.00165	0.00165
8	0.088767	0.00235	0.002	0.002	0.002
9	0.10900	0.00275	0.00235	0.00235	0.00235
10	0.130	0.00315	0.0027	0.0027	0.0027
11	0.151	0.00360	0.0031	0.0031	0.0031
12	0.172	0.00405	0.0035	0.0035	0.0035
13	0.193	0.00450	0.0039	0.0039	0.0039
14	0.214	0.00500	0.00435	0.00435	0.00435
15	0.235	0.00550	0.0048	0.0048	0.0048
16	0.256	0.00600	0.00525	0.00525	0.00525
17	0.277	0.00655	0.00575	0.00575	0.00575
18	0.298	0.00710	0.00625	0.00625	0.00625
19	0.319	0.00765	0.00675	0.00675	0.00675
20	0.340	0.00825	0.0073	0.0073	0.0073
21	0.361	0.00885	0.00785	0.00785	0.00785
22	0.382	0.00950	0.0084	0.0084	0.0084
23	0.403	0.01015	0.009	0.009	0.009
24	0.424	0.01085	0.0096	0.0096	0.0096
25	0.445	0.01155	0.0102	0.0102	0.0102
26	0.466	0.01230	0.01085	0.01085	0.01085
27	0.487	0.01305	0.0115	0.0115	0.0115
28	0.508	0.01385	0.01215	0.01215	0.01215
29	0.529	0.01465	0.01285	0.01285	0.01285
30	0.550	0.01550	0.01355	0.01355	0.01355
31	0.571	0.0164	0.01425	0.01425	0.01425
32	0.592	0.0173	0.015	0.015	0.015
33	0.613	0.0183	0.01575	0.01575	0.01575
34	0.634	0.0195	0.0165	0.0165	0.0165
35	0.655	0.0203	0.0173	0.0173	0.0173
36	0.676	0.0223	0.0181	0.0181	0.0181
37	0.697	0.0243	0.0189	0.0189	0.0189
38	0.718	0.0263	0.01975	0.01975	0.01975
39	0.739	0.0293	0.0206	0.0206	0.0206
40	0.760	0.0323	0.02145	0.02145	0.02145

TABLE 4(A) (Continued)

Index	All Grids	Grid 1	Grid 2	Grid 3	Grid 4
	X(m)	Y(m)	Y(m)	Y(m)	Y(m)
41	0.781	0.0353	0.02235	0.02235	0.02235
42	0.802	0.0393	0.02325	0.02325	0.02325
43	0.823	0.0433	0.02415	0.02415	0.02415
44	0.845	0.0473	0.0251	0.0251	0.0251
45	0.862	0.0513	0.02605	0.02605	0.02605
46	0.889	0.0563	0.02705	0.0270	0.0270
47	0.911	0.0613	0.02805	0.028	0.028
48	0.933	0.0663	0.02955	0.029	0.029
49	0.955	0.0723	0.03105	0.030	0.030
50	0.977	0.0783	0.03305	0.0315	0.0315
51	1.000	0.0853	0.03505	0.0330	0.0330
52	1.021	0.0933	0.03755	0.0345	0.0345
53	-	-	0.04005	0.0365	0.0365
54	-	-	0.04303	0.0385	0.0385
55	-	-	0.04605	0.0405	0.0405
56	-	-	0.04955	0.0430	0.0430
57	-	-	0.05305	0.0455	0.0455
58	-	-	0.05705	0.0485	0.0480
59	-	-	0.06105	0.0515	0.051
60	-	-	0.06555	0.055	0.054
61	-	-	0.07005	0.0585	0.057
62	-	-	0.07505	0.0625	0.0605
63	-	-	0.0801	0.0665	0.0640
64	-	-	0.0861	0.071	0.0675
65	-	-	0.0933	0.0755	0.0715
66	-	-	-	0.0805	0.0755
67	-	-	-	0.0860	0.0795
68	-	-	-	0.0933	0.0840
69	-	-	-	-	0.0885
70	-	-	-	-	0.0933

TABLE 4(B)

X-direction Grid Spacings for $S_\infty = 35^0/oo$

Index	All Grids Y(m)	Grid 1 X(m)	Grid 2 X(m)	Grid 3 X(m)
1	0.0000	0.0000	0.000	0.0000
2	0.00025	0.0003	0.0003	0.00025
3	0.0005	0.0007	0.0007	0.00060
4	0.00075	0.0013	0.0012	0.00125
5	0.00105	0.0022	0.0019	0.0021
6	0.00135	0.0037	0.0027	0.00325
7	0.00165	0.0060	0.0042	0.00470
8	0.002	0.0095	0.0062	0.00655
9	0.00235	0.0147	0.0092	0.00885
10	0.0027	0.0224	0.0137	0.01165
11	0.0031	0.0341	0.0197	0.01505
12	0.0035	0.0508	0.0277	0.01915
13	0.0039	0.0773	0.0457	0.02415
14	0.00435	0.0940	0.0607	0.03020
15	0.0048	0.111	0.0757	0.0377
16	0.00525	0.128	0.0907	0.0460
17	0.00575	0.145	0.1057	0.0560
18	0.00625	0.162	0.1207	0.068
19	0.00675	0.179	0.1357	0.080
20	0.0073	0.196	0.1507	0.092
21	0.00785	0.213	0.1657	0.104
22	0.0084	0.230	0.1807	0.116
23	0.009	0.247	0.1957	0.128
24	0.0096	0.264	0.2107	0.140
25	0.0102	0.281	0.2257	0.152
26	0.01085	0.298	0.2407	0.164
27	0.0115	0.315	0.2557	0.176
28	0.01215	0.332	0.2707	0.188
29	0.01285	0.349	0.2857	0.200
30	0.01355	0.366	0.3007	0.212
31	0.01425	0.383	0.3157	0.224
32	0.015	0.0400	0.3307	0.236
33	0.01575	0.0417	0.3457	0.248
34	0.0165	0.0434	0.3607	0.260
35	0.0173	0.451	0.3757	0.272
36	0.0181	0.468	0.3907	0.284
37	0.0189	0.485	0.4057	0.296
38	0.01975	0.502	0.4207	0.308
39	0.0206	0.519	0.4357	0.320
40	0.02145	0.536	0.4507	0.332

TABLE 4(B) (Continued)

Index	All Grids Y(m)	Grid 1 X(m)	Grid 2 X(m)	Grid 3 X(m)
41	0.02325	0.555	0.4657	0.344
42	0.02325	0.570	0.4807	0.356
43	0.02415	0.582	0.4957	0.368
44	0.0251	0.604	0.5107	0.380
45	0.02605	0.621	0.5257	0.392
46	0.02705	0.638	0.5407	0.404
47	0.02805	0.653	0.5557	0.416
48	0.02955	0.672	0.5707	0.428
49	0.03105	0.689	0.5857	0.440
50	0.03305	0.706	0.6007	0.452
51	0.03505	0.723	0.6157	0.464
52	0.03755	0.740	0.6307	0.476
53	0.04005	0.757	0.6457	0.488
54	0.04303	0.774	0.6607	0.500
55	0.04605	0.791	0.6757	0.512
56	0.04955	0.808	0.6907	0.524
57	0.05305	0.825	0.7057	0.536
58	0.05705	0.842	0.7207	0.548
59	0.06105	0.859	0.7357	0.560
60	0.06555	0.876	0.7507	0.572
61	0.07005	0.893	0.7657	0.583
62	0.07505	0.910	0.7807	0.594
63	0.0801	0.927	0.7957	0.605
64	0.0861	0.9445	0.8107	0.616
65	0.0933	0.962	0.8257	0.627
66	-	0.980	0.8407	0.638
67	-	1.000	0.8557	0.650
68	-	1.021	0.8707	0.662
69	-	-	0.8857	-
70	-	-	0.9007	-
71	-	-	0.9167	-
72	-	-	0.9327	-
73	-	-	0.9487	-
74	-	-	0.9652	-
75	-	-	0.9817	-
76	-	-	1.000	-
77	-	-	1.021	-

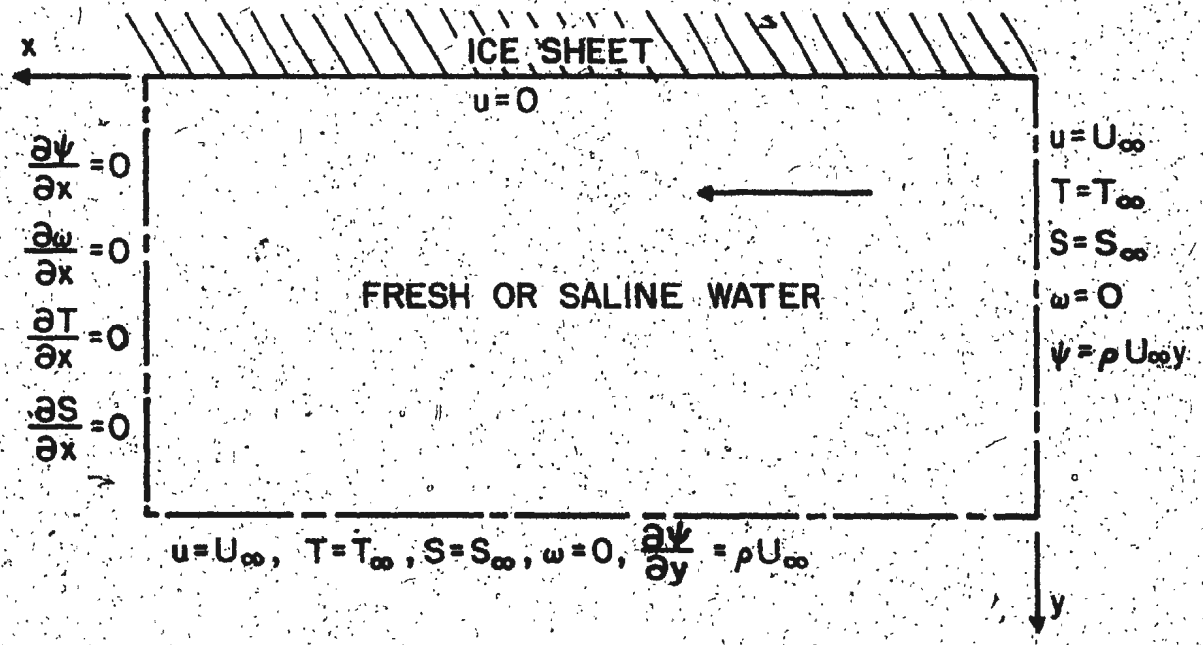

Figure 1

Schematic Diagram of the Flow Field with Boundary Conditions

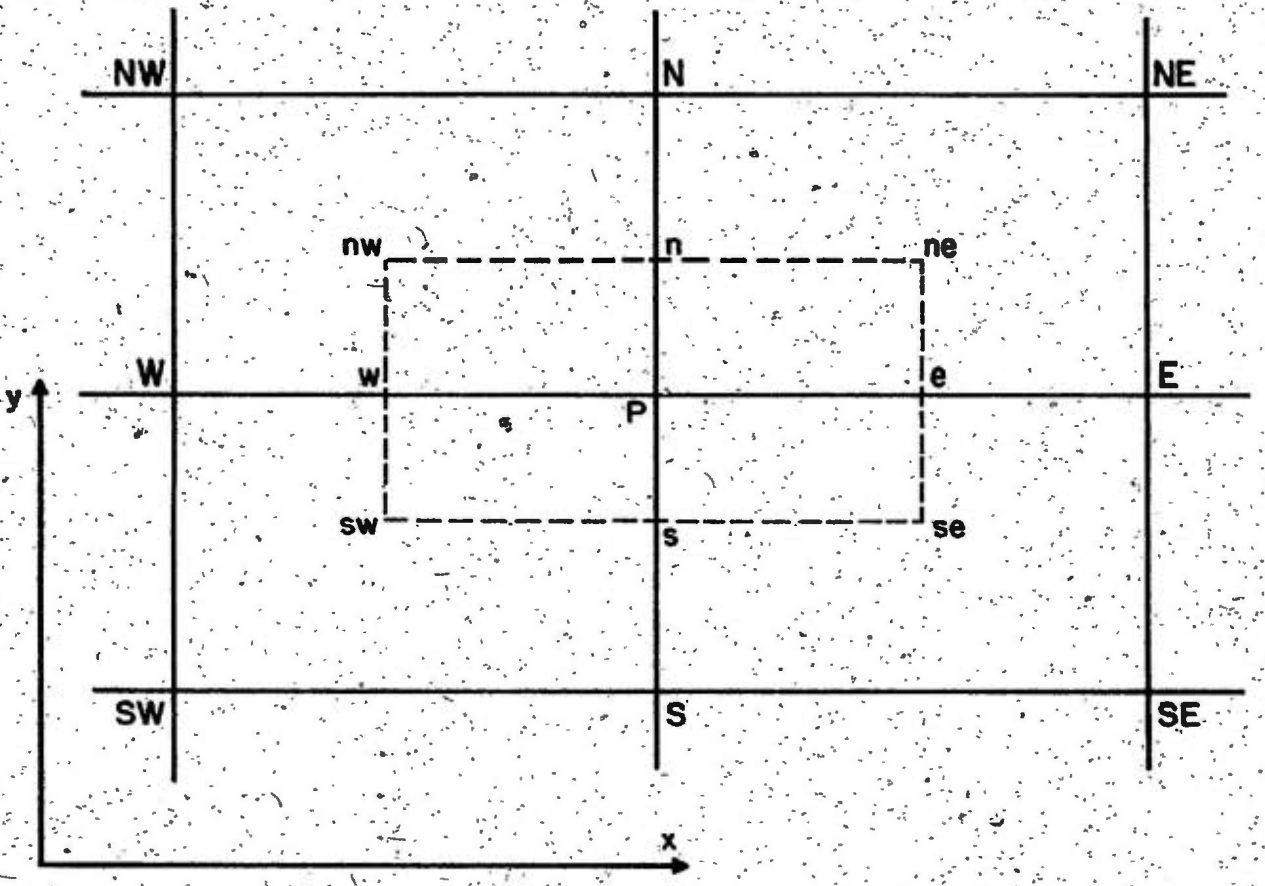

Figure 2

Illustration of a Portion of the Finite-Difference Grid; the Dotted Lines Enclose the Area of Integration

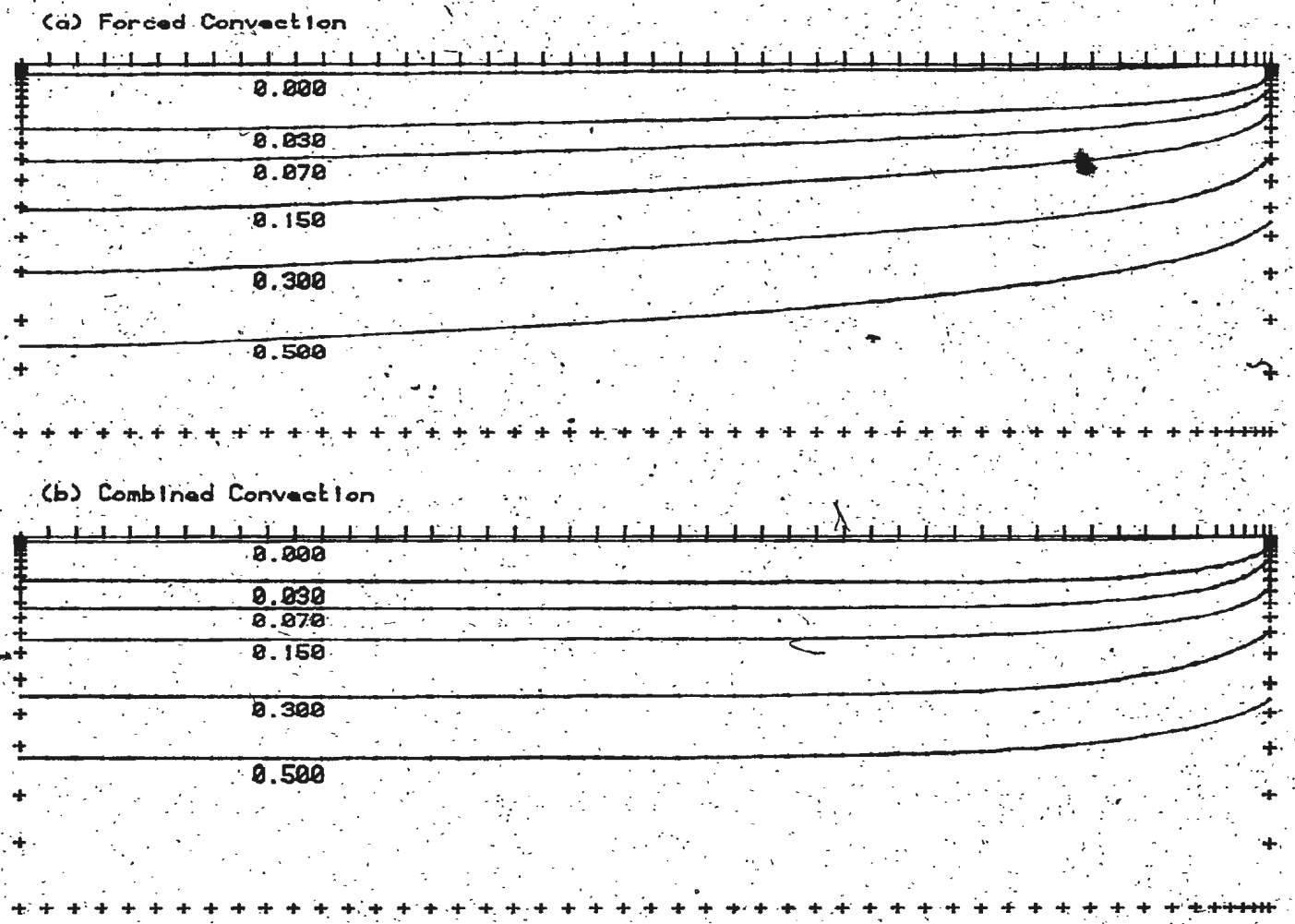

Figure 3 Streamlines for U_∞ = 0.025 m/s, T_∞ = 2.00 °C, S_∞ = 0. ppt

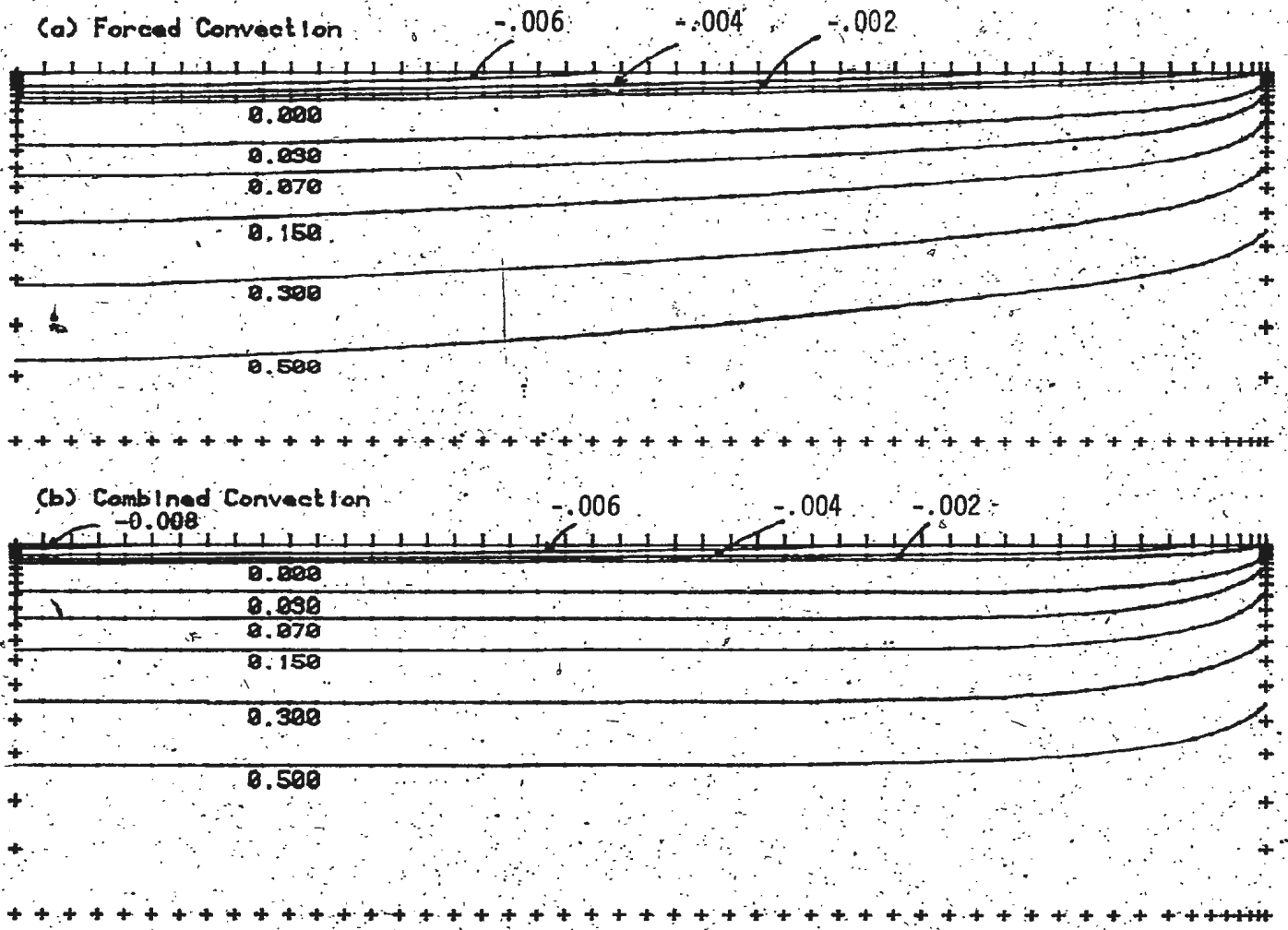

Figure 4 Streamlines for U_∞ = 0.025 m/s, T_∞ = 20.00 °C, S_∞ = 0. ppt

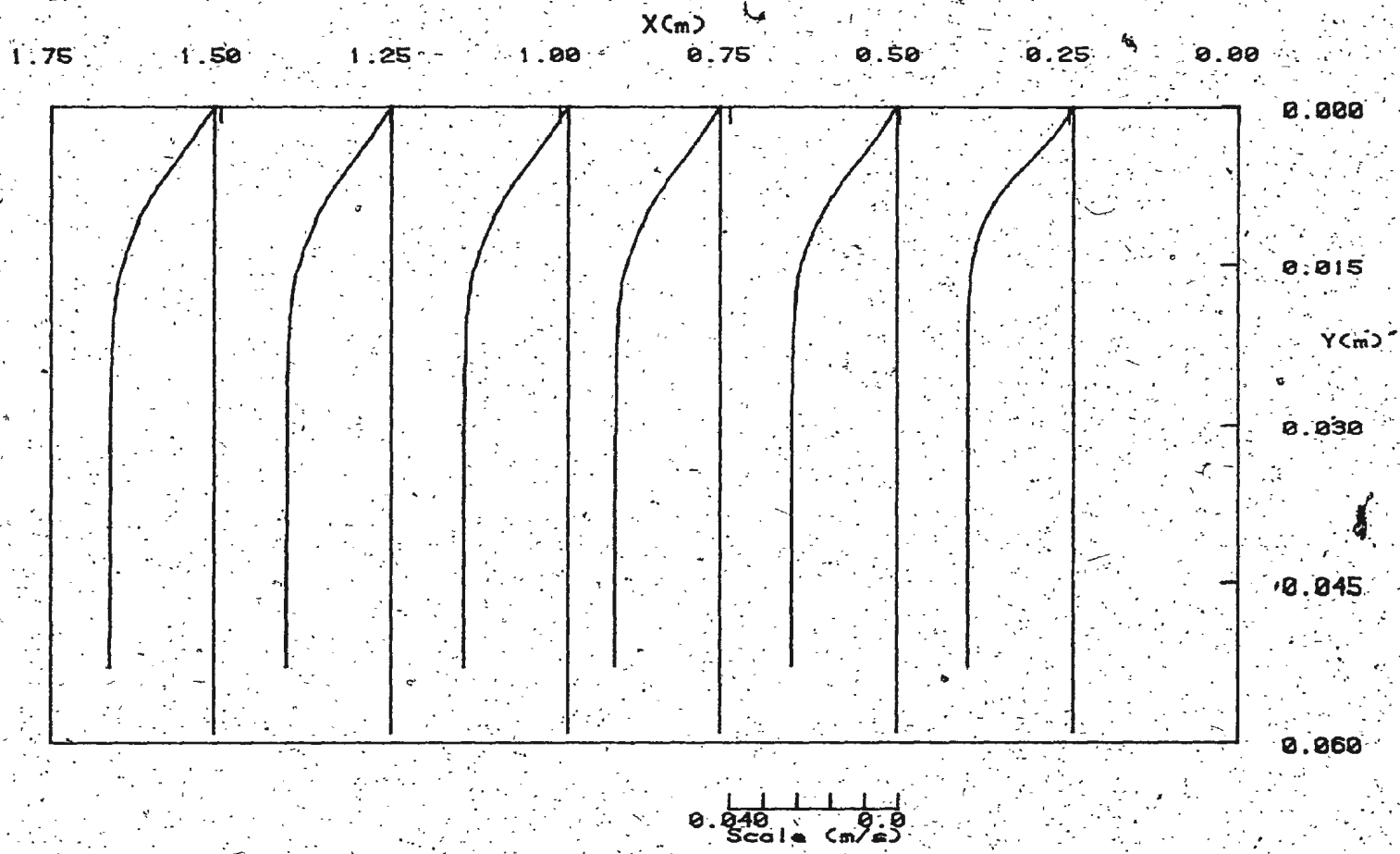

Figure 5(a) Velocity Profiles for T_∞ = 20.00 °C, S_∞ = 0. ppt, U_∞ = 0.025 m/s for Combined Convection

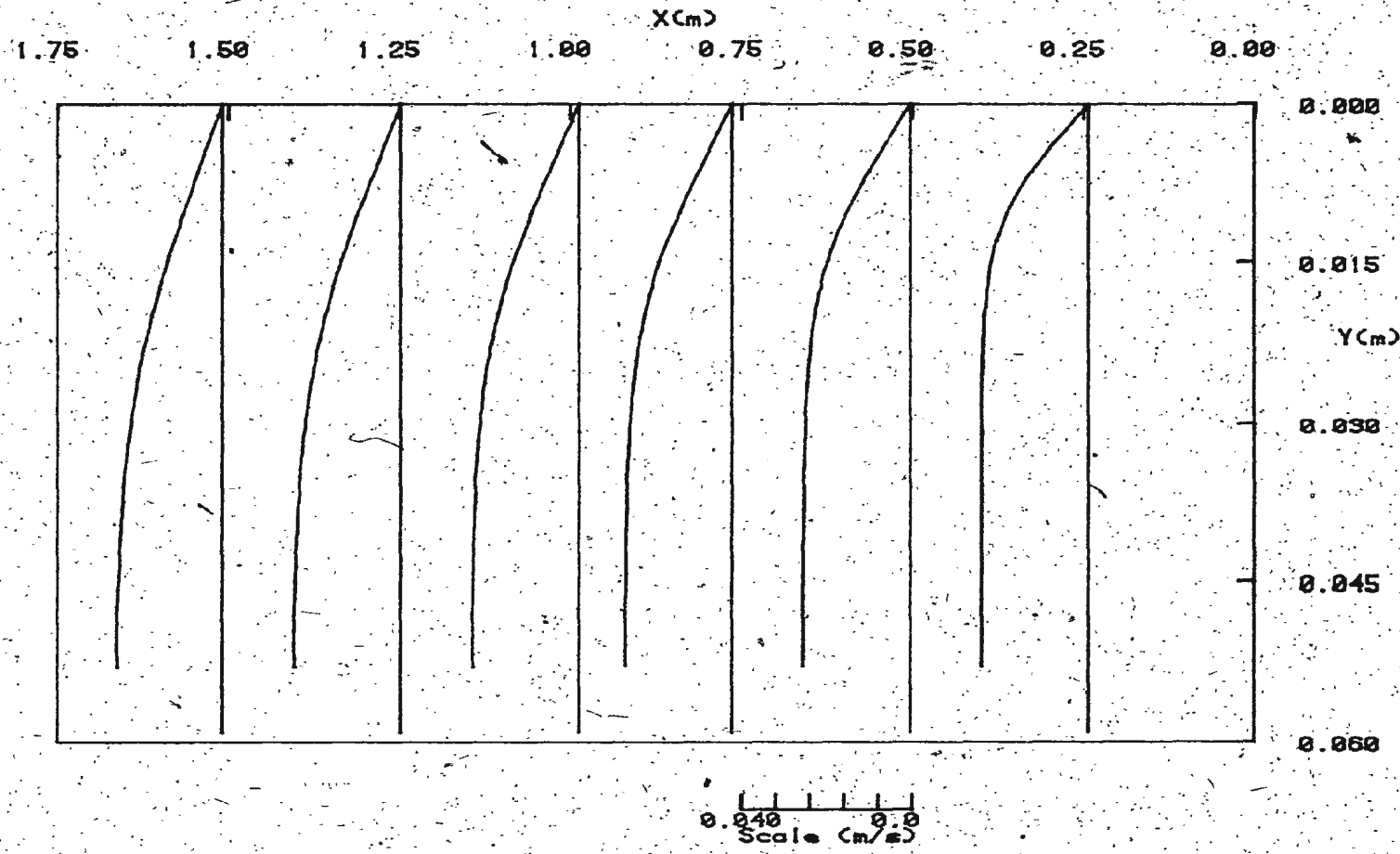

Figure 5(b) Velocity Profiles for $T_\infty = 20.00\ ^\circ C$, $S_\infty = 0.$ ppt, $U_\infty = 0.025$ m/s for Forced Convection

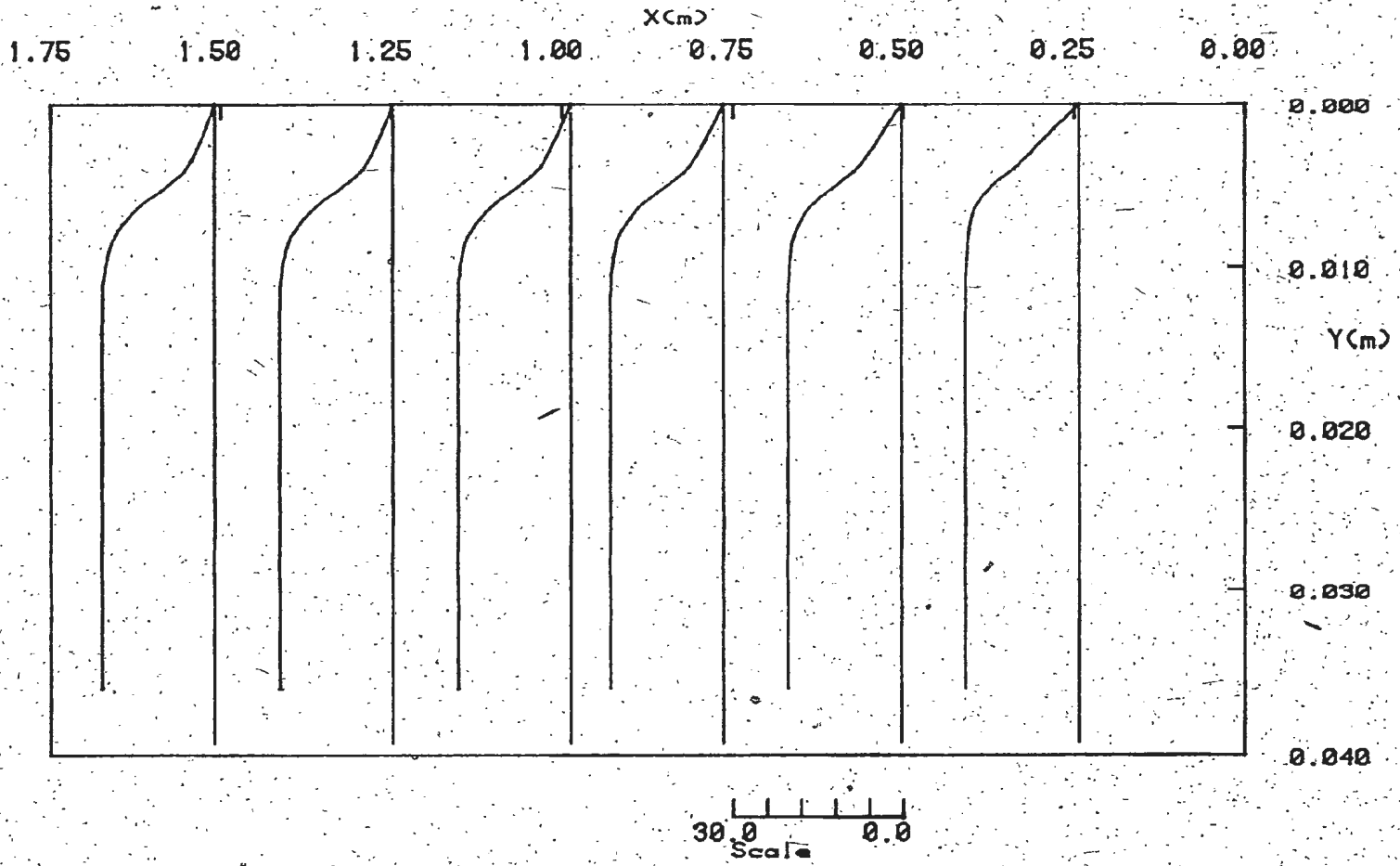

Figure 6(a) Temperature Profiles for T_∞ = 20.00°C, S_∞ = 0. ppt, U_∞ = 0.025 m/s for Combined Convection

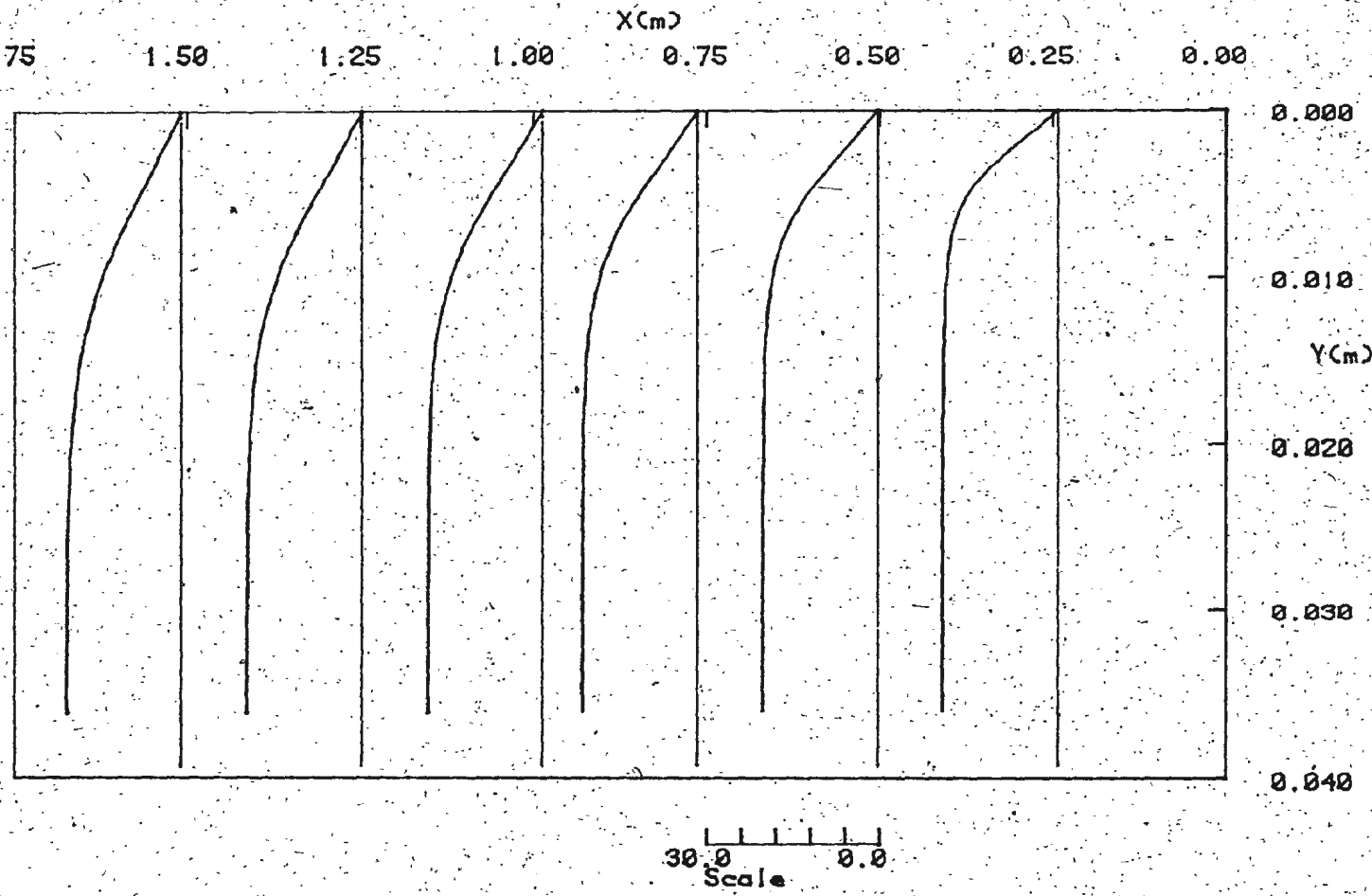

Figure 6(b) Temperature Profiles for T_∞ = 20.00 °C, S_∞ = 0. ppt, U_∞ = 0.025 m/s for Forced Convection

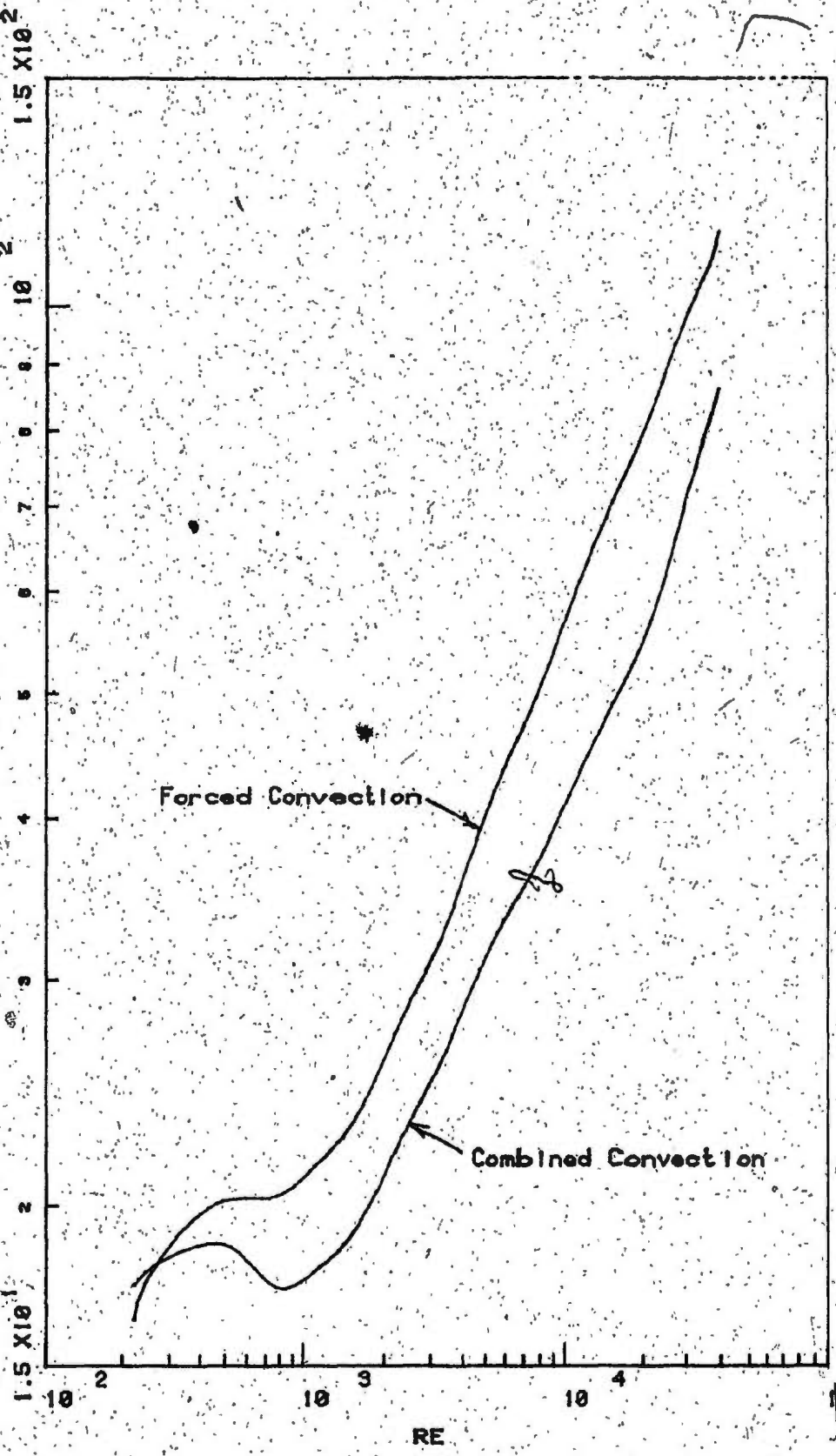

Figure 7 Nusselt Number as a Function of Reynolds Number for U_∞ = 0.025 m/s, S_∞ = 0. ppt., T_∞ = 20.0°C

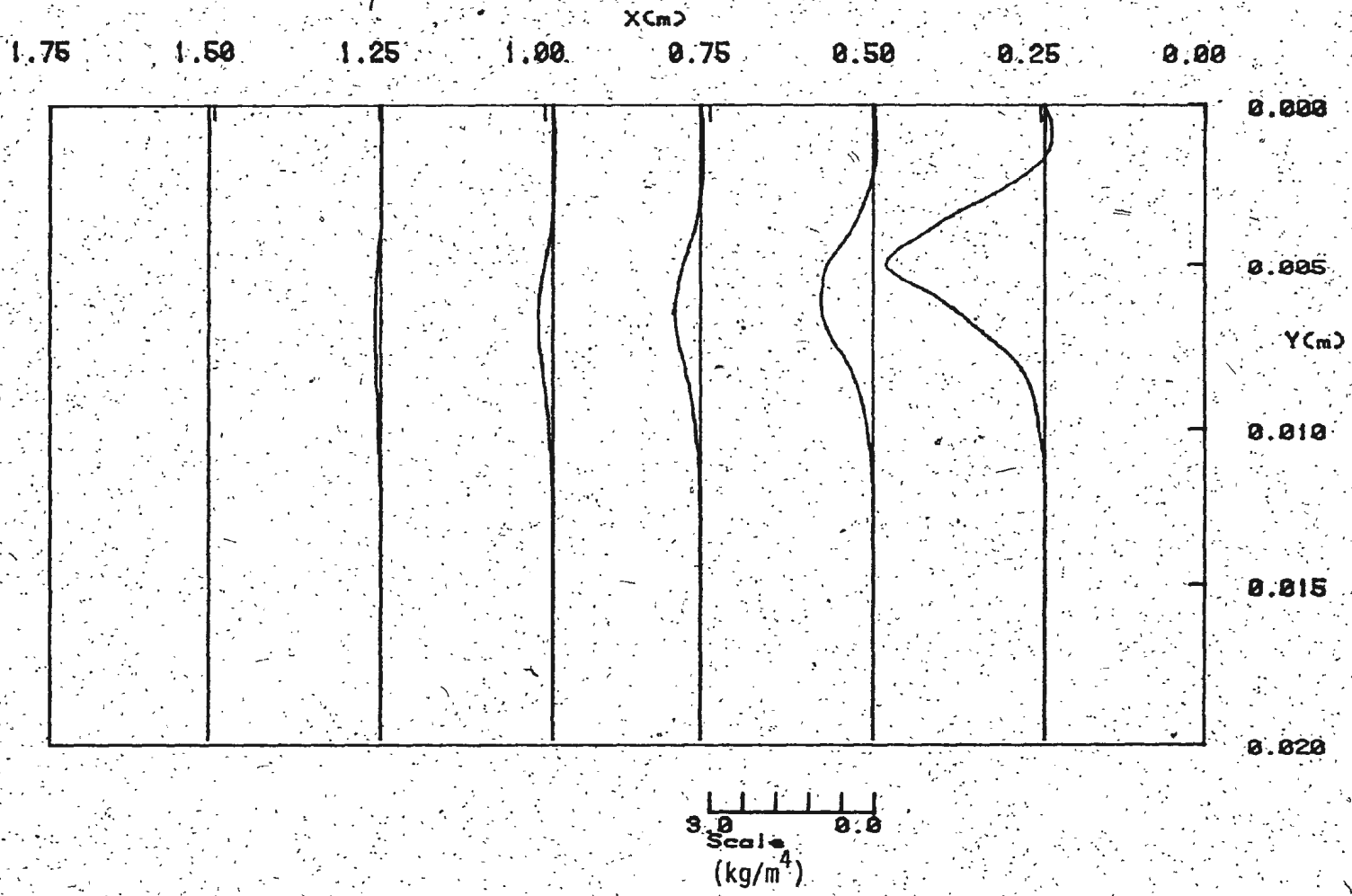

Figure 8(a) Density Gradient Profiles for T_∞ = 20.00 °C, S_∞ = 0. ppt, U_∞ = 0.025 m/s

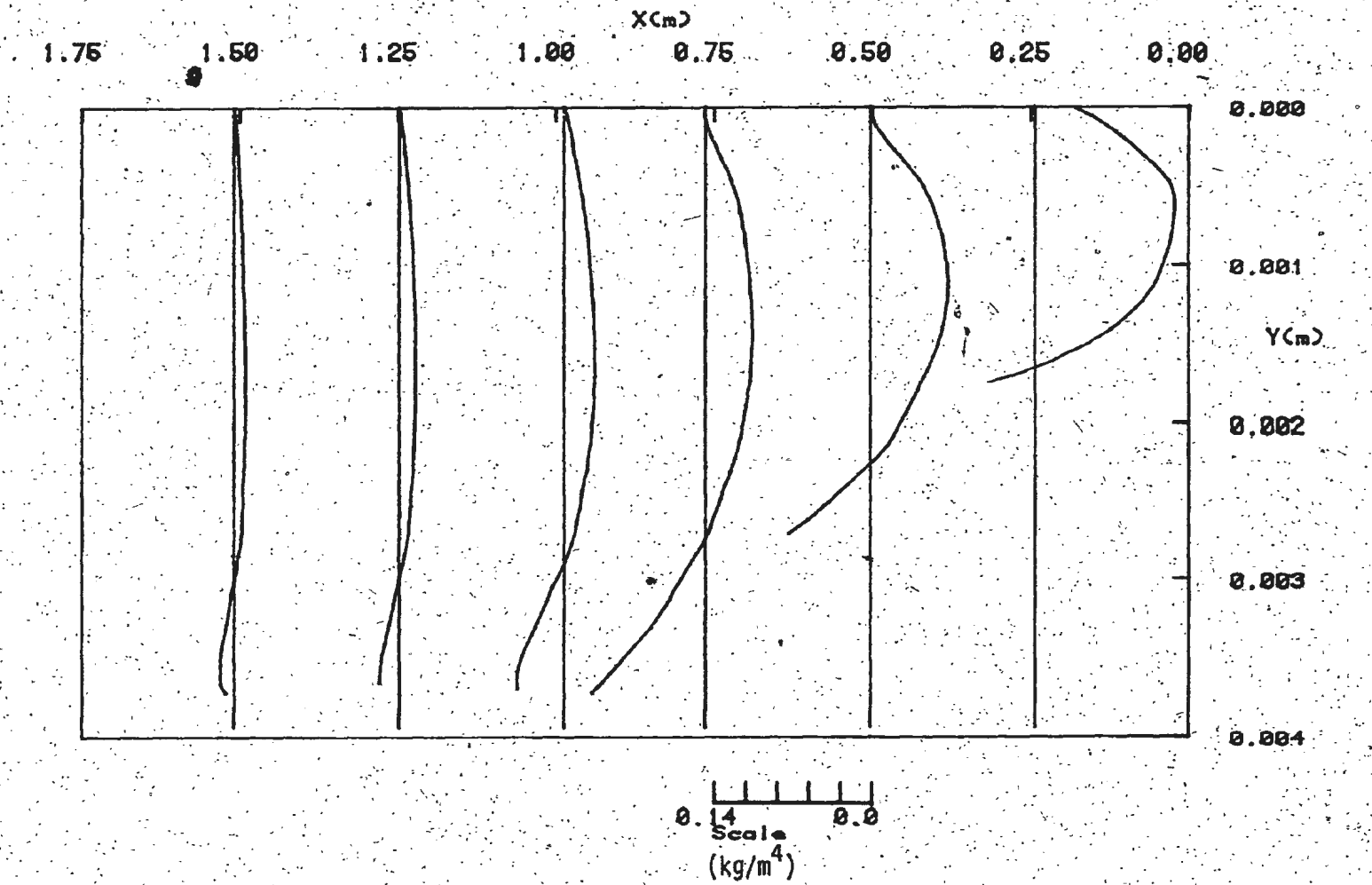

Figure 8(b) Density Gradient Profiles for T_∞ = 20.00°C, S_∞ = 0. ppt, U_∞ = 0.025 m/s

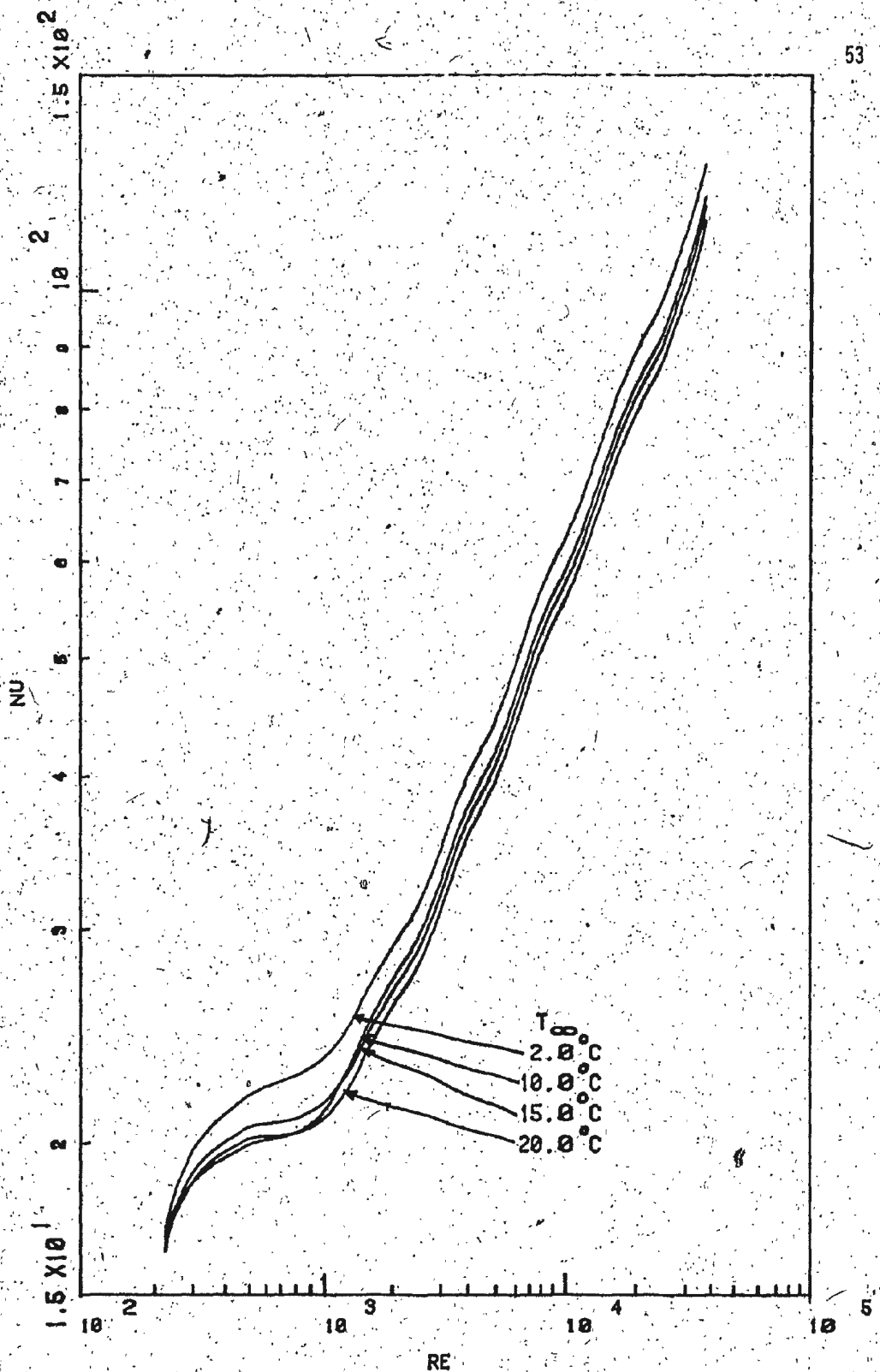

Figure 9(a) Nusselt Number as a Function of Reynolds Number at Various T_∞ for U_∞ = 0.025 m/s, S_∞ = 0. ppt. for Forced Convection

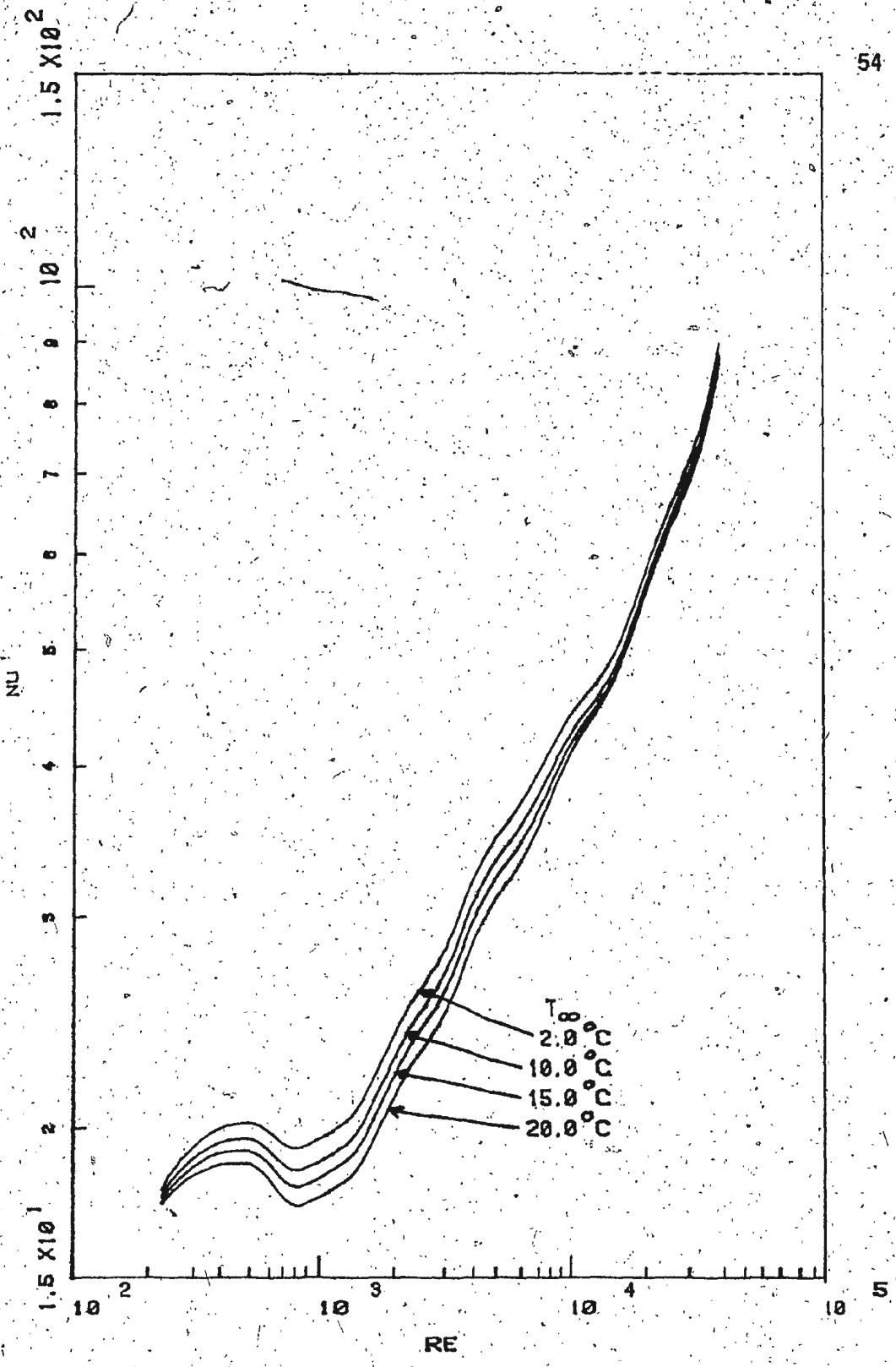

Figure 9(b) Nusselt Number as a Function of Reynolds Number at Various T_∞ for U_∞ = 0.025 m/s, S_∞ = 0. ppt. For Combined Convection

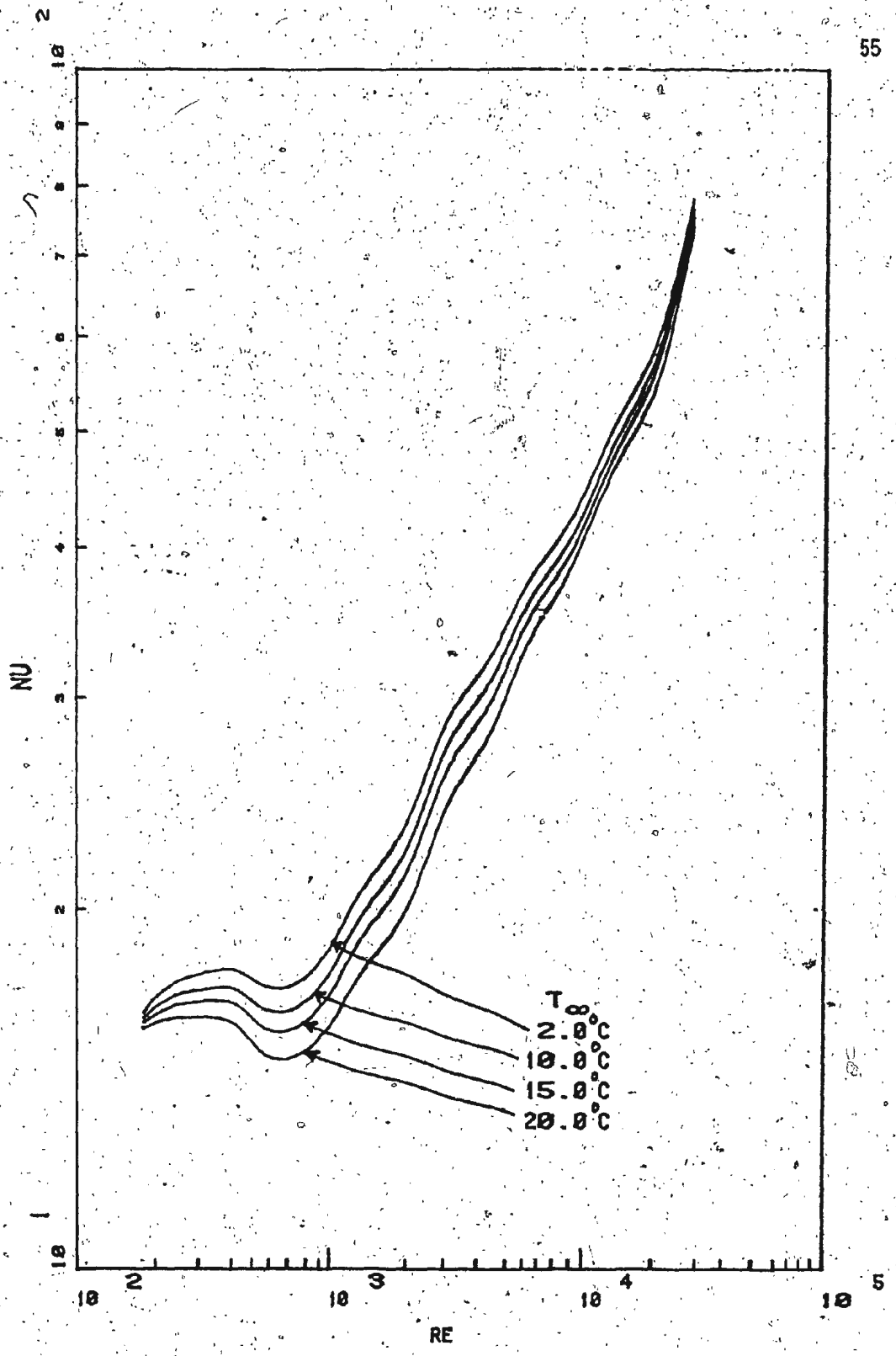

Figure 10 Nusselt Number as a Function of Reynolds Number at Various T_∞ for U_∞ = 0.020 m/s, S_∞ = 0. ppt. for Combined Convection

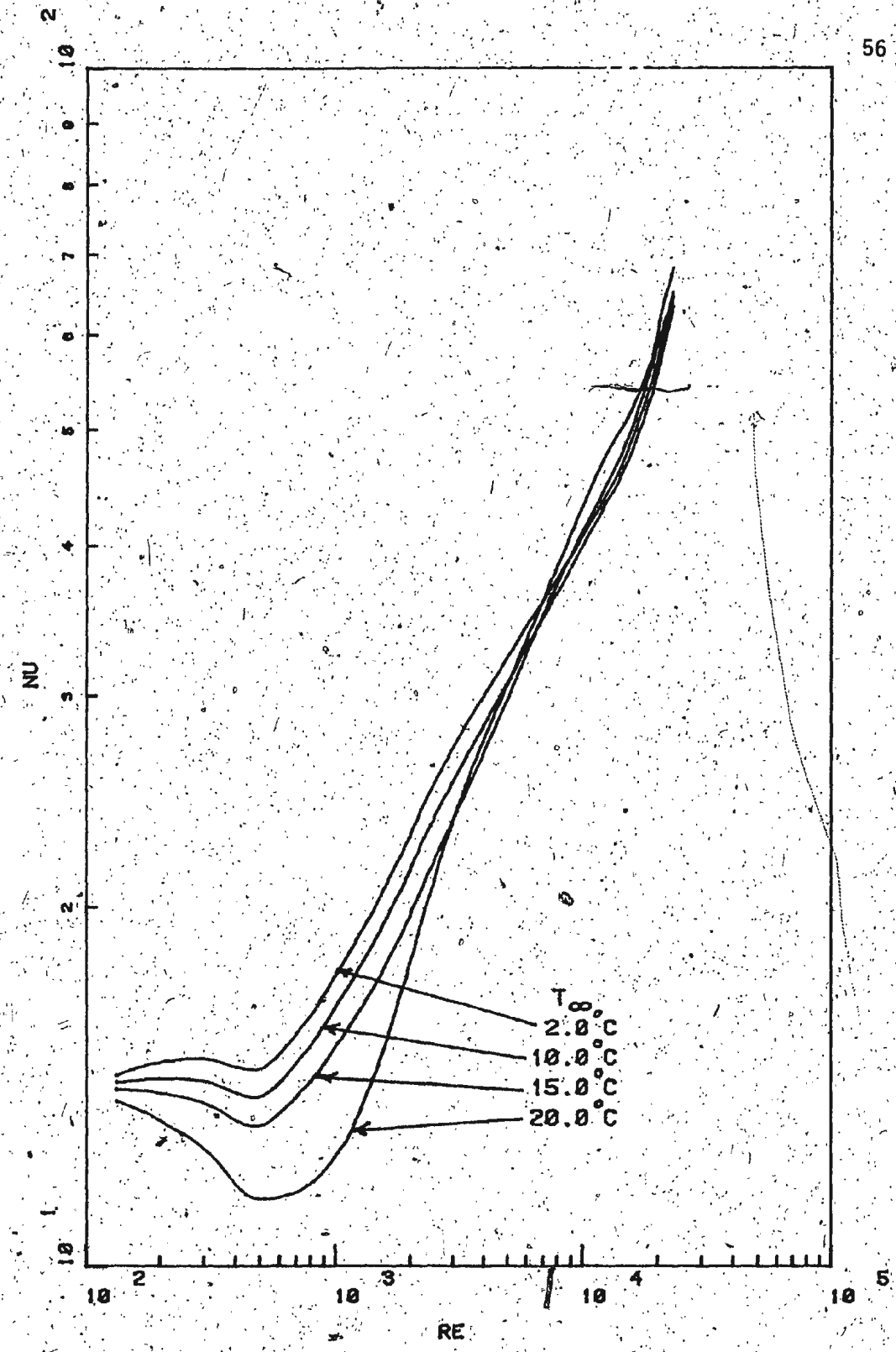

Figure 11 Nusselt Number as a Function of Reynolds Number at Various T_∞ for U_∞ = 0.015 m/s, S_∞ = 0. ppt. for Combined Convection

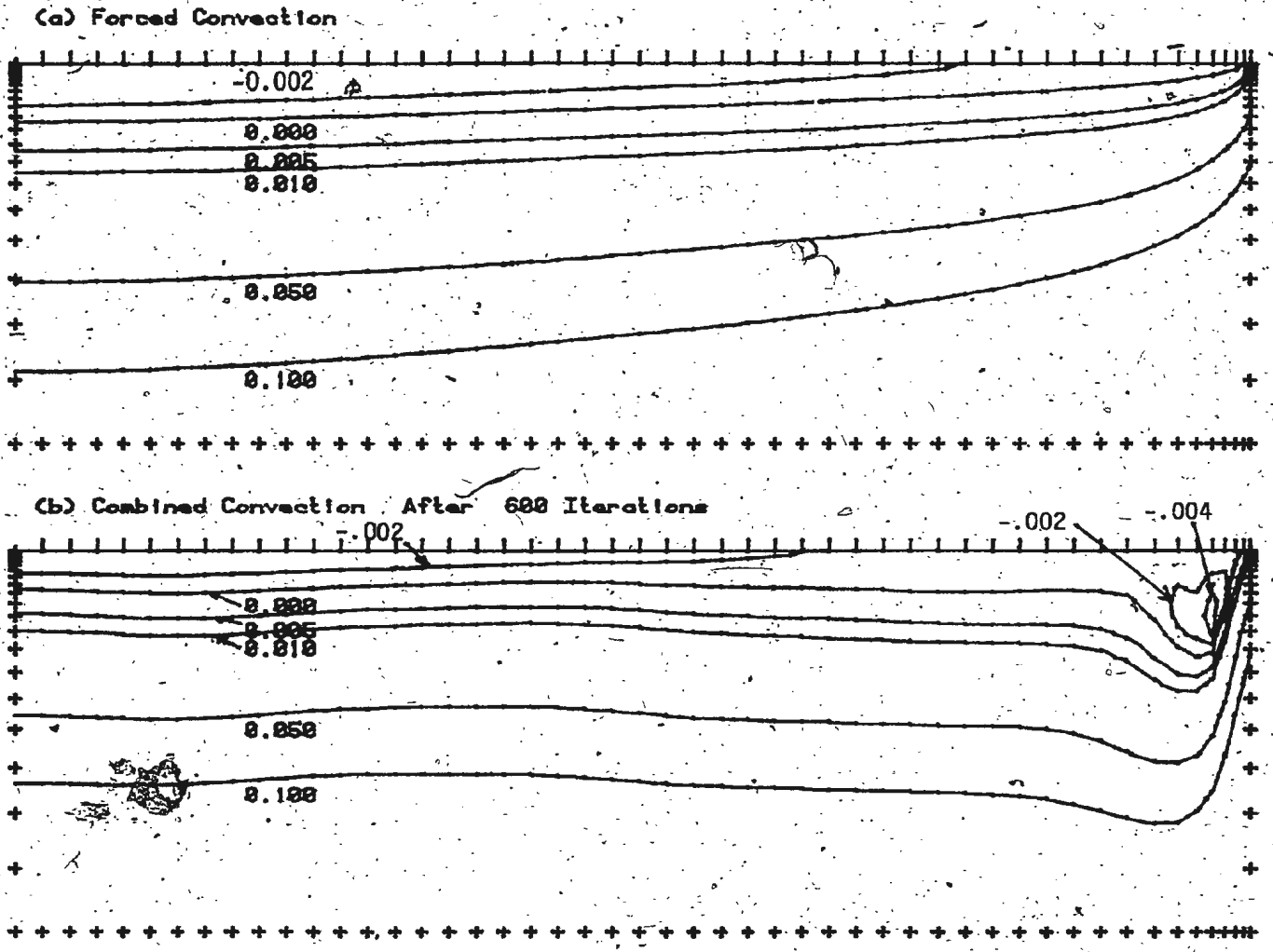

Figure 12 Streamlines for U_∞ = 0.010 m/s, T_∞ = 15.00 °C, S_∞ = 0. ppt

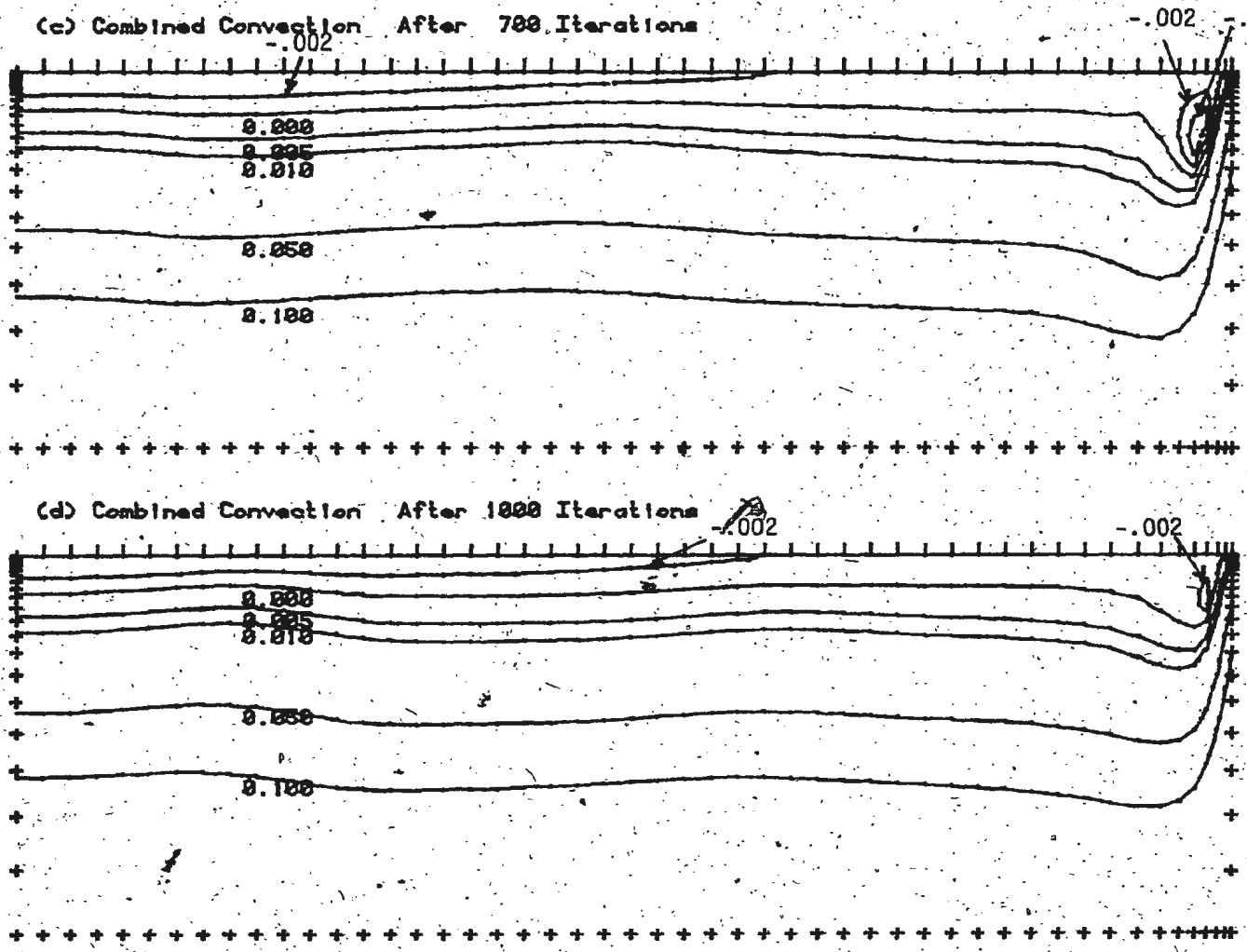

Figure 12 Streamlines for U_∞ = 0.010 m/s, T_∞ = 15.00 °C, S_∞ = 0. ppt

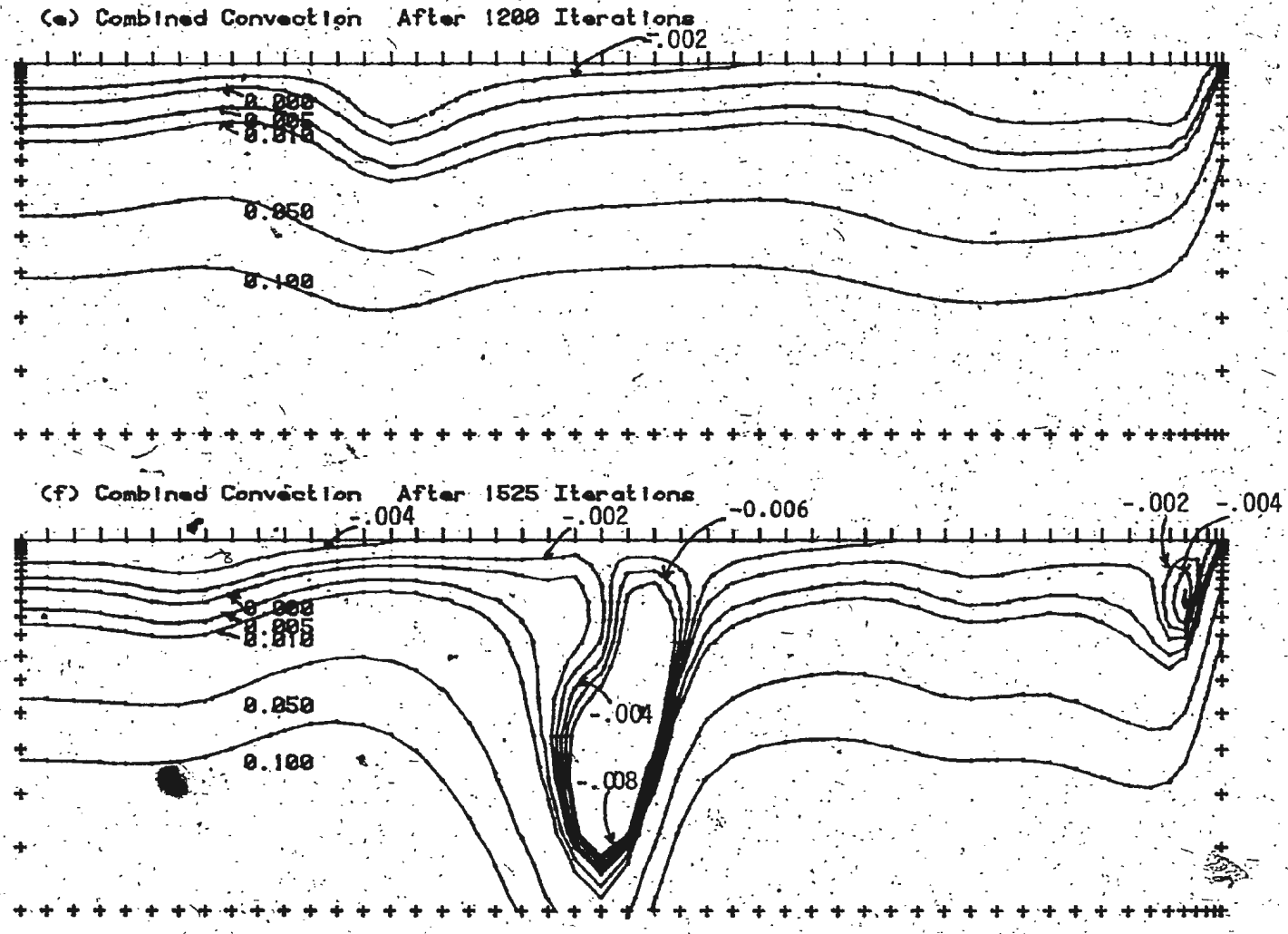

Figure 12 Streamlines for U_∞ = 0.010 m/s, T_∞ = 15.00 °C, S_∞ = 0. ppt

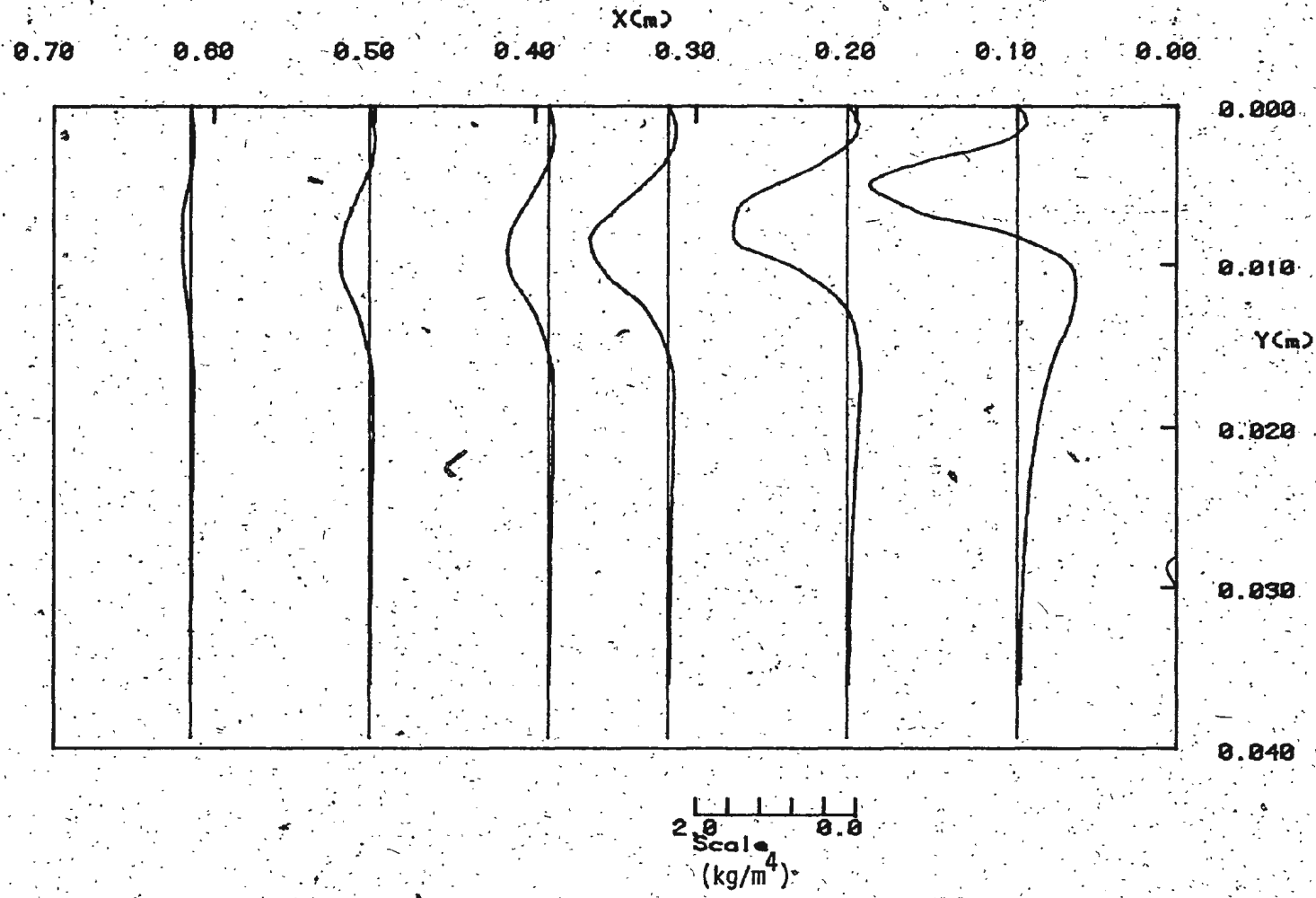

Figure 18 Density Gradient Profiles for T_∞ = 15.00°C, S_∞ = 0. ppt, U_∞ = 0.010 m/s for Combined Convection After 700 Iterations

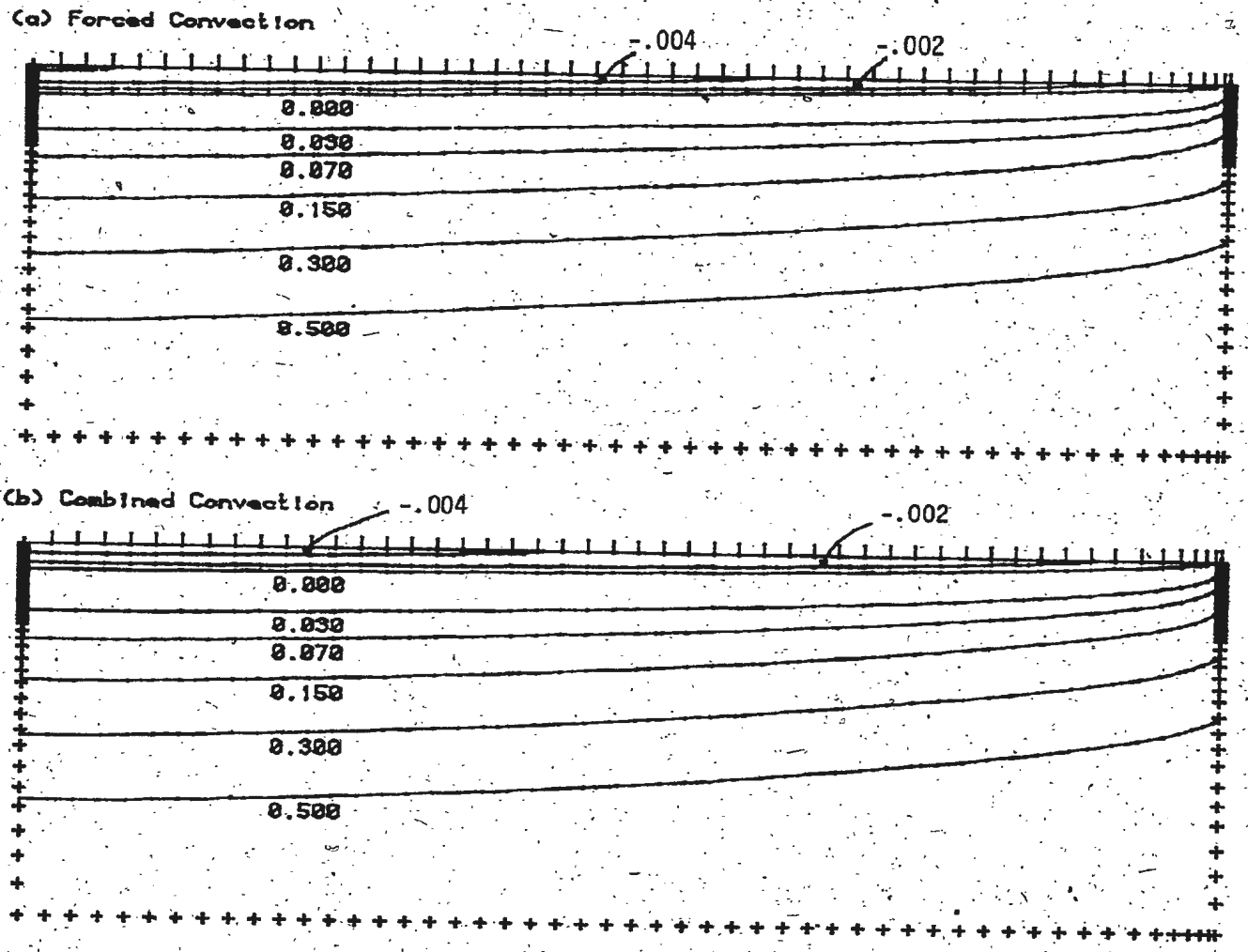

Figure 14 Streamlines for U_∞ = 0.025 m/s, T_∞ = 20.00 °C, S_∞ = 5. ppt

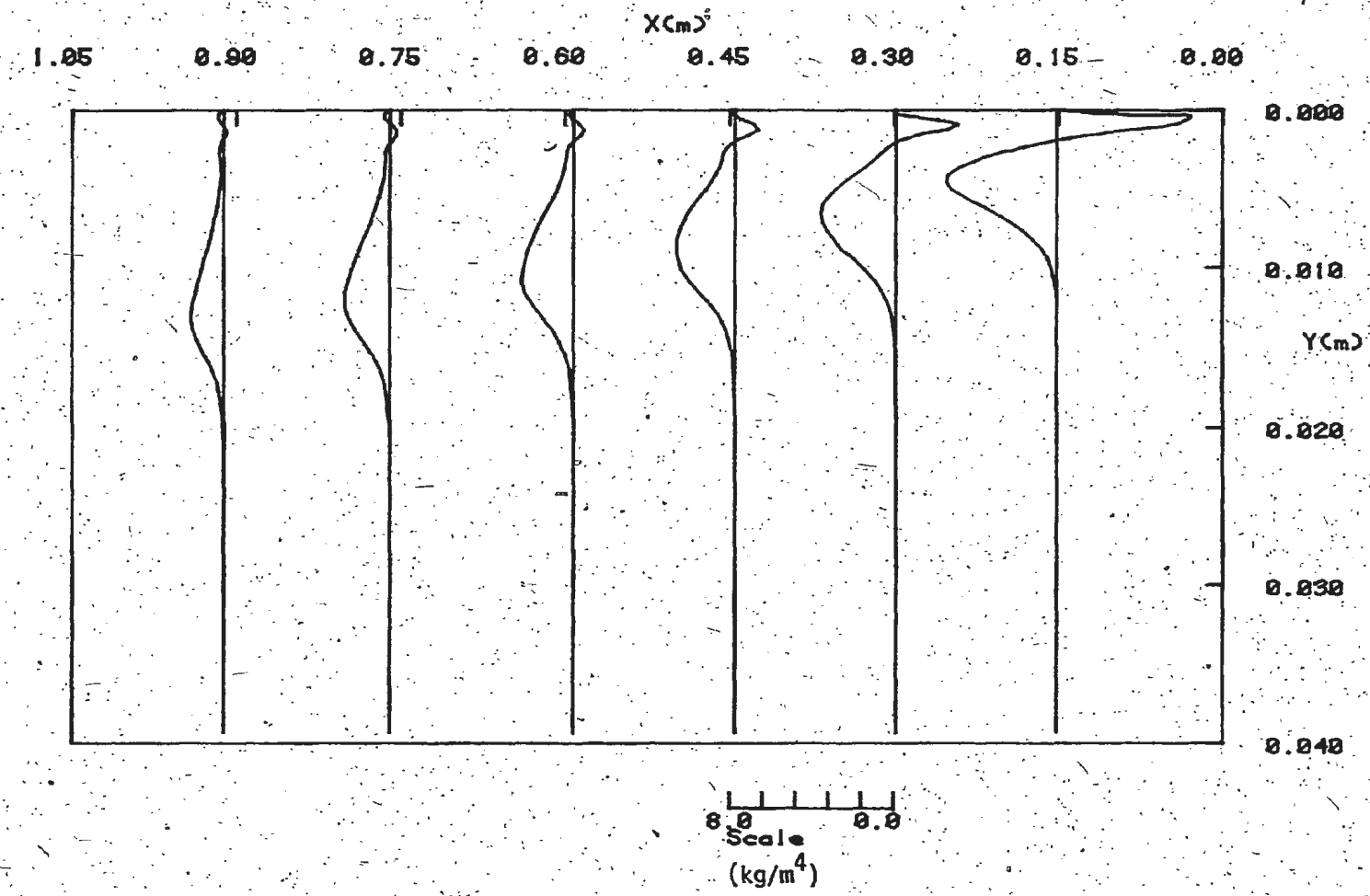

Figure 15 Density Gradient Profiles for T_∞ = 20.00 °C, S_∞ = 5. ppt, U_∞ = 0.025 m/s

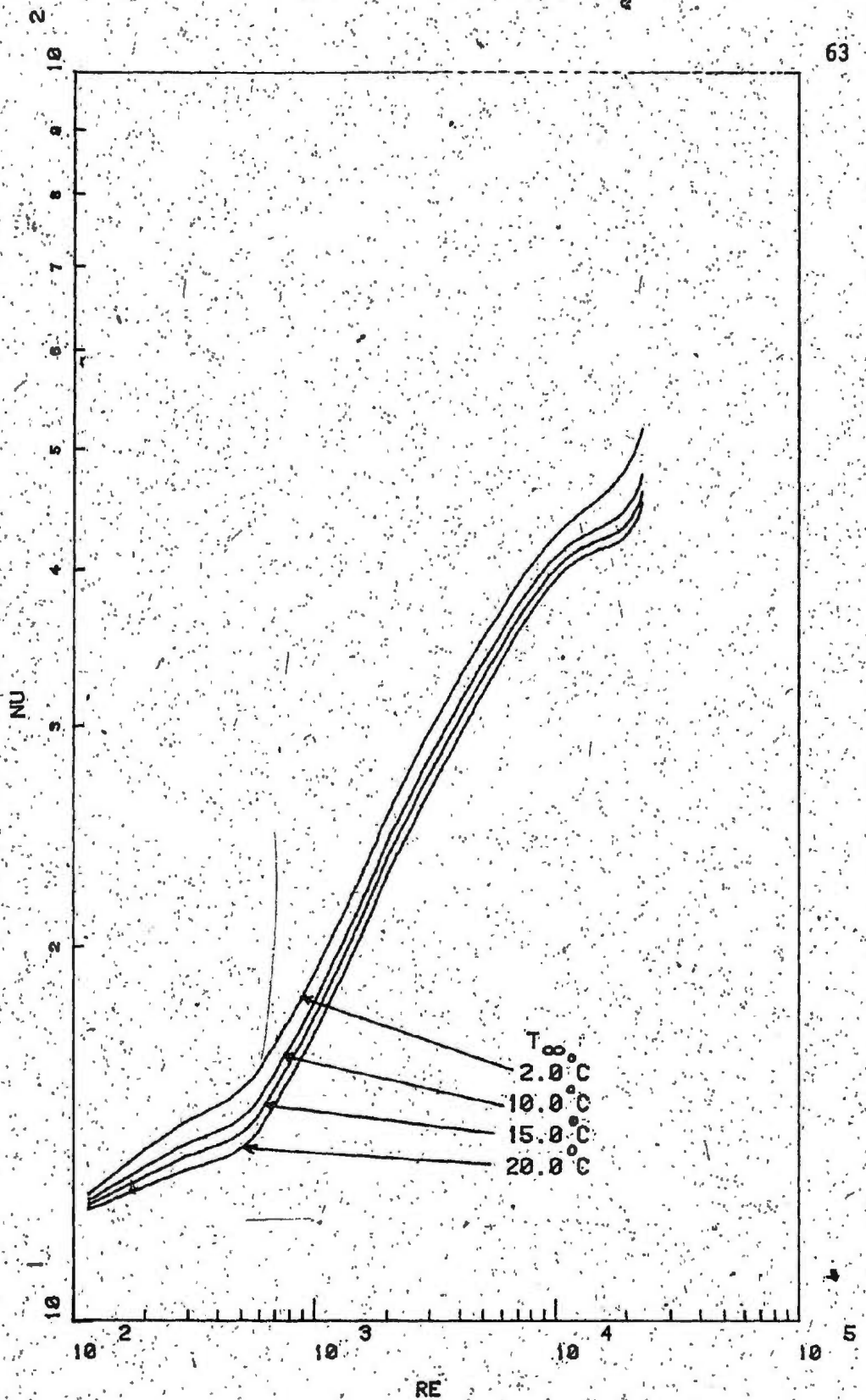

Figure 16 Nusselt Number as a Function of Reynolds Number at Various T_∞ for U_∞ = 0.025 m/s, S_∞ = 5. ppt. for Combined Convection

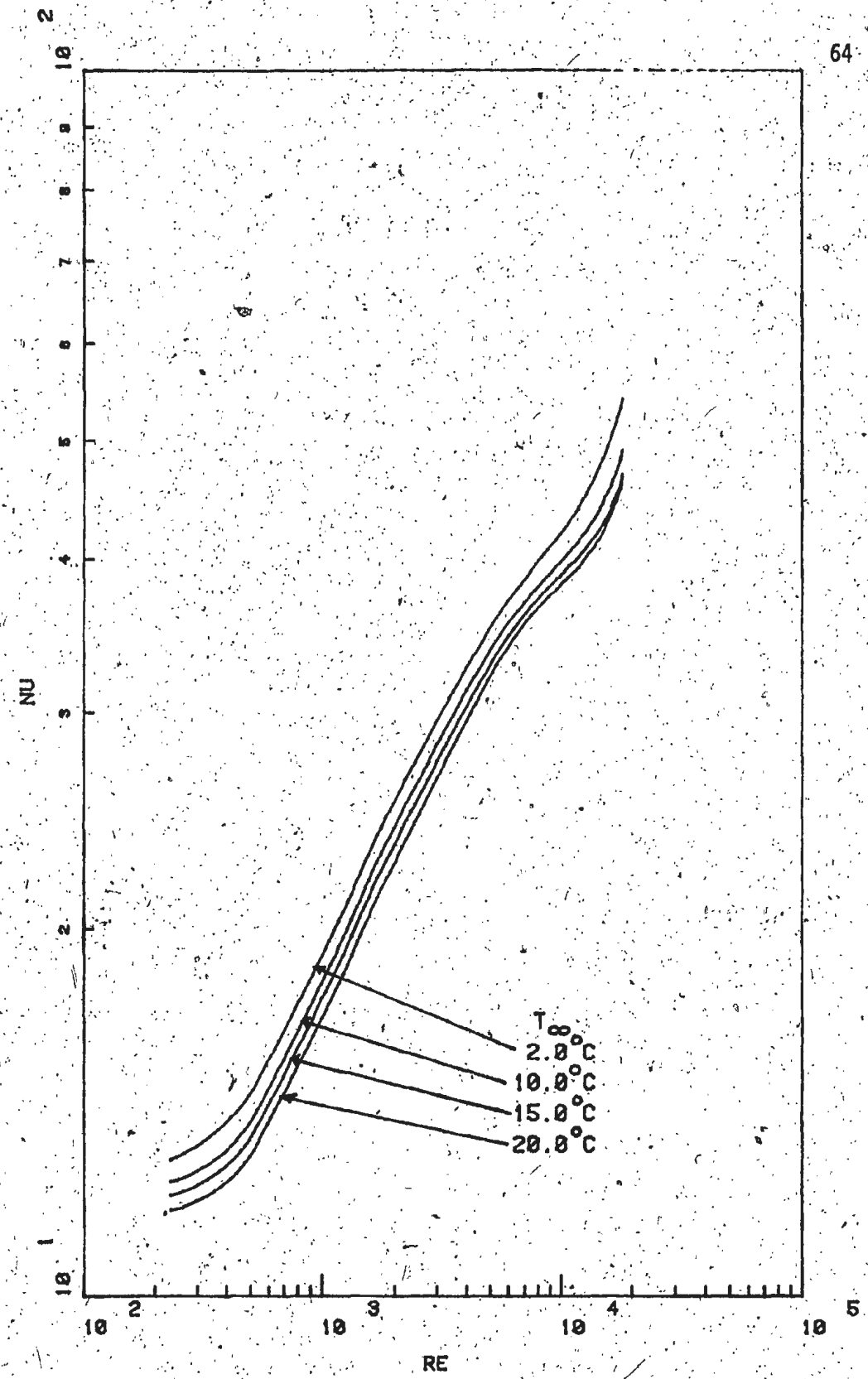

Figure 17. Nusselt Number as a Function of Reynolds Number at Various T_∞ for U_∞ = 0.020 m/s, S_∞ = 5. ppt. for Combined Convection

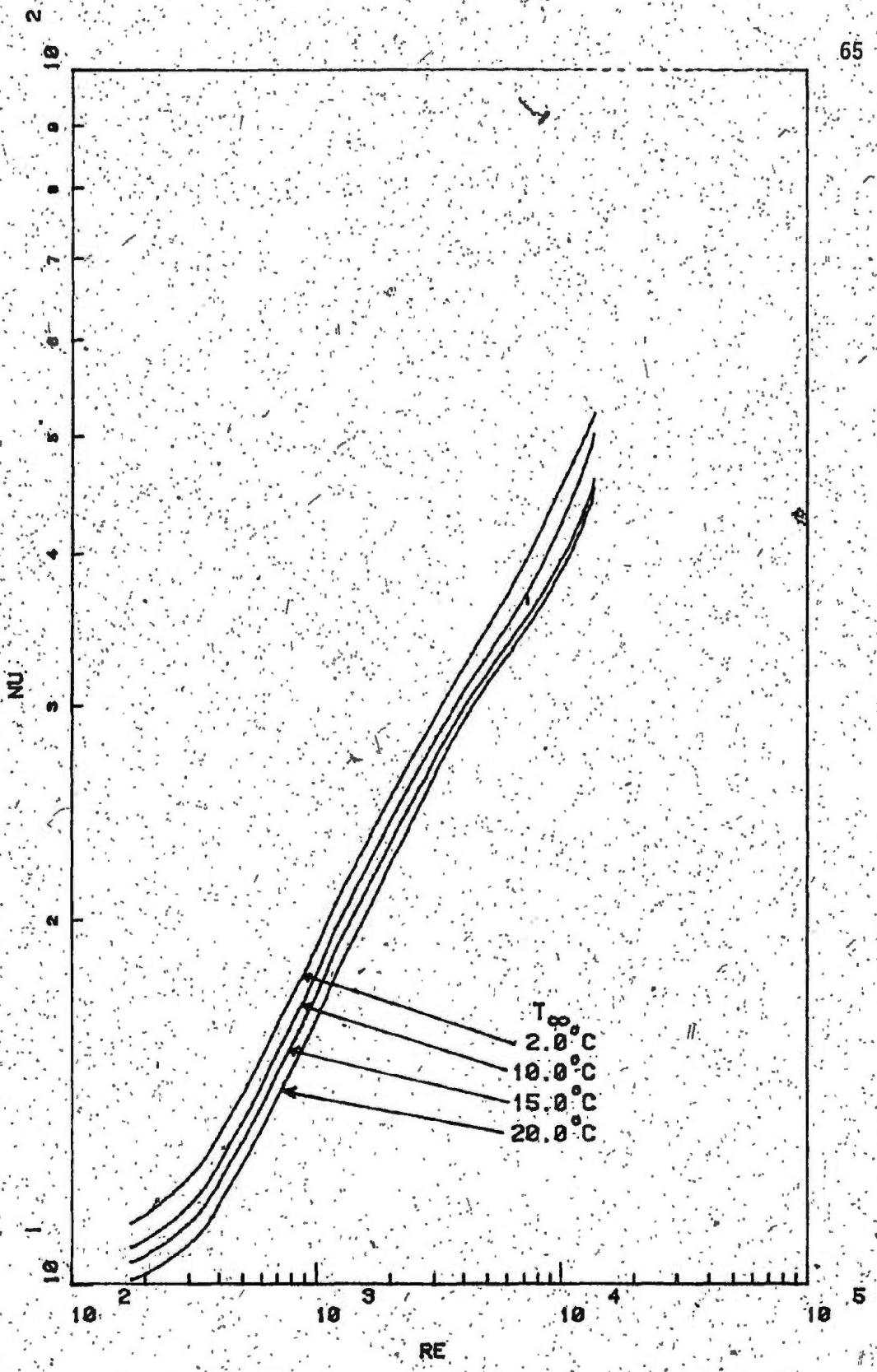

Figure 18 Nusselt Number as a Function of Reynolds Number at Various T_∞ for U_∞ = 0.015 m/s, S_∞ = 5. ppt. for Combined Convection

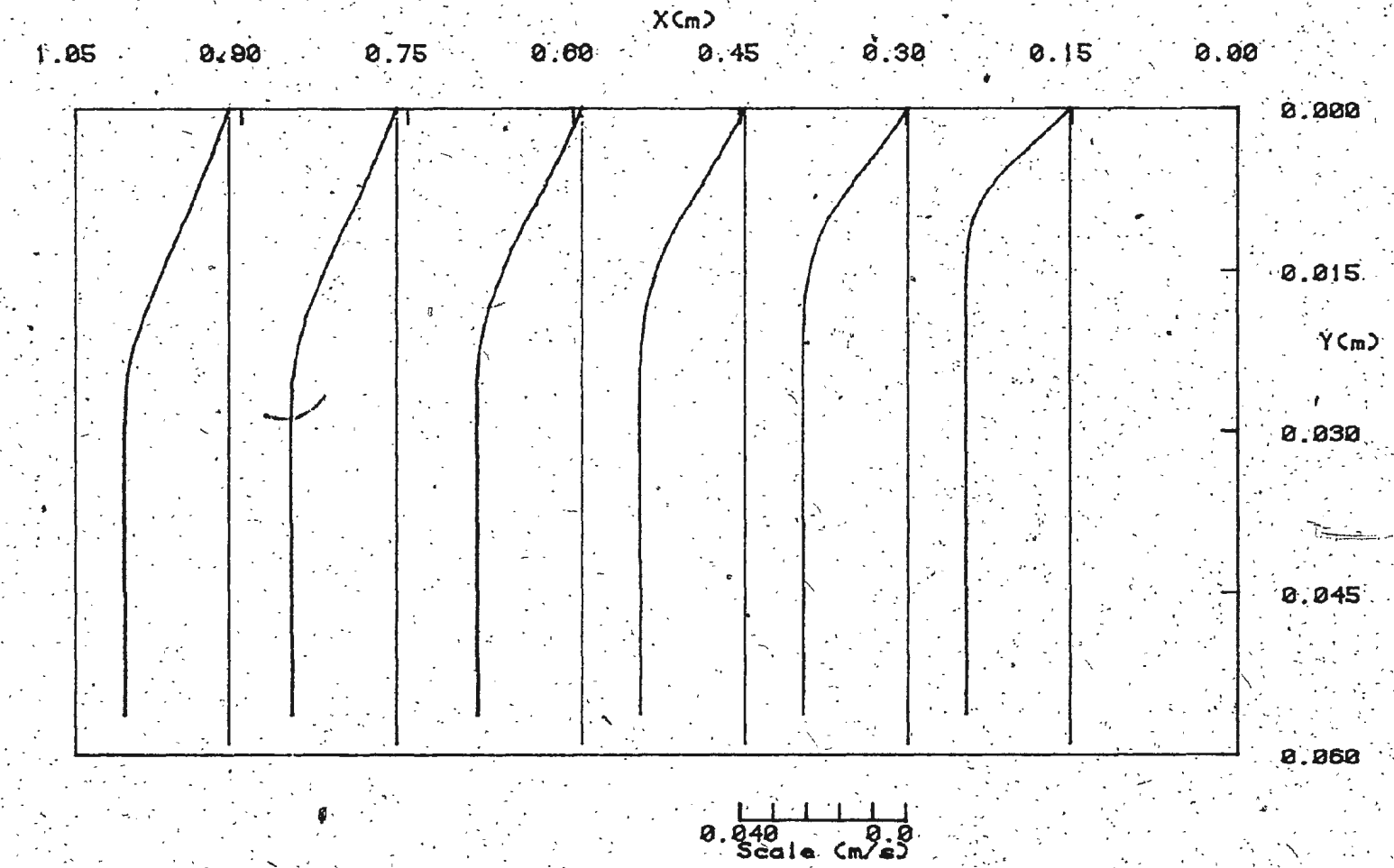

Figure 19(a) Velocity Profiles for T_∞ = 20.00 °C, S_∞ = 5. ppt, U_∞ = 0.025 m/s for Combined Convection

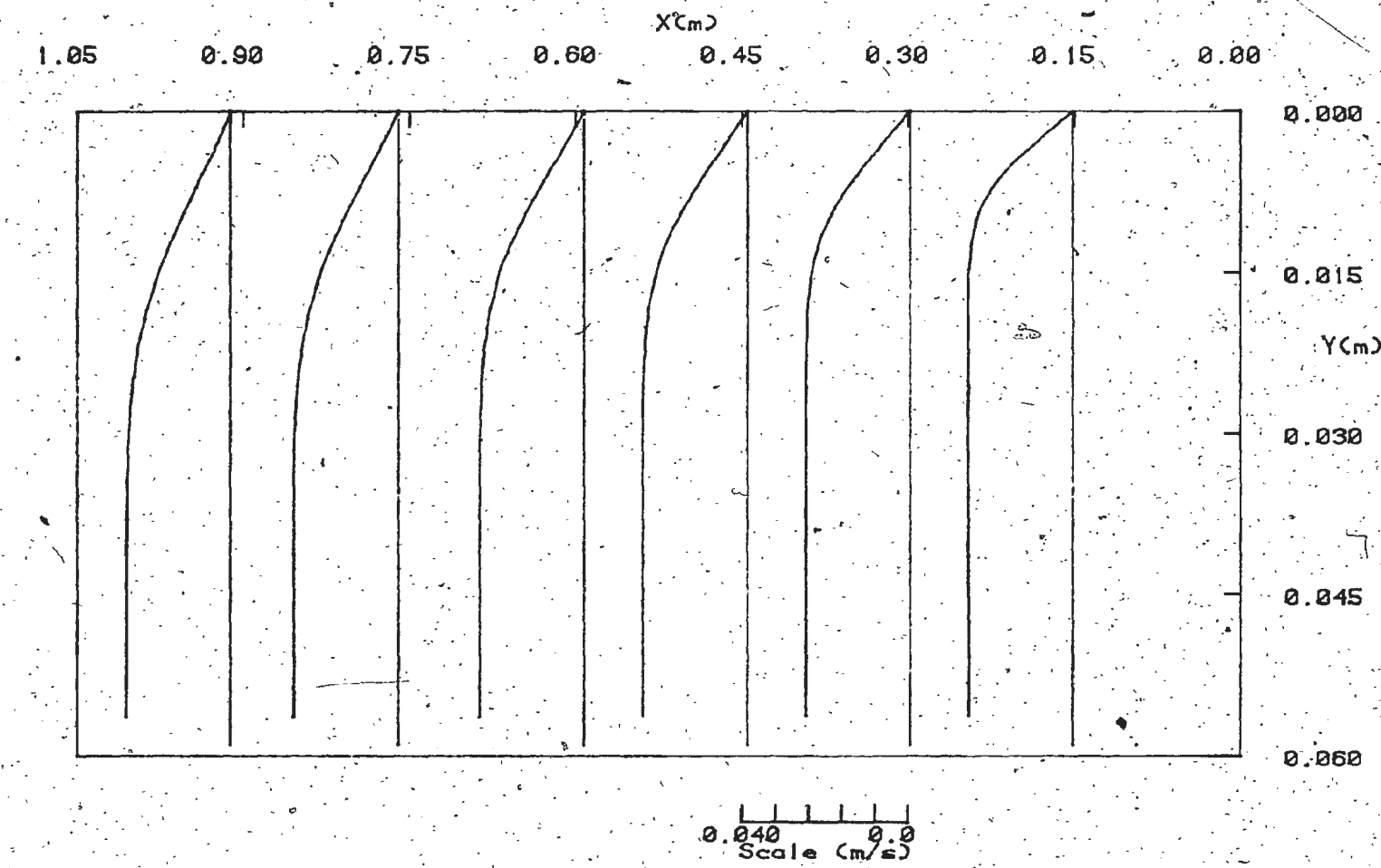

Figure 19(b) Velocity Profiles for $T_\infty = 20.00^\circ C$, $S_\infty = 5.$ ppt, $U_\infty = 0.025$ m/s for Forced Convection

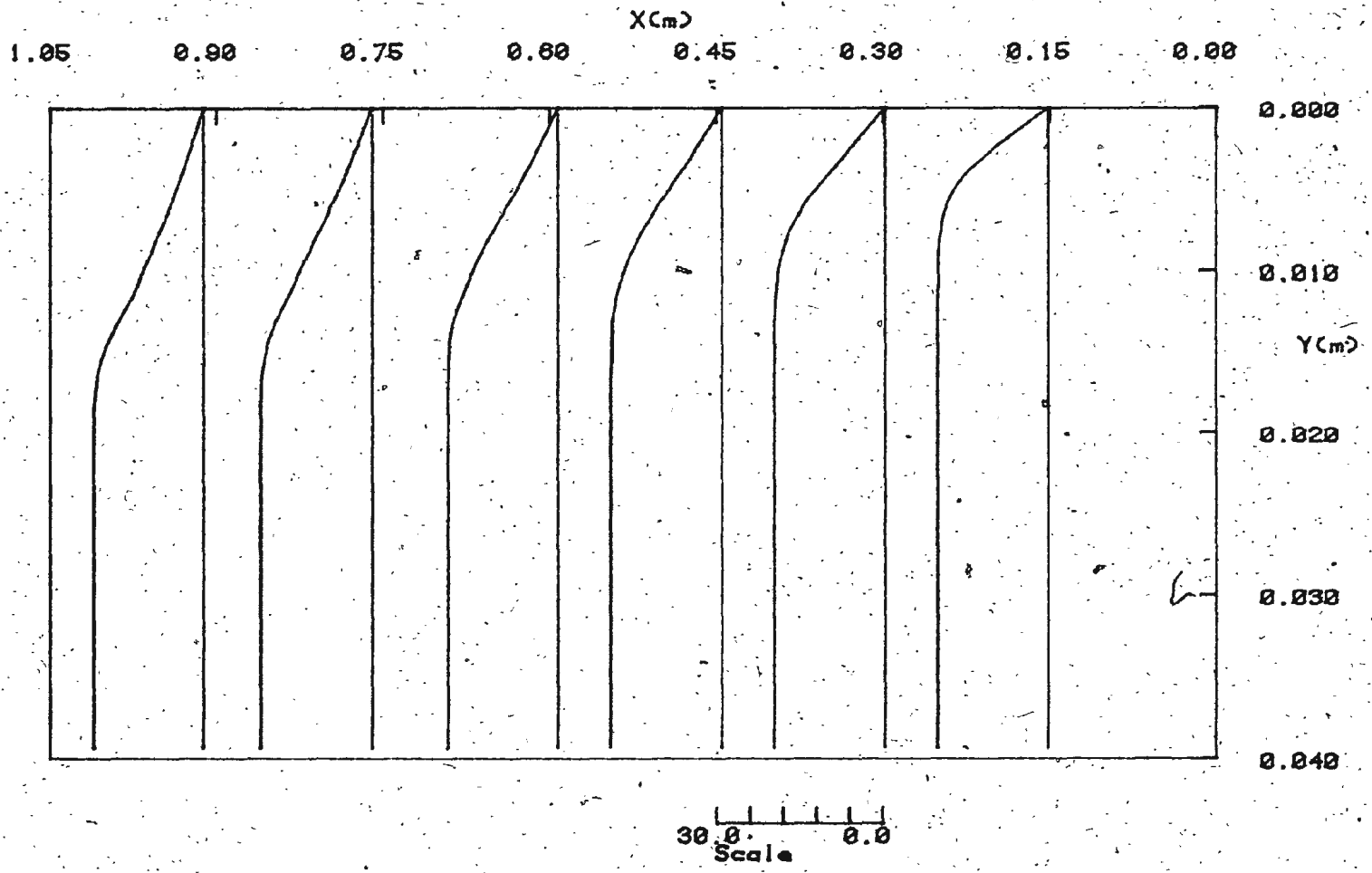

Figure 20(a) Temperature Profiles for T_{∞} = 20.00°C, S_{∞} = 5. ppt, U_{∞} = 0.025 m/s for Combined Convection

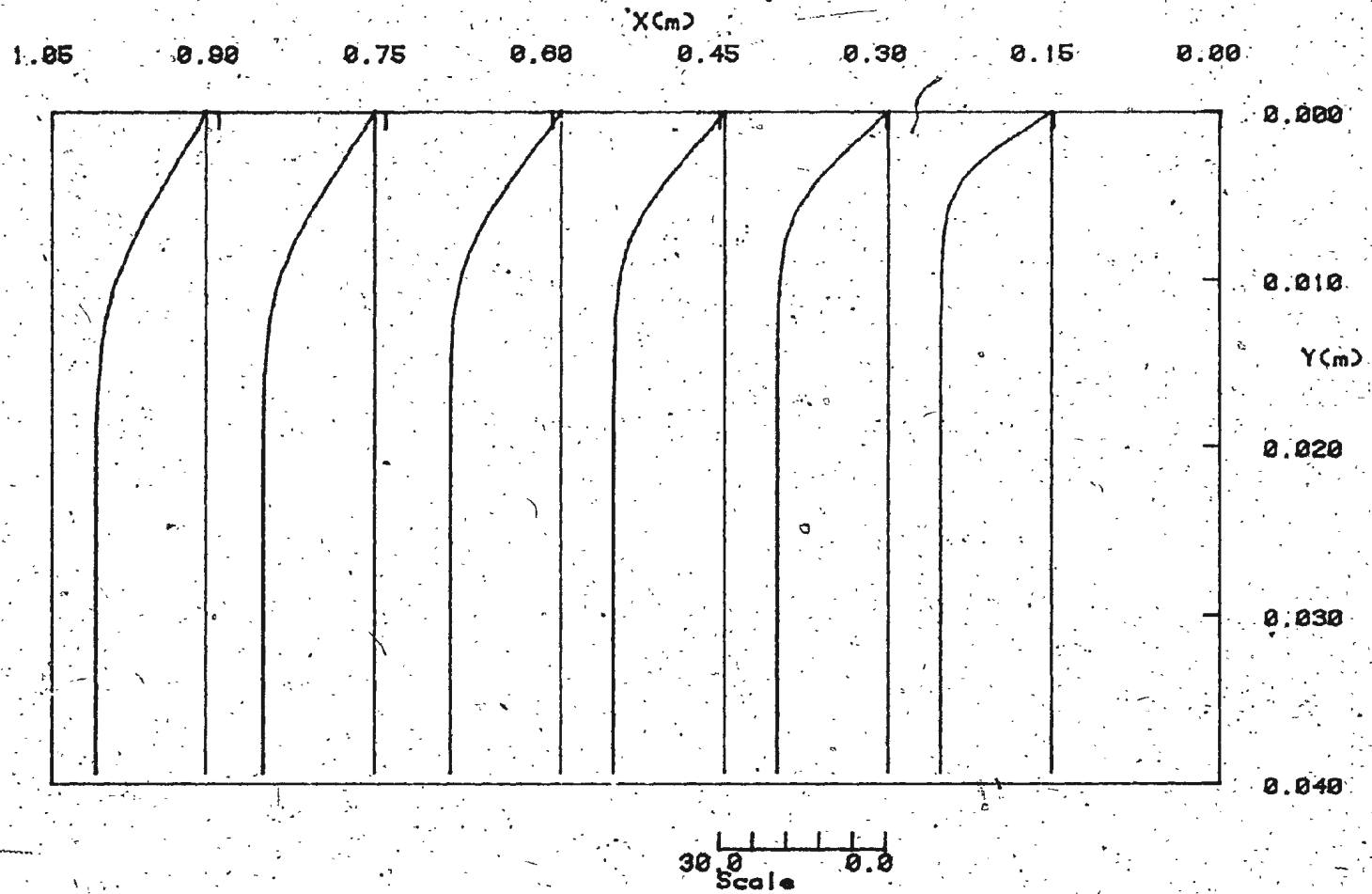

Figure 20(b) Temperature Profiles for T_∞ = 20.00°C, S_∞ = 5. ppt, U_∞ = 0.025 m/s for Forced Convection

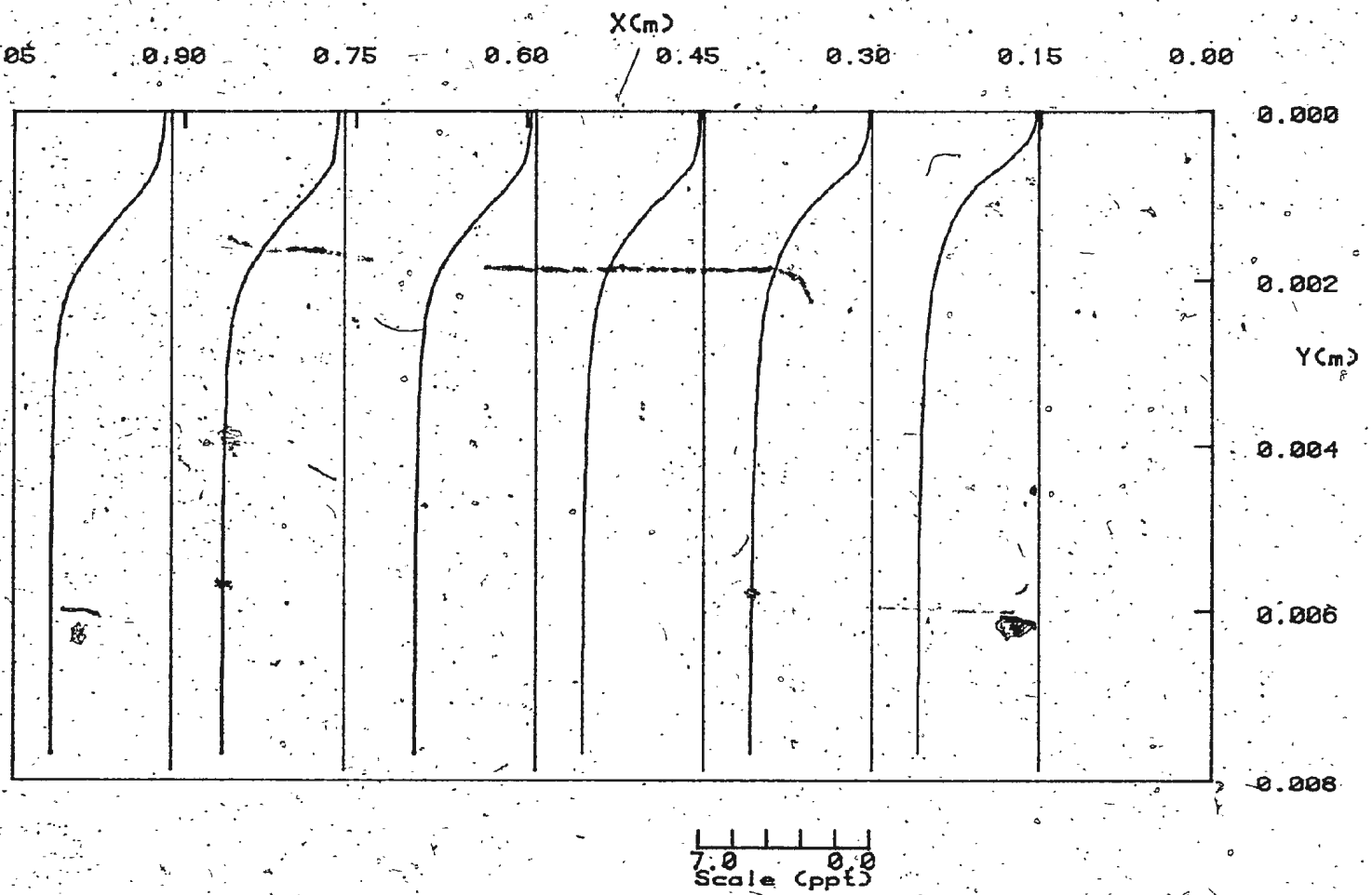

Figure 21(a). Salinity Profiles for T_∞ = 20.00 °C, S_∞ = 5. ppt, U_∞ = 0.025 m/s for Combined Convection

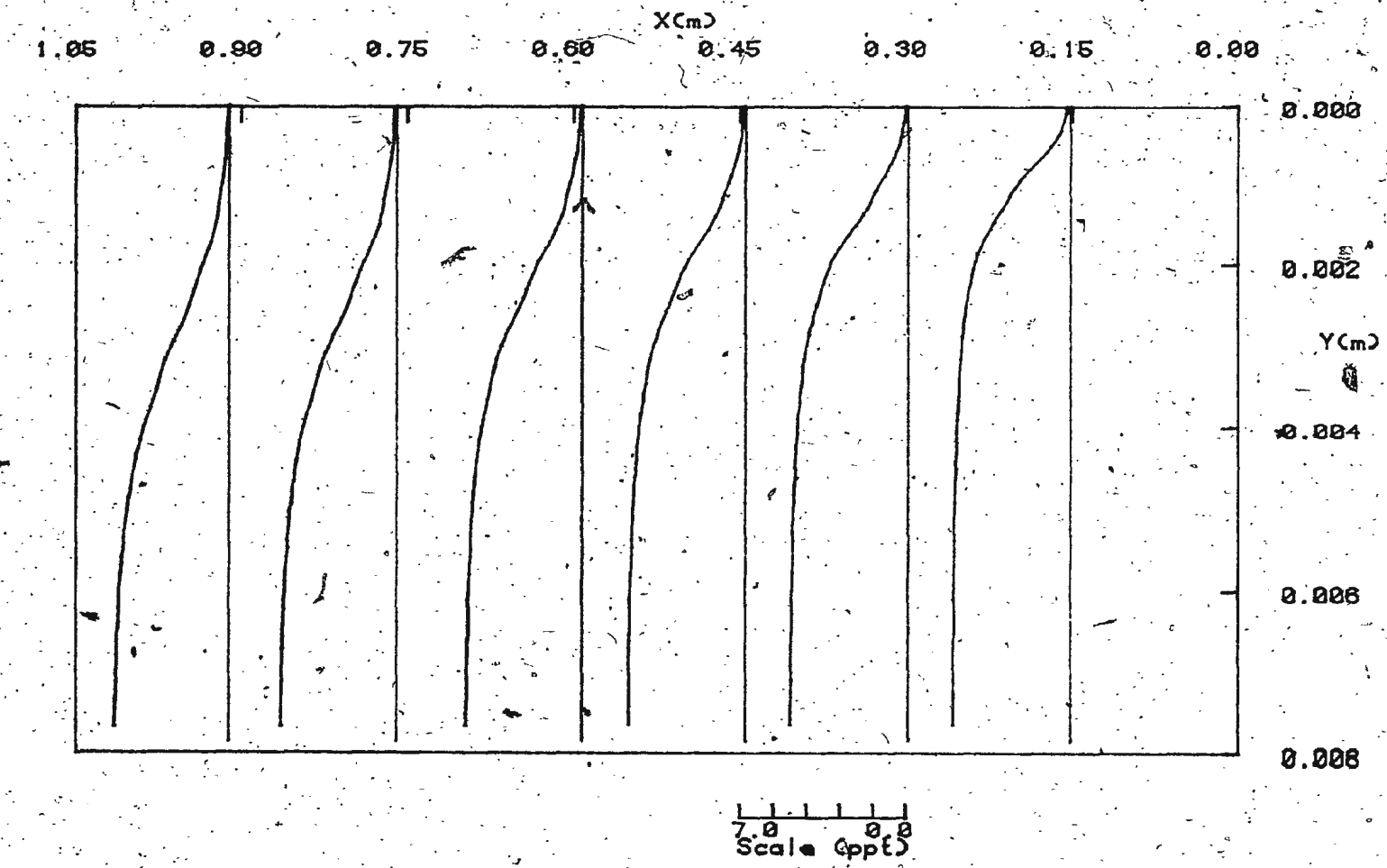

Figure 21(b) Salinity Profiles for $T_\infty = 20.00^\circ C$, $S_\infty = 5.$ ppt, $U_\infty = 0.025$ m/s for Forced Convection

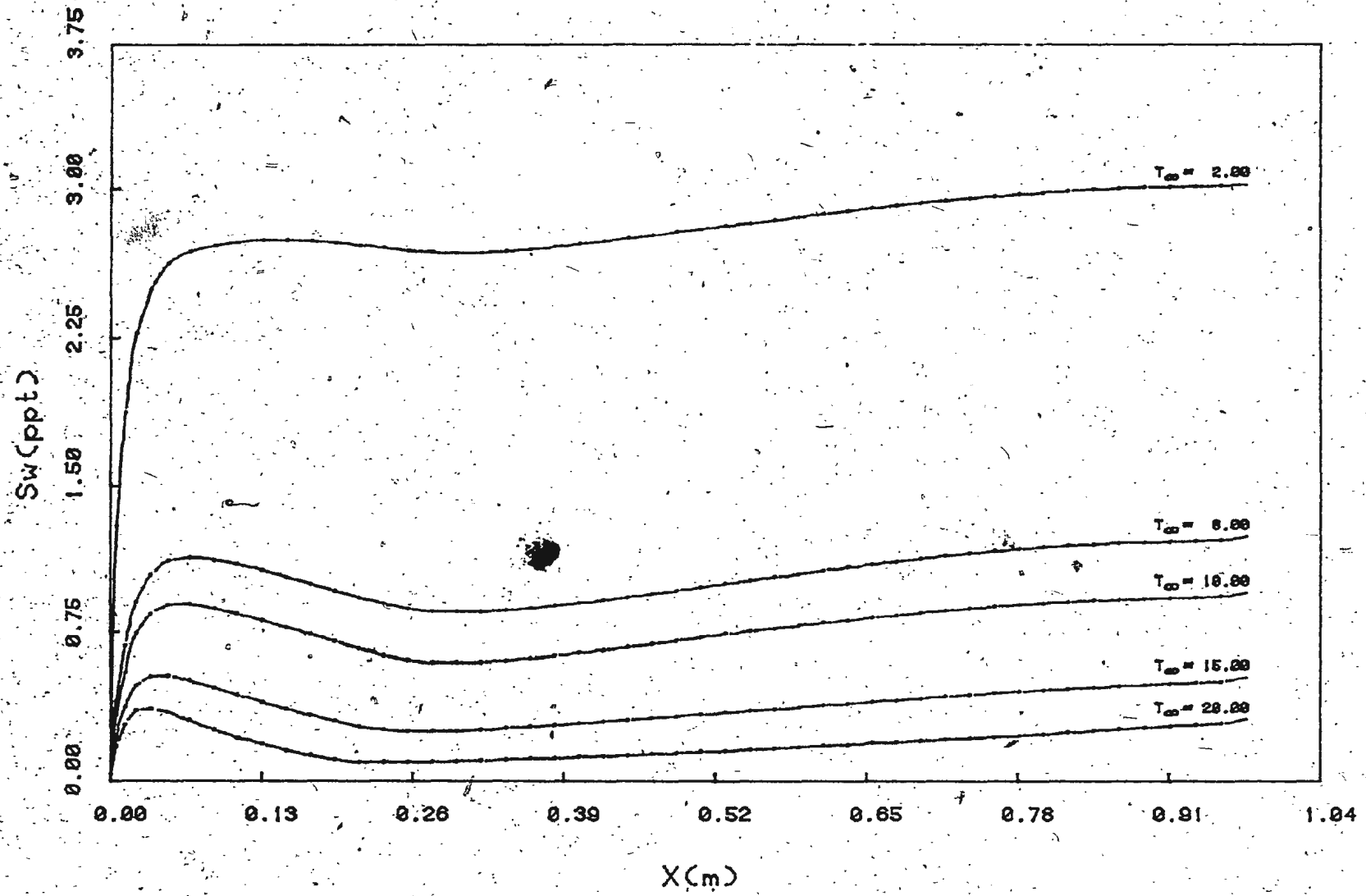

Figure 22(a) Wall Salinity as a Function of Distance along the Plate at various T_∞ for U_∞ = 0.025 m/s, S_∞ = 5. ppt. for Combined Convection

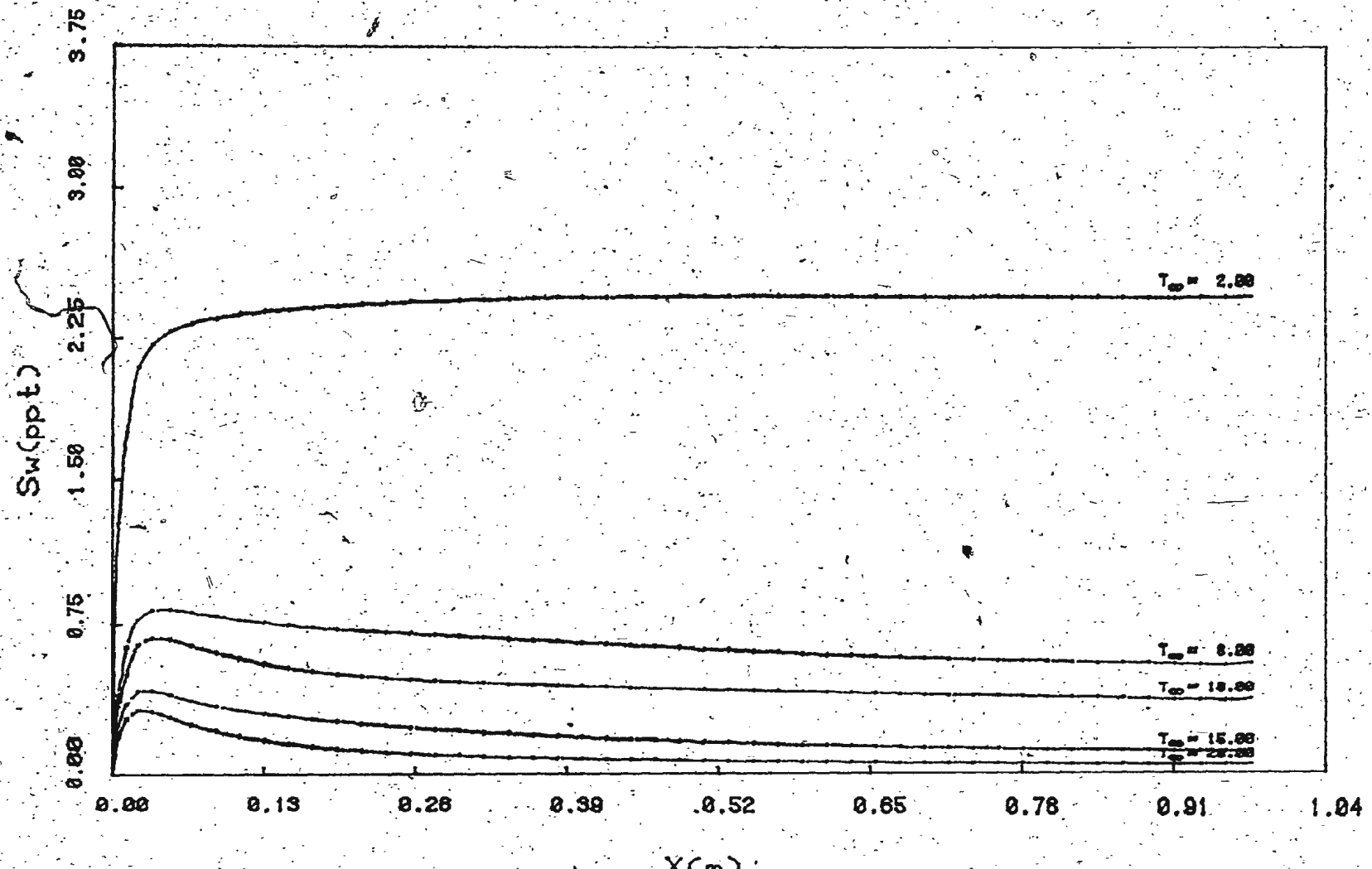

Figure 22(b) Wall Salinity as a Funation of Distance along the Plate at various T_∞ for U_∞ = 0.025 m/s, S_∞ = 5. ppt. for Forced Convection

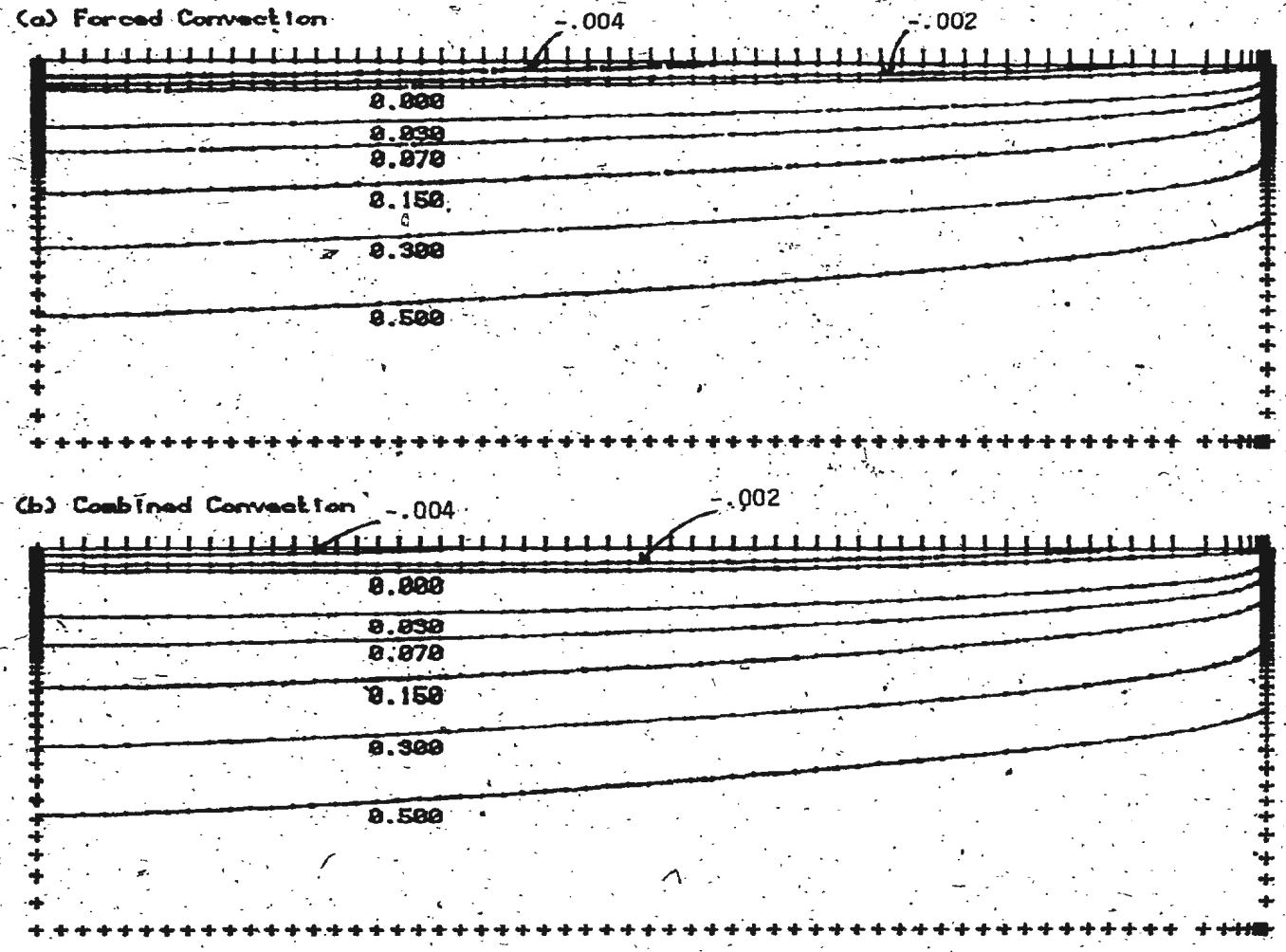

Figure 23 Streamlines for U_∞ = 0.025 m/s, T_∞ = 20.00 °C, S_∞ = 35. ppt

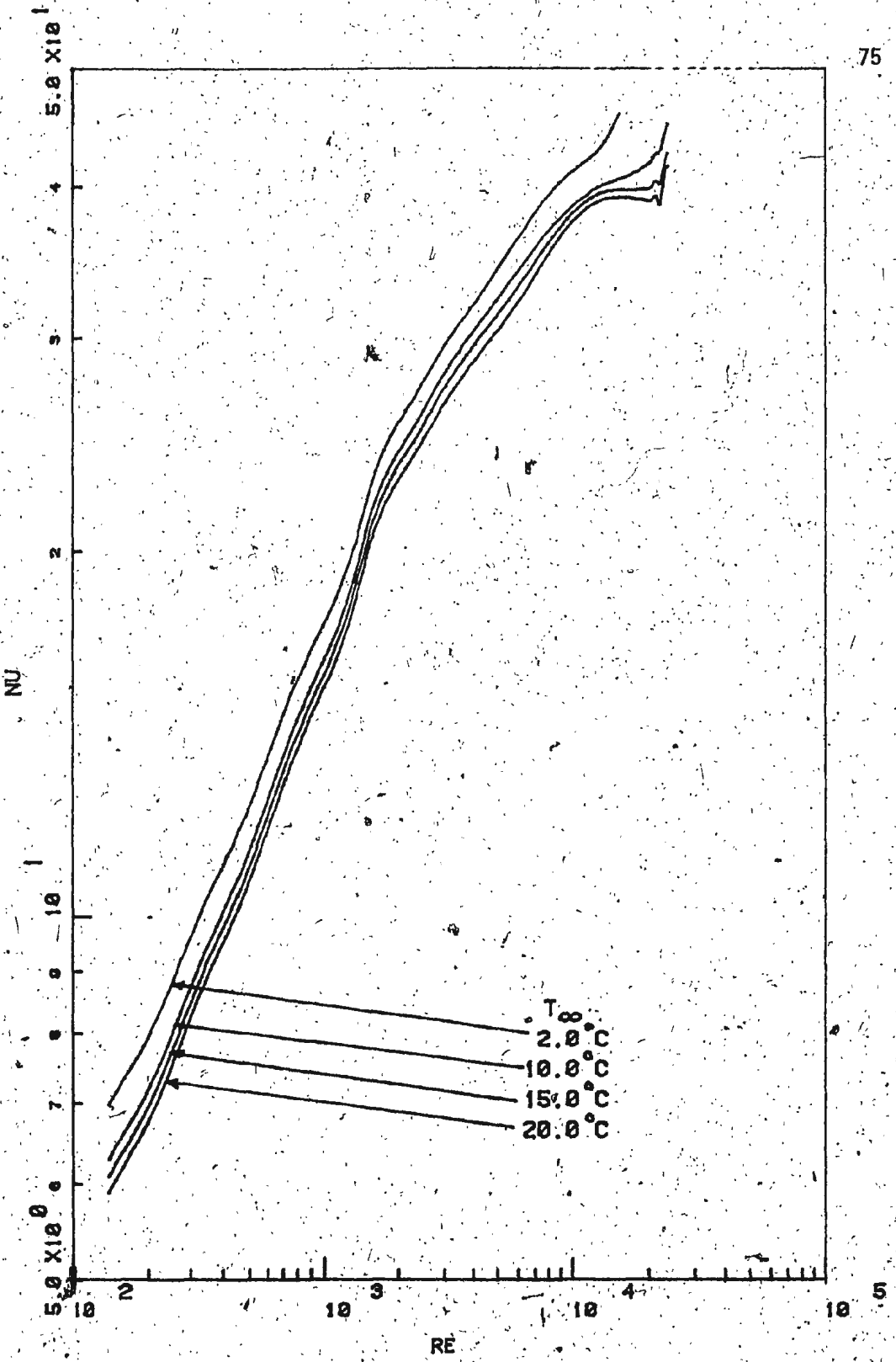

Figure 24 Nusselt Number as a Function of Reynolds Number at Various T_∞ for U_∞ = 0.025 m/s, S_∞ = 35. ppt. for Combined Convection

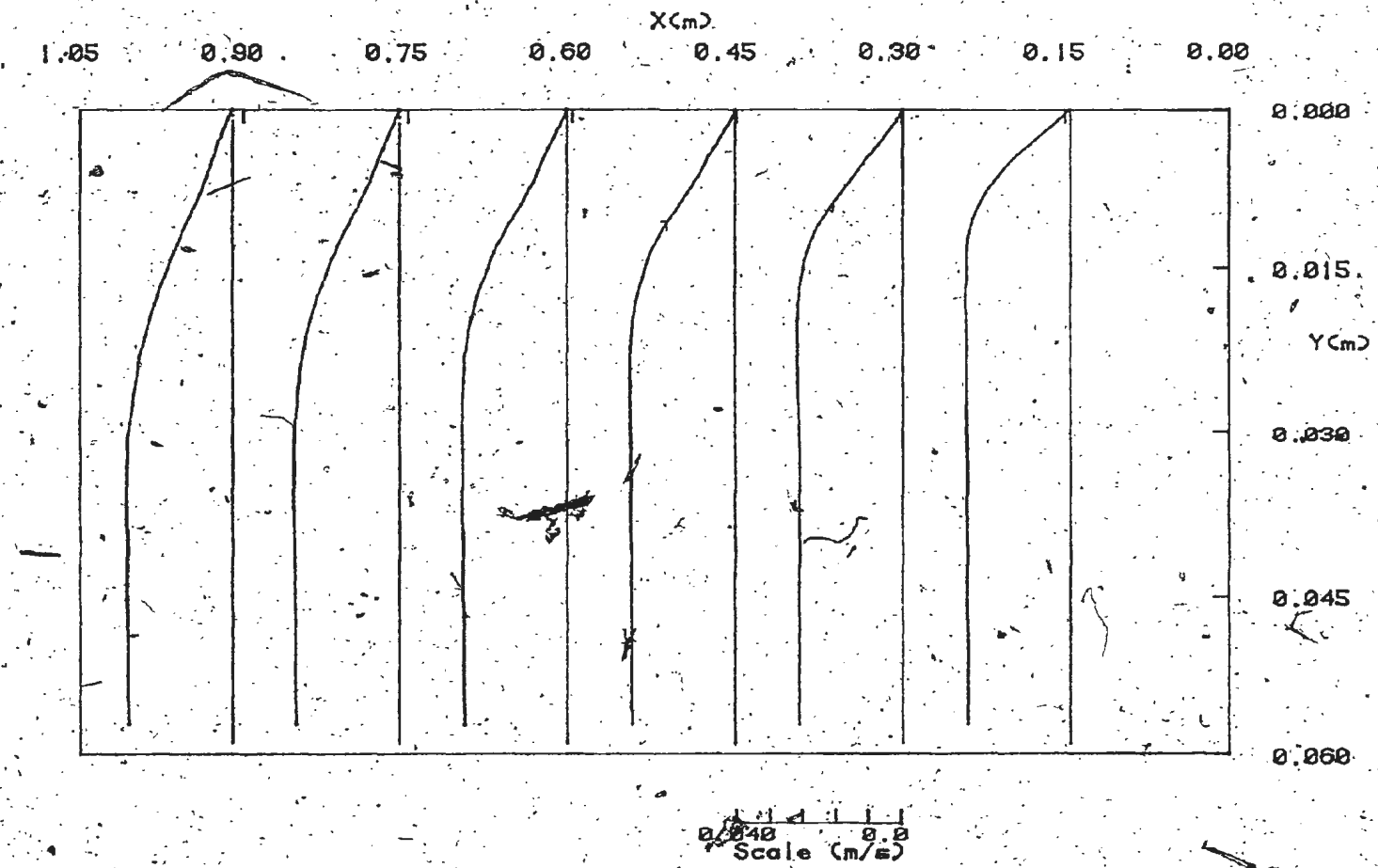

Figure 25(a) Velocity Profiles for T_∞ = 20.00 °C, S_∞ = 35. ppt, U_∞ = 0.025 m/s for Combined Convection

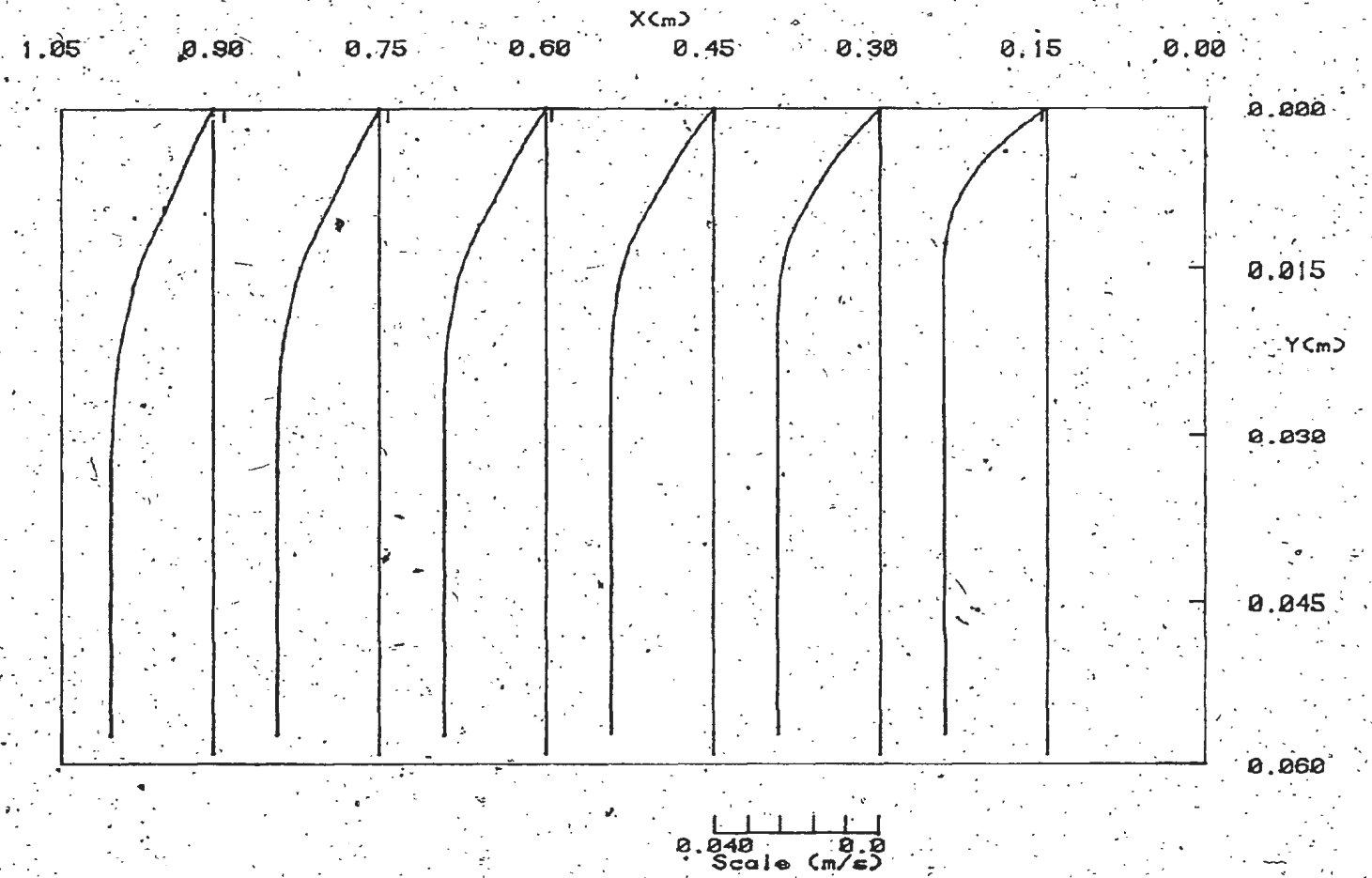

Figure 25(b) Velocity Profiles for T_∞ = 20.00 °C, S_∞ = 35.0 ppt, U_∞ = 0.025 m/s for Forced Convection

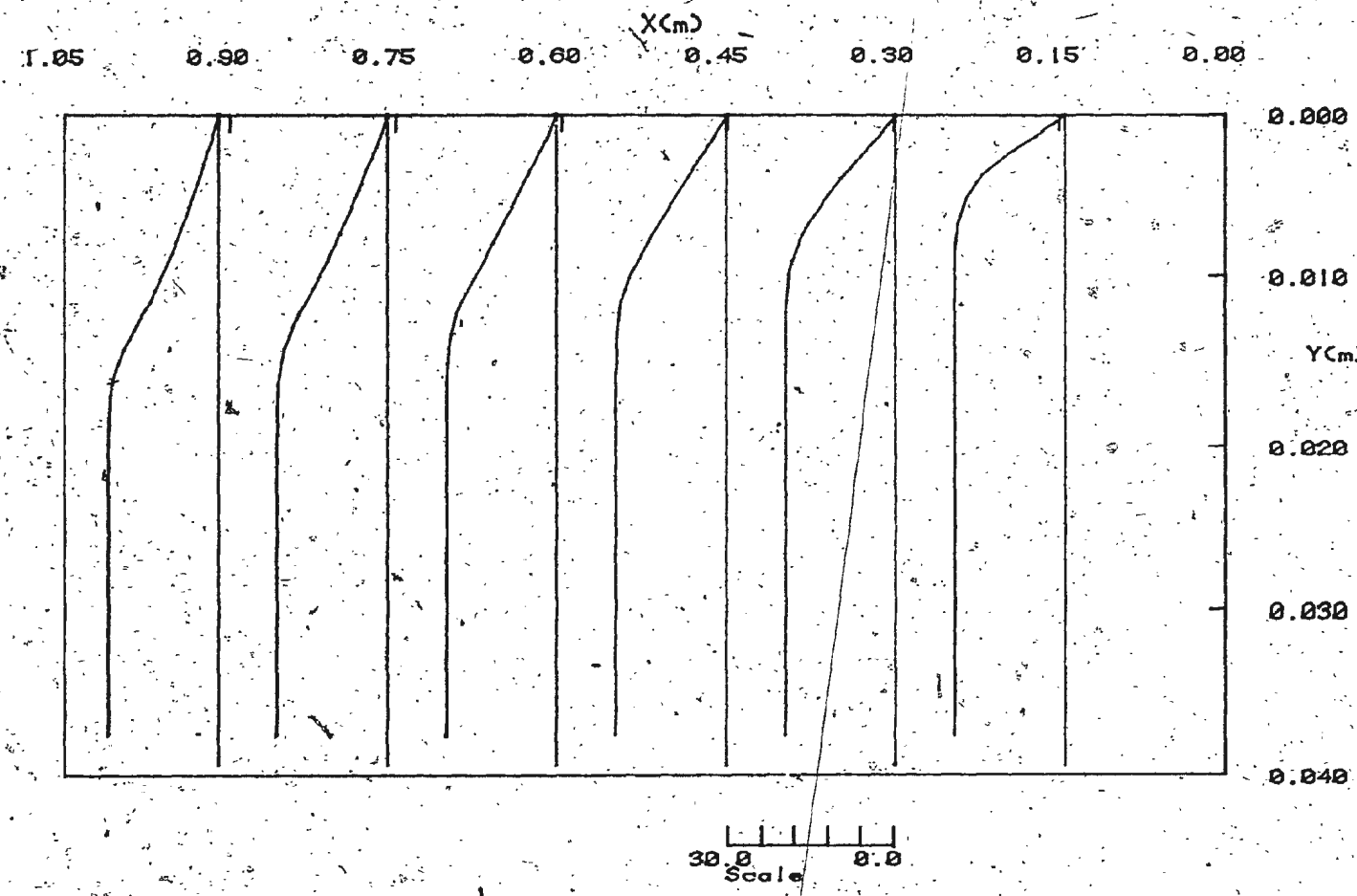

Figure 26(a) Temperature Profiles for $T_\infty = 20.00^\circ C$, $S_\infty = 35.$ ppt, $U_\infty = 0.025$ m/s for Combined Convection

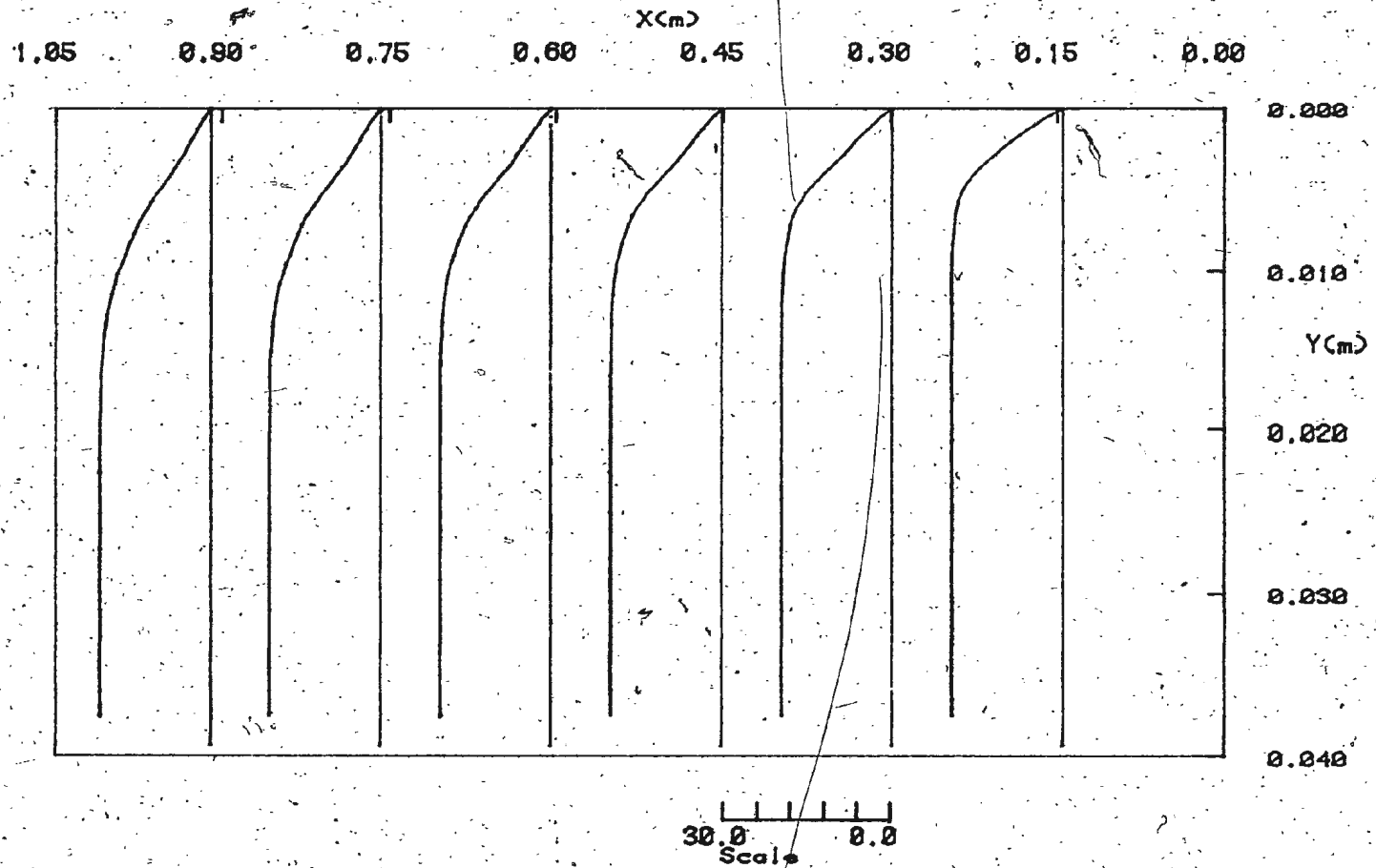

Figure 26(b) Temperature Profiles for T_∞ = 20.00 °C, S_∞ = 35. ppt, U_∞ = 0.025 m/s for Forced Convection

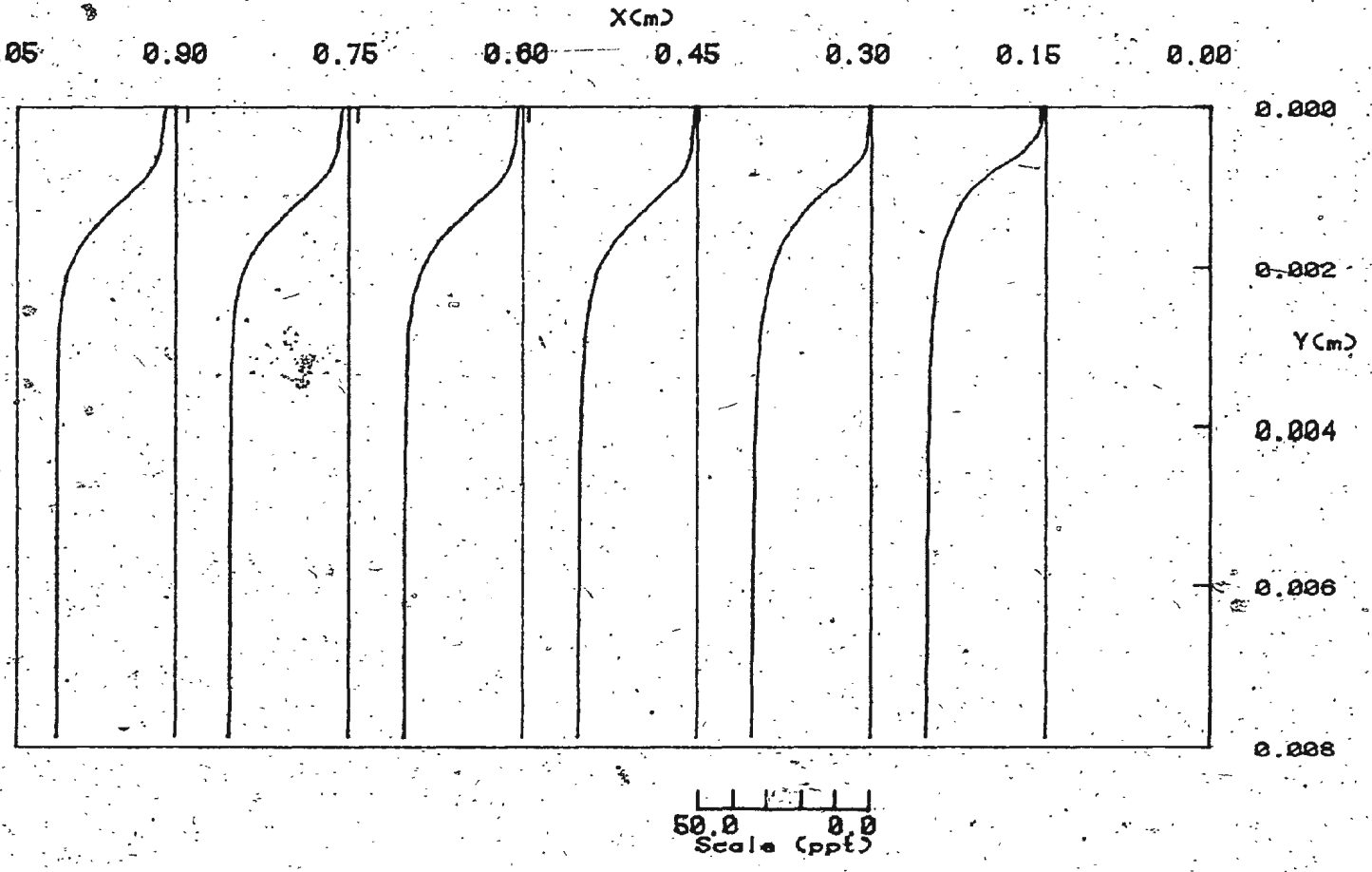

Figure 27(a) Salinity Profiles for T_∞ = 20.00°C, S_∞ = 35. ppt, U_∞ = 0.025 m/s for Combined Convection

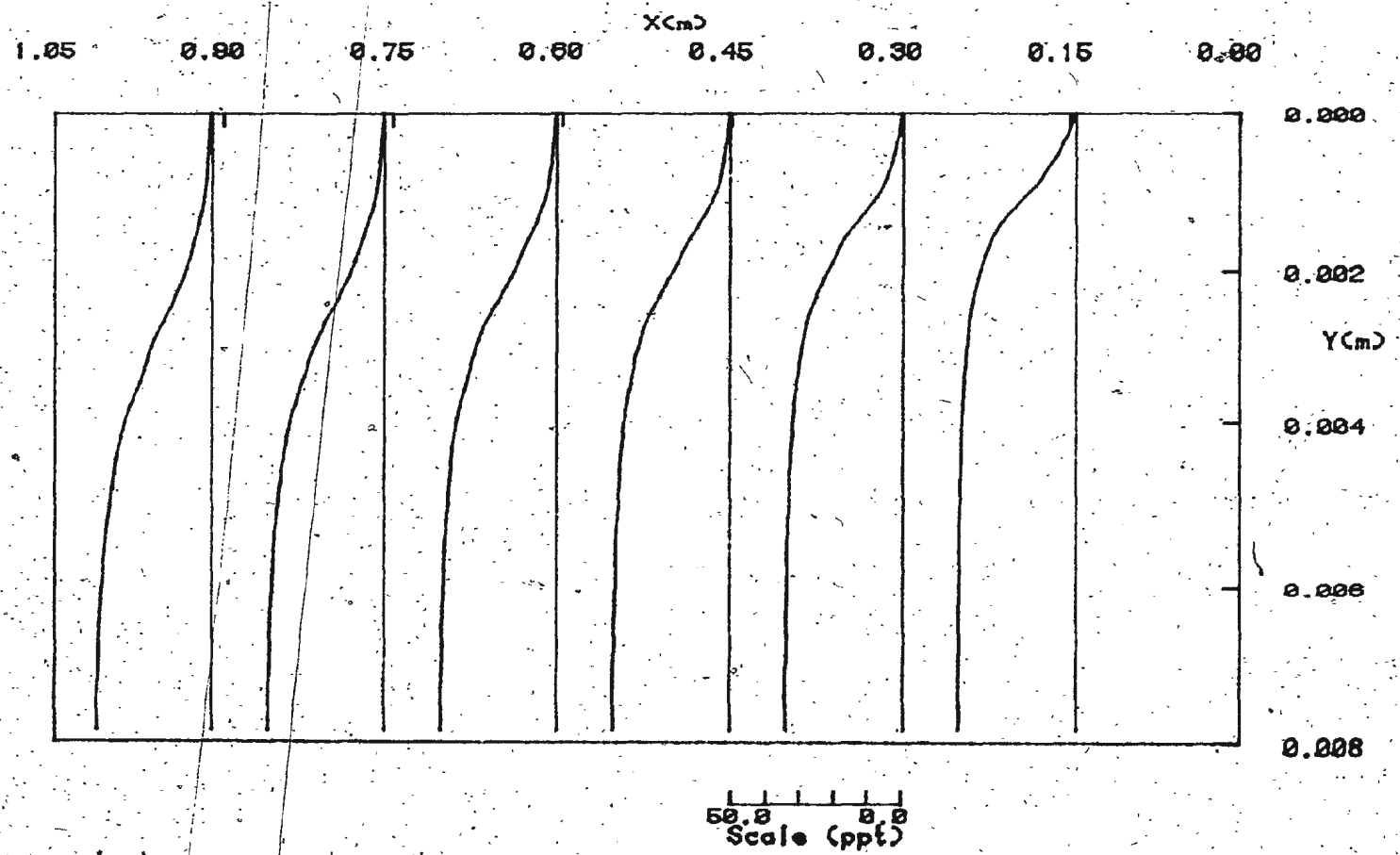

Figure 27(b) Salinity Profiles for T_∞ = 20.00°C, S_∞ = 35. ppt, U_∞ = 0.025 m/s for Forced Convection

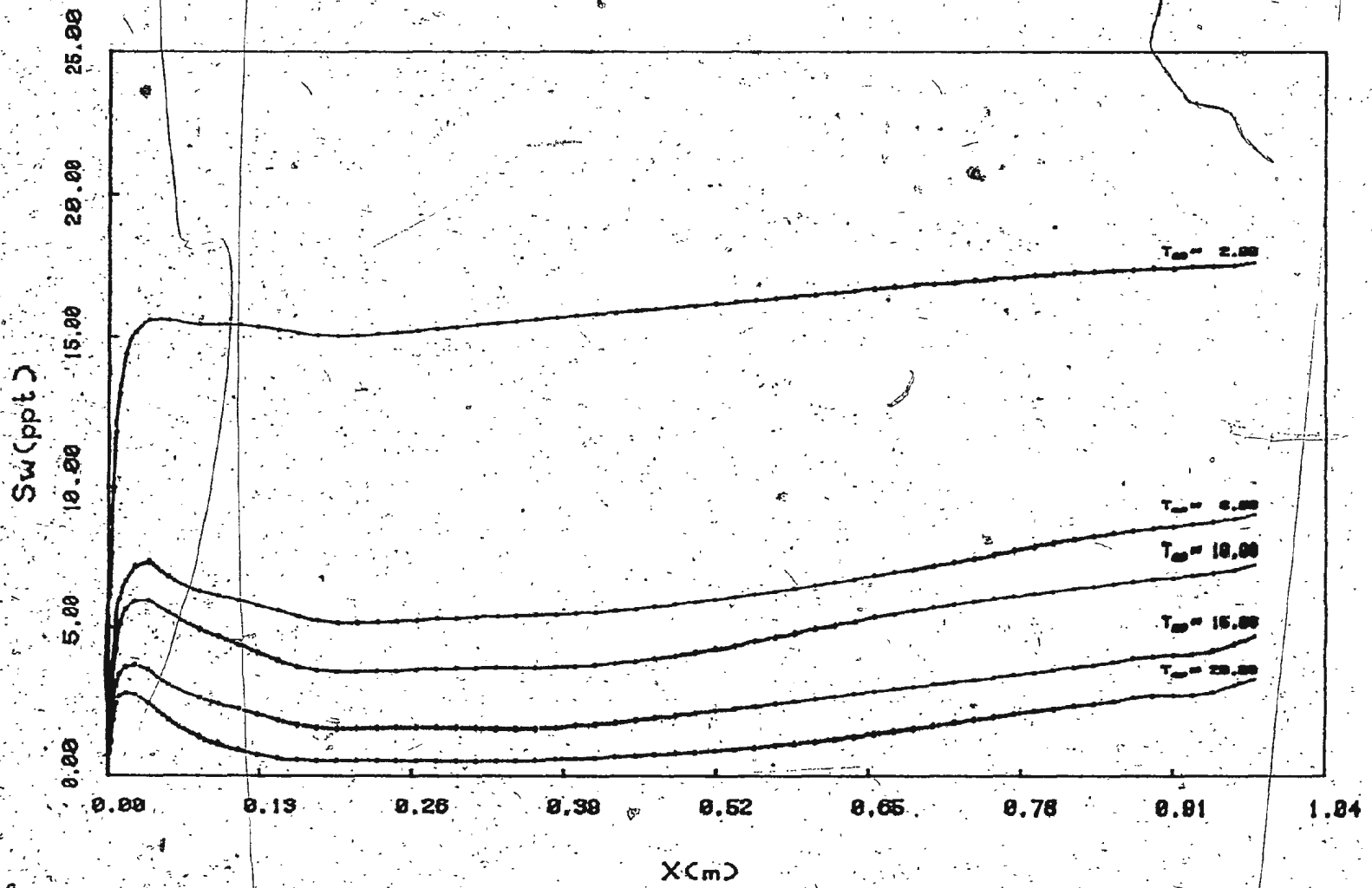

Figure 28(a) Wall Salinity as a Function of Distance along the Plate at various T_∞ for U_∞ = 0.025 m/s, S_∞ = 35. ppt. for Combined Convection

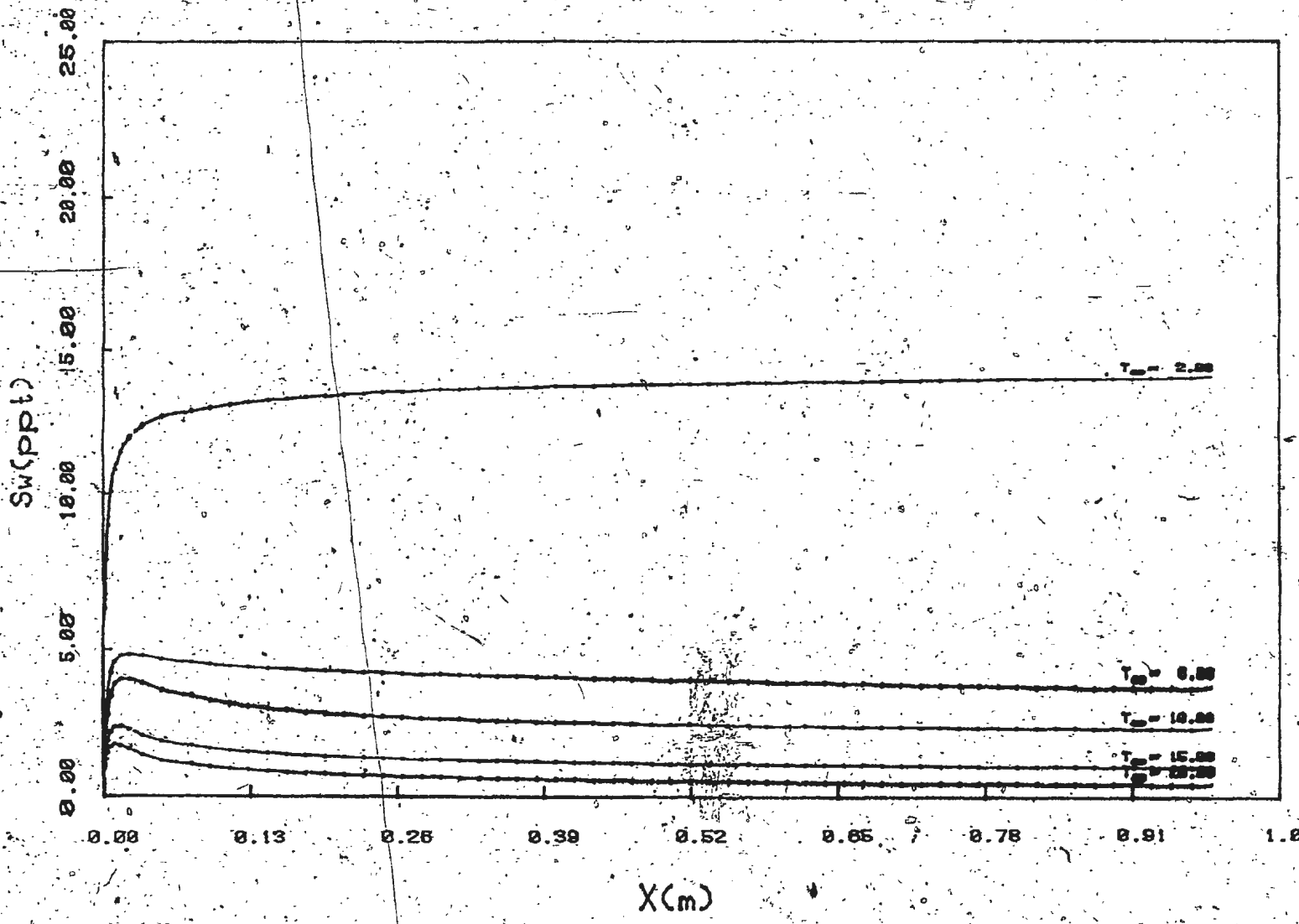

Figure 28(b) Wall Salinity as a Function of Distance along the Plate at various T_∞ for U_∞ = 0.025 m/s, S_∞ = 35. ppt. for Forced Convection

APPENDIX A

FINITE DIFFERENCE APPROXIMATIONS

Equation (7) is

$$a_\phi \frac{\partial}{\partial x}\{\phi\frac{\partial\psi}{\partial y}\} - a_\phi \frac{\partial}{\partial y}\{\phi\frac{\partial\psi}{\partial x}\} - \frac{\partial}{\partial x}\{b_\phi \frac{\partial}{\partial x}(c_\phi\phi)\}$$

$$- \frac{\partial}{\partial y}\{b_\phi \frac{\partial}{\partial y}(c_\phi\phi)\} + d_\phi = 0 \qquad \text{(A-1)}$$

where ϕ is the dependent variable of the general elliptical equation, symbols a_ϕ, b_ϕ, c_ϕ and d_ϕ are identified in table 1. Integration of the above equation was done by using the techniques of Spalding [19] and Gosman et al. [15] as is summarized in this Appendix. For the purpose of the derivation of the finite difference equation, the field of interest has been covered by a rectangular grid, and the nodes of the finite difference grid correspond with the intersections of the grid lines. In figure 2, a typical node P is shown with surrounding nodes N, S, E and W. The finite difference equation will eventually be expressed primarily in terms of the values of the variables at these nodes, and to a lesser extent in terms of the values on the nodes labelled NE, NW, SE and SW. The double integral of equation (A-1) which is to be evaluated, is

$$\int_{y_s}^{y_n}\int_{x_w}^{x_e} a_\phi \left\{\frac{\partial}{\partial x}\left(\phi\frac{\partial\psi}{\partial y}\right) - \frac{\partial}{\partial y}\left(\phi\frac{\partial\psi}{\partial x}\right)\right\} dx\, dy$$

$$- \int_{y_s}^{y_n}\int_{x_w}^{x_e} \left\{\frac{\partial}{\partial x}\left(b_\phi \frac{\partial}{\partial x}(c_\phi\phi)\right) + \frac{\partial}{\partial y}\left(b_\phi \frac{\partial}{\partial y}(c_\phi\phi)\right)\right\} dx\, dy -$$

$$+ \int_{y_s}^{y_n}\int_{x_w}^{x_e} d_\phi\, dx\, dy = 0 \qquad \text{(A-2)}$$

where the integration limits are the coordinates of the sides of the rectangle in figure 2. Inspection of equation (A-2) reveals that all the terms but the last could be formally integrated once if a_ϕ were a constant. Since a_ϕ is constant, integrating equation (A-2) once, gives

$$a_\phi \left[\int_{y_s}^{y_n} \{\phi_e \left(\frac{\partial\psi}{\partial y}\right)_e - \phi_w \left(\frac{\partial\psi}{\partial y}\right)_w\}\, dy - \int_{x_w}^{x_e} \{\phi_n \left(\frac{\partial\psi}{\partial x}\right)_n - \phi_s \left(\frac{\partial s}{\partial x}\right)_s\, dx\right]$$

Convection terms

$$- \int_{y_s}^{y_n} \{ b_{\phi_e} \left(\frac{\partial}{\partial x}(c_\phi\phi)\right)_e - b_{\phi_w} \left(\frac{\partial}{\partial x}(c_\phi\phi)\right)_w \}\, dy$$

Diffusion terms

$$- \int_{x_w}^{x_e} \{b_{\phi_n} \left(\frac{\partial}{\partial y}(c_\phi\phi)\right)_n - b_{\phi_s} \left(\frac{\partial}{\partial y}(c_\phi\phi)\right)_s\}\, dx$$

$$+ \int_{y_s}^{y_n}\int_{x_w}^{x_e} d_\phi\, dx\, dy = 0 \qquad \text{(A-3)}$$

Source term

where those quantities which appear with the subscripts m, s, e or w are to be evaluated along the side of the rectangle.

Since there are convection terms in ω, T and S equations, equation (A-3) can be integrated by Spalding's [19] finite difference techniques following the methods of Runchal [20].

The complexities in solving equation (A-3) results primarily from the possible variation of fluid properties. In order to simplify the equation (A-3), all fluid properties can be assumed constant except for the density variation in body forces during the processes of calculation. Therefore the final general finite difference equation will become

$$\phi_P = \frac{(C_E-A_E)\phi_E + (C_W-A_W)\phi_W + (C_N-A_N)\phi_N + (C_S-A_S)\phi_S + d_{\phi,P}\, V_P}{C_E + C_W + C_N + C_S + A_E + A_W + A_N + A_S} \qquad \text{(A-4)}$$

where

$$C_E = \tfrac{1}{2}\,[B_E + |A_E| + |B_E - |A_E||]$$

$$C_W = \tfrac{1}{2}\,[B_W + |A_W| + |B_W - |A_W||]$$

$$C_N = \tfrac{1}{2}\,[B_N + |A_N| + |B_N - |A_N||]$$

$$C_S = \tfrac{1}{2}\,[B_S + |A_S| + |B_S - |A_S||]$$

in which

$$A_E = a_\phi[(\psi_{SE} + \psi_S - \psi_{NE} - \psi_N) + |\psi_{SE} + \psi_S - \psi_{NE} - \psi_N|]/8$$

$$A_W = a_\phi[(\psi_{NW} + \psi_N - \psi_{SW} - \psi_S) + |\psi_{NW} + \psi_N - \psi_{SW} - \psi_S|]/8$$

$$A_N = a_\phi[(\psi_{NE} + \psi_E - \psi_{NW} - \psi_W) + |\psi_{NE} + \psi_E - \psi_{NW} - \psi_W|]/8$$

$$A_S = a_\phi[(\psi_{SW} + \psi_W - \psi_{SE} - \psi_E) + |\psi_{SW} + \psi_W - \psi_{SE} - \psi_E|]/8$$

$$B_E = \frac{b_{\phi,E} + b_{\phi,P}}{4} \frac{y_N - y_S}{X_E - X_P} C_\phi$$

$$B_W = \frac{b_{\phi,W} + b_{\phi,P}}{4} \frac{y_N - y_S}{X_P - X_W} C_\phi$$

$$B_N = \frac{b_{\phi,S} + b_{\phi,P}}{4} \frac{X_E - X_W}{Y_P - Y_S} C_\phi$$

$$B_S = \frac{b_{\phi,S} + b_{\phi,P}}{4} \frac{X_E - X_W}{Y_P - Y_S} C_\phi$$

$$V_P = \left(\frac{X_E - X_W}{2}\right)\left(\frac{Y_N - Y_S}{2}\right)$$

For stream function calculations, since there are no convection terms, equation (A-3) can be integrated following the methods of Gosman et al. [15] which gives

$$\psi_P = \frac{(B'_E)\psi_E + (B'_W)\psi_W + (B'_N)\psi_N + (B'_S)\psi_S + \rho_P W_P}{B'_E + B'_W + B'_N + B'_S} \qquad (A\text{-}5)$$

where

$$B'_E = \frac{2}{(x_E - x_P)(x_E - x_W)}$$

$$B'_W = \frac{2}{(x_P - x_W)(x_E - x_W)}$$

$$B'_N = \frac{2}{(y_N - y_P)(y_N - y_S)}$$

$$B'_S = \frac{2}{(y_P - y_S)(y_N - y_S)}$$

Method for Solving Gradients of Various Variables

Consider a gradient of ϕ at the point P in x-direction as shown below:

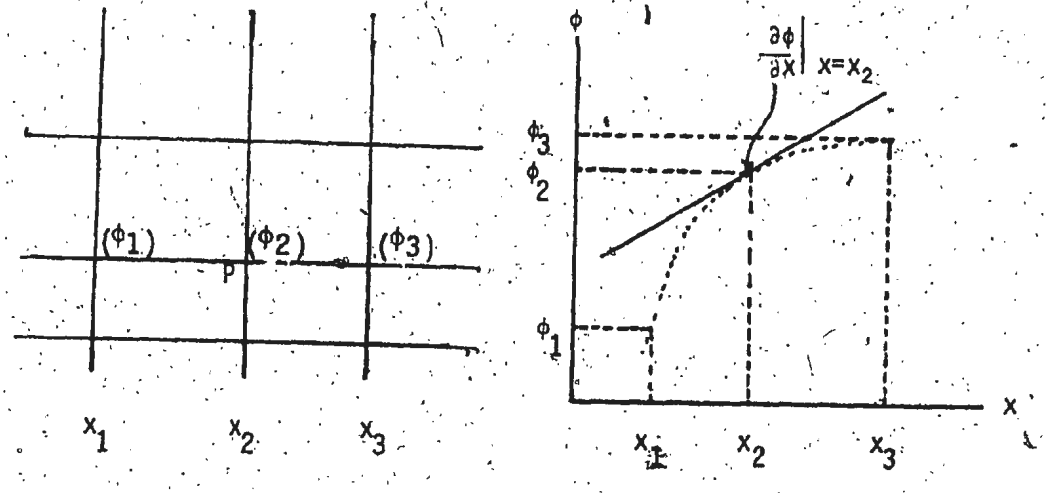

The following quadratic equation can be chosen to satisfy (x_1,ϕ_1), (x_2,ϕ_2) and (x_3,ϕ_3) with three arbitrary constants

$$\phi = ax^2 + bx + C \qquad \text{(A-6)}$$

At $x = x_1$

$$\phi_1 = ax_1^2 + bx_1 + C \qquad \text{(A-7)}$$

At $x = x_2$

$$\phi_2 = ax_2^2 + bx_2 + C \qquad \text{(A-8)}$$

At $x = x_3$

$$\phi_3 = ax_3^2 + bx_3 + C \qquad \text{(A-9)}$$

Carrying out the elimination of C from equations (A-7), (A-8) and (A-9) leads to

$$a = \frac{(\phi_3 - \phi_1)(x_2 - x_1) - (\phi_2 - \phi_1)(x_3 - x_1)}{(x_2 - x_1)(x_3 - x_2)(x_3 - x_1)} \qquad \text{(A-10)}$$

and

$$b = \frac{(\phi_3 - \phi_2) - a(x_3^2 - x_2^2)}{(x_3 - x_2)} \qquad \text{(A-11)}$$

Differentiating equation (A-6) with respect to x gives

$$\frac{\partial \phi}{\partial x} = 2ax + b$$

$$\therefore \left.\frac{\partial \phi}{\partial x}\right|_{x=x_2} = 2ax_2 + b \qquad \text{(A-12)}$$

Substituting the values of a and b from equations (A-10) and (A-11) into the equation (A-12) results to

$$\left.\frac{\partial \phi}{\partial x}\right|_{x=x_2} = \frac{\phi_3 - \phi_2}{x_3 - x_2} - \frac{\phi_3 - \phi_1}{x_3 - x_1} + \frac{\phi_2 - \phi_1}{x_2 - x_1}$$

$$= \frac{\dfrac{(\phi_3 - \phi_2)(x_2 - x_1)}{(x_3 - x_2)} + \dfrac{(\phi_2 - \phi_1)(x_3 - x_2)}{(x_2 - x_1)}}{(x_3 - x_1)} \qquad \text{(A-13)}$$

Solution Procedure

In order to solve the finite difference equations, the following steps are to be followed:

(i) Selection of grids in X and Y-directions. For adequate convergence, nodes should be closely spaced in the region where variables change rapidly.

(ii) Provide initial values of various variables.

(iii) Solve the finite difference equations with associated boundary conditions.

(iv) Calculated new values of the variables are then used as the improved initial values and return to step (iii). This process is to be repeated until convergence is reached.

In order to reduce the execution time for convergence, relaxation technique is used. The relationship between a new value and an old value of the variable is given by

$$\phi_{P_{new}} = \phi_{P_{old}} + RP\,(\phi_{P_{new}} - \phi_{P_{old}}) \qquad \text{(A-14)}$$

where ϕ_P is the dependent variable and RP is called the relaxation parameter which lies between 0 and 1.

APPENDIX B

```
C      FILE NAME:    GRI68.FTN
C      ************************************************************
C      *                  INITIALISATION PROGRAM                  *
C      ************************************************************
       INCLUDE 'COMMON.FTN'
       DIMENSION X(66)
       BYTE ALPHA(80)
       COMMON/VORTIC/W1(M),W2(M),W3(M),RPW,RSDUW
       COMMON/STRFN/F1(M),F2(M),F3(M),RPF,RSDUF
       COMMON/TEM/T1(M),T2(M),T3(M),RPT,RSDUT
       COMMON/SAL/S1(M),S2(M),S3(M),RPS,RSDUS
       COMMON/VSQ/VSQ1(M),VSQ2(M),VSQ3(M),V2
       COMMON/SOR/SOR1(M),SOR2(M),SOR3(M),RPSOR
       COMMON/CONVE/AE(M),AW(M),AN(M),AS(M),AT(M)
       COMMON/DEN/RO1(M),RO2(M),RO3(M)
       COMMON/BW/BWE,BWW,BWEW,BWN(M),BWS(M),BWNS(M)
       COMMON/BF/BFE,BFW,BFEW,BFN(M),BFS(M),BFNS(M)
       COMMON/BT/BTE,BTW,BTEW,BTN(M),BTS(M),BTNS(M)
       COMMON/BS/BSE,BSW,BSEW,BSN(M),BSS(M),BSNS(M)
       COMMON/XY/Y(M),DDY(M),Y32,Y22,DY,DYY,X1,X2,X3
       COMMON/PROP/THECON,FUSION,DIFCL
       COMMON/VAR/JJ,JNM,JN,TINF,SALINF,VELINF
       DATA W1,F1,T1,S1,VSQ1,SOR1,RO1/455*0./
       DATA X/0.,.0003,.0007,.0013,.0022,.0037,.006,.0095,.0147,.0224
     *,.0341,.0508,.0773,.094,.111,.128,.145,.162,.179,.196,.213,.23
     *,.247,.264,.281,.298,.315,.332,.349,.366,.383,.4,.417,.434,.451
     *,.468,.485,.502,.519,.536,.553,.57,.587,.604,.621,.638,.655,.672
     *,.689,.706,.723,.74,.757,.774,.791,.808,.825,.842,.859,.876,.893
     *,.91,.927,.9445,.962,.98,1.0,1.021/
       DATA PR,SC,ZMUREF/7.0,813.2,.001075/
       TYPE*,' ENTER NAME OF FILE TO BE CREATED'
       READ(5,1005)ALPHA
1005   FORMAT(80A1)
       ALPHA(80)=0
       OPEN(UNIT=1,TYPE='NEW',ACCESS='DIRECT',INITIALSIZE=70,
     *  RECORDSIZE=480,ASSOCIATEVARIABLE=III,NAME=ALPHA)
```

```
      TYPE 1
1     FORMAT(' II,IN')
      ACCEPT *,II,IN
      TYPE 3
3     FORMAT(' VELINF, TINF, SALINF, CC')
      ACCEPT *,VELINF,TINF,SALINF,CC
      DO 5 J=2,JNM
      D=2./(Y(J+1)-Y(J-1))
      BFS(J)=D/(Y(J)-Y(J-1))
      BFN(J)=D/(Y(J+1)-Y(J))
      BFNS(J)=BFS(J)+BFN(J)
      BWS(J)=ZMUREF*BFS(J)
      BWN(J)=ZMUREF*BFN(J)
      BWNS(J)=BWN(J)+BWS(J)
      BTS(J)=BWS(J)/PR
      BTN(J)=BWN(J)/PR
      BTNS(J)=BTS(J)+BTN(J)
      BSS(J)=BWS(J)/SC
      BSN(J)=BWN(J)/SC
      BSNS(J)=BSS(J)+BSN(J)
5     DDY(J)=Y(J+1)-Y(J-1)
      Y32=Y(3)**2
      Y22=Y(2)**2
      DY=Y(2)*Y32-Y(3)*Y22
      DYY=Y(JN)-Y(JNM)
      K=0
      III=1
      INM=IN-1
      WRITE(1'III)II,INM,IN,PR,SC,ZMUREF,VELINF,TINF,SALINF,
     *JJ,JNM,JN,THECON,FUSION,DIFCL,BWN,BWS,BWNS,BFN,BFS,BFNS,Y
      WRITE(1'III)DDY,BTN,BTS,BTNS,BSN,BSS,BSNS,Y32,Y22,DY,DYY
     *,RPW,RPF,RPT,RPS,RPSOR,CC
      III=3
      CALL DENSIT(SALINF,TINF,ROINF)
      X1=0.
      DO 10 I=1,68
```

```
      IF(I.EQ.1.OR.I.EQ.68) GO  TO 11
      DX=2./(X(I+1)-X(I-1))
      BFW=DX/(X(I)-X(I-1))
      BFE=DX/(X(I+1)-X(I))
      BFEW=BFW+BFE
      BWW=ZMUREF*BFW
      BWE=ZMUREF*BFE
      BWEW=BWE+BWW
      BTE=BWE/PR
      BTW=BWW/PR
      BTEW=BTE+BTW
      BSW=BWW/SC
      BSE=BWE/SC
      BSEW=BSW+BSE
11    XI=X(I)
      IF(XI.EQ.0.)GO TO12
      DEL=4.64*XI/SQRT(ROINF*VELINF*XI/ZMUREF)
      GO TO 14
12    DEL=0.
14    F1(1)=0.
      IF(I.NE.1)W1(1)=-2.
      T1(1)=0.
      S1(1)=0.
      CALL DENSIT(0.,0.,RO1(1))
      U1=0.
      DO 13 J=2,JN
      U=VELINF
      IF(Y(J).GT.DEL)GO TO15
      YBD=Y(J)/DEL
      U=VELINF*(1.5*YBD-.5*YBD**3)
15    F1(J)=F1(J-1)+ROINF*U*(Y(J)-Y(J-1))
      IF(I.NE.1)W1(J)=-(U-U1)/(Y(J)-Y(J-1))
      T1(J)=U/VELINF*TINF
      S1(J)=U/VELINF*SALINF
      VSQ1(J)=0.
      SOR1(J)=0.
```

```
      U1=U
      CALL DENSIT(S1(J),T1(J),RO1(J))
13    CONTINUE
10    WRITE(1,'III)W1,F1,T1,S1,VSQ1,SOR1,RO1,BWE,BWW,BWEW,
     *BFE,BFW,BFEW,BTE,BTW,BTEW,BSE,BSW,BSEW,RSDUW,RSDUF
     *,RSDUT,RSDUS,X1,K
      CLOSE(UNIT=1)
      STOP
      END
      BLOCK DATA
      INCLUDE 'COMMON.FTN'
      COMMON/VORTIC/W1(M),W2(M),W3(M),RPW,RSDUW
      COMMON/STRFN/F1(M),F2(M),F3(M),RPF,RSDUF
      COMMON/TEM/T1(M),T2(M),T3(M),RPT,RSDUT
      COMMON/SAL/S1(M),S2(M),S3(M),RPS,RSDUS
      COMMON/VSQ/VSQ1(M),VSQ2(M),VSQ3(M),V2
      COMMON/SOR/SOR1(M),SOR2(M),SOR3(M),RPSOR
      COMMON/CONVE/AE(M),AW(M),AN(M),AS(M),AT(M)
      COMMON/DEN/RO1(M),RO2(M),RO3(M)
      COMMON/BW/BWE,BWW,BWEW,BWN(M),BWS(M),BWNS(M)
      COMMON/BF/BFE,BFW,BFEW,BFN(M),BFS(M),BFNS(M)
      COMMON/BT/BTE,BTW,BTEW,BTN(M),BTS(M),BTNS(M)
      COMMON/BS/BSE,BSW,BSEW,BSN(M),BSS(M),BSNS(M)
      COMMON/XY/Y(M),DDY(M),Y32,Y22,DY,DYY,X1,X2,X3
      COMMON/PROP/THECON,FUSION,DIFCL
      COMMON/VAR/JJ,JNM,JN,VELINF,TINF,SALINF
      DATA RPW,RPF,RPT,RPS,RPSOR/.5,.8,.8,.8,.2/
      DATA RSDUW,RSDUF,RSDUT,RSDUS/4*0./
      DATA Y/0.,.00025,.0005,.00075,.00105,.00135,.00165,.002,.00235
     *,.0027,.0031,.0035,.0039,.00435,.0048,.00525,.00575,.00625,.00675
     *,.0073,.00785,.0084,.009,.0096,.0102,.01085,.0115,.01215,.01285
     *,.01355,.01425,.015,.01575,.0165,.0173,.0181,.0189,.01975,.0206
     *,.02145,.02235,.02325,.02415,.0251,.02605,.02705,.02805,.02955
     *,.03105,.03305,.03505,.03755,.04005,.04305,.04605,.04955,.05305
     *,.05705,.06105,.06555,.07005,.07505,.0801,.0861,.0933/
      DATA THECON,FUSION,DIFCL/.596,334944.,12.9E-10/
```

```
      DATA JJ,JNM,JN/2,64,65/
      DATA BWE,BWW,BWEW,BFE,BFW,BFEW,BTE,BTW,
     *BTEW,BSE,BSW,BSEW/12*0./
      DATA BWN,BWS,BWNS,BFN,BFS,BFNS,BTN,BTS,BTNS,
     *BSN,BSS,BSNS,DDY/845*0./
      END
      SUBROUTINE DENSIT(S,T,D)
      SIGMA0=(-0.093+0.8149*S-0.000482*S**2+0.0000068*S**3)
      SIGT=-((T-3.98)**2)/503.570*(T+283.)/(T+67.26)
      AT=T/1000.*(4.7867-0.098185*T+0.0010843*T**2)
      BT=T/1000000.*(18.030-0.8164*T+0.01667*T**2)
      SIGMAT=SIGT+(SIGMA0+0.1324)*(1.-AT+BT*(SIGMA0-0.1324))
      D=SIGMAT+1000.
      RETURN
      END


C          FILE NAME:       COMMON.FTN
      PARAMETER M=65
```

APPENDIX C

```
C       FILE NAME:      FOR500.FTN
C     **********************************************************************
C     *          PROGRAM FOR FORCED CONVECTION SOLUTION                    *
C     **********************************************************************
      INCLUDE 'COMMON.FTN'
      BYTE ALPHA(80)
      COMMON/VORTIC/W1(M),W2(M),W3(M),RPW,RSDUW
      COMMON/STRFN/F1(M),F2(M),F3(M),RPF,RSDUF
      COMMON/TEM/T1(M),T2(M),T3(M),RPT,RSDUT
      COMMON/SAL/S1(M),S2(M),S3(M),RPS,RSDUS
      COMMON/VSO/VSO1(M),VSO2(M),VSO3(M),V2
      COMMON/SOR/SOR1(M),SOR2(M),SOR3(M),RPSOR
      COMMON/CONVE/AE(M),AW(M),AN(M),AS(M),AT(M)
      COMMON/DEN/RO1(M),RO2(M),RO3(M)
      COMMON/BW/BWE,BWW,BWEW,BWN(M),BWS(M),BWNS(M)
      COMMON/BF/BFE,BFW,BFEW,BFN(M),BFS(M),BFNS(M)
      COMMON/BT/BTE,BTW,BTEW,BTN(M),BTS(M),BTNS(M)
      COMMON/BS/BSE,BSW,BSEW,BSN(M),BSS(M),BSNS(M)
      COMMON/XY/Y(M),DDY(M),Y32,Y22,DY,DYY,X1,X2,X3
      COMMON/PROP/THECON,FUSION,DIFCL
      COMMON/VAR/JJ,JNM,JN,TINF,SALINF,VELINF
      DATA RSW,RSF,RST,RSS/4*0./
      DATA V1/0./
      DATA NMAX/500/
      RSDUW=0.
      RSDUF=0.
      RSDUT=0.
      RSDUS=0.
      KKK=7*(21)+18
      TYPE*,' ENTER NAME OF DATA FILE'
      READ(5,857)ALPHA
857   FORMAT(80A1)
      ALPHA(80)=0
      OPEN(UNIT=1,TYPE='OLD',ACCESS='DIRECT',NAME=ALPHA,
     *  ASSOCIATEVARIABLE=III,FORM='UNFORMATTED'
     *  )
```

```
      III=1
      READ(1'III)II,INM,IN,PR,SC,ZMUREF,VELINF,TINF,SALINF,
     *JJ,JNM,JN,THECON,FUSION,DIFCL,BWN,BWS,BWNS,BFN,BFS,BFNS,Y
      READ(1'III)DDY,BTN,BTS,BTNS,BSN,BSS,BSNS,Y32,Y22,DY,DYY
     *,RPW,RPF,RPT,RPS,RPSOR,CC
      WRITE(5,202)
      READ(5,201)NMAX
  104 III=3
      READ(1'III)W1,F1,T1,S1,VSQ1,SOR1,RO1,BWE,BWW,BWEW
     *,BFE,BFW,BFEW,BTE,BTW,BTEW,BSE,BSW,BSEW,RW,RF,RT,RS
     *,X1,K
      WMAX=-2.
      FMAX=F1(JN)
      READ(1'III)W2,F2,T2,S2,VSQ2,SOR2,RO2,BWE,BWW,BWEW
     *,BFE,BFW,BFEW,BTE,BTW,BTEW,BSE,BSW,BSEW,RW,RF,RT,RS
     *,X2,K
  202 FORMAT(' ENTER NMAX')
  201 FORMAT(I5)
      I=II
      V1=0.
  102 III=I+3
      READ(1'III)W3,F3,T3,S3,VSQ3,SOR3,RO3,BWE3,BWW3,BWEW3
     *,BFE3,BFW3,BFEW3,BTE3,BTW3,BTEW3,BSE3,BSW3,BSEW3,
     *RSDUW3,RSDUF3,RSDUT3,RSDUS3,X3,K
      K=K+1
      DX=(X3-X1)*2.
      J=JJ
    6 JP=J+1
      JM=J-1
      DV=DX*DDY(J)
      STNW=F1(JP)
      STWME=F1(J)-F3(J)
      STSW=F1(JM)
      STNMS=F2(JP)-F2(JM)
      STSE=F3(JM)
      STNE=F3(JP)
```

```
      G1PW=(STNMS+STNW-STSW)/DV
      G1PE=(STNMS+STNE-STSE)/DV
      G2PS=(STWME+STSW-STSE)/DV
      G2PN=(STWME+STNW-STNE)/DV
      AE(J)=ABS(G1PE)-G1PE
      AW(J)=ABS(G1PW)+G1PW
      AS(J)=ABS(G2PS)+G2PS
      AN(J)=ABS(G2PN)-G2PN
      AT(J)=AE(J)+AW(J)+AN(J)+AS(J)
      IF(J.EQ.JNM) GO TO 62
      J=J+1
      GOTO 6
62    CONTINUE
      J=JJ
1     ANUM=(AE(J)+BWE)*W3(J)+(AW(J)+BWW)*W1(J)
     * +(AN(J)+BWN(J))*W2(J+1)+(AS(J)+BWS(J))*W2(J-1)
     * +SOR2(J)
      ADNM=AT(J)+BWEW+BWNS(J)
      IF(ADNM.EQ.0.)GO TO 11
      CALL RESID(W2(J),ANUM,ADNM,WMAX,RPW,RSDUW)
11    IF(J.EQ.JNM)GOTO12
      J=J+1
      GOTO1
12    CONTINUE
      J=JJ
4     ANUM=BFE*F3(J)+BFW*F1(J)
     * +BFN(J)*F2(J+1)+BFS(J)*F2(J-1)
     * +W2(J)*RO2(J)
      ADNM=BFEW+BFNS(J)
      IF(ADNM.EQ.0.)GOTO41
      CALL RESID(F2(J),ANUM,ADNM,FMAX,RPF,RSDUF)
41    IF(J.EQ.JNM)GOTO42
      J=J+1
      GOTO4
42    CONTINUE
      J=JJ
```

```
2       ANUM=CAE(J)+BTE)*T3(J)+(AW(J)+BTW)*T1(J)
     *  +(AN(J)+BTN(J))*T2(J+1)+(AS(J)+BTS(J))*T2(J-1)
        ADNM=AT(J)+BTEW+BTNS(J)
        IF(ADNM.EQ.0.)GOTO21
        CALL RESID(T2(J),ANUM,ADNM,TINF,RPT,RSDUT)
21      IF(J.EQ.JNM)GOTO22
        J=J+1
        GOTO2
22      CONTINUE
        J=JJ
3       ANUM=CAE(J)+BSE)*S3(J)+(AW(J)+BSW)*S1(J)
     *  +(AN(J)+BSN(J))*S2(J+1)+(AS(J)+BSS(J))*S2(J-1)
        ADNM=AT(J)+BSEW+BSNS(J)
        IF(ADNM.EQ.0.)GOTO31
        CALL RESID(S2(J),ANUM,ADNM,SALINF,RPS,RSDUS)
31      IF(J.EQ.JNM)GOTO32
        J=J+1
        GOTO3
32      CONTINUE
        DX=X2-X1
        KSAL=0
250     T2(1)=-0.003-0.0527*S2(1)-0.00004*(S2(1)**2.)
        DTDY=(Y32*(T2(2)-T2(1))-Y22*(T2(3)-T2(1)))/DY
        V2=THECON/RO2(1)/FUSION*DTDY
        SNEW=DIFCL*S2(2)/(V2*Y(2)+DIFCL)
        SNEW=S2(1)-(S2(1)-SNEW)*.5
D       TYPE*,KSAL,SNEW,S2(1),T2(1)
        IF(KSAL.GT.67)GOTO251
        IF(SNEW.EQ.S2(1)) GO TO 251
        IF(S2(1).EQ.0.) GO TO 252
        IF(ABS(1.-SNEW/S2(1)).LT.CC)GO TO 251
252     S2(1)=SNEW
        KSAL=KSAL+1
        GO TO 250
251     S2(1)=SNEW
        IF(S2(1).LT.0.)S2(1)=0.
```

```
      F2(1)=F1(1)-(RO1(1)*V1+RO2(1)*V2)/2.*DX
      U2=DIFF(F2(3),F2(2),F2(1),Y(3),Y(2),Y(1))/RO2(2)
      W2(1)=(V2-V1)/DX-U2/Y(2)
      F2(JN)=F2(JNM)+VELINF*RO2(JN)*DYY
      DO10 J=1,JN
10    CALL DENSIT(S2(J),T2(J),RO2(J))
      VSQ2(1)=V2**2/2.
100   III=I+2
      WRITE(1,'III)W2,F2,T2,S2,VSQ2,SOR2,RO2,BWE,BWW,
     *BWEW,BFE,BFW,BFEW,BTE,BTW,BTEW,BSE,BSW,BSEW,
     *RSDUW,RSDUF,RSDUT,RSDUS,X2,K
      IF(I.EQ.INM) GO TO 101
C  UPDATE**********************************************
      J=1
110   W1(J)=W2(J)
      W2(J)=W3(J)
      F1(J)=F2(J)
      F2(J)=F3(J)
      T1(J)=T2(J)
      T2(J)=T3(J)
      S1(J)=S2(J)
      S2(J)=S3(J)
      VSQ1(J)=VSQ2(J)
      VSQ2(J)=VSQ3(J)
      SOR1(J)=SOR2(J)
      SOR2(J)=SOR3(J)
      RO1(J)=RO2(J)
      RO2(J)=RO3(J)
      IF(J.EQ.JN)GO TO 72
      J=J+1
      GO TO 110
72    BWE=BWE3
      BWW=BWW3
      BWEW=BWEW3
      BFE=BFE3
      BFW=BFW3
```

```
      BFEW=BFEW3
      BTE=BTE3
      BTW=BTW3
      BTEW=BTEW3
      BSE=BSE3
      BSW=BSW3
      BSEW=BSEW3
      X1=X2
      X2=X3
      V1=V2
C RESIDUALS**********************************************
      RSW=AMAX1(RSW,RSDUW)
      RSF=AMAX1(RSF,RSDUF)
      RST=AMAX1(RST,RSDUT)
      RSS=AMAX1(RSS,RSDUS)
      RSDUW=0.
      RSDUF=0.
      RSDUT=0.
      RSDUS=0.
      I=I+1
      GOTO 102
 101  WRITE(1'III)W2,F2,T2,S2,VSQ2,SOR2,RO2,BWE3,BWW3,
     *BWEW3,BFE3,BFW3,BFEW3,BTE3,BTW3,BTEW3,BSE3,BSW3,
     *BSEW3,RSW,RSF,RST,RSS,X3,K*
      WRITE(6,109)K,RSW,RSF,RST,RSS
 109  FORMAT(I5,4E11.4)
      IF(AMAX1(RSW,RSF,RST,RSS).LT.CC.OR.K.EQ.NMAX)
     *GO TO 103
      RSW=0.
      RSF=0.
      RST=0.
      RSS=0.
      GO TO 104
 103  CONTINUE
      STOP
      END
```

```
      SUBROUTINE RESID(OLD,ANUM,ADNM,AMAX,RP,RSD)
      RS1=ANUM/ADNM-OLD
      OLD=OLD+RP*RS1
      RSD=AMAX1(RSD,ABS(RS1/AMAX))
      RETURN
      END
      SUBROUTINE DENSIT(S,T,D)
      SIGMA0=(-0.093+0.8149*S-0.000482*S**2+0.0000068*S**3)
      SIGT=-((T-3.98)**2)/503.570*(T+283.)/(T+67.26)
      AT=T/1000.*(4.7867-0.098185*T+0.0010843*T**2)
      BT=T/1000000.*(18.030-0.8164*T+0.01667*T**2)
      SIGMAT=SIGT+(SIGMA0+0.1324)*(1.-AT+BT*(SIGMA0-0.1324))
      D=SIGMAT+1000.
      RETURN
      END
      FUNCTION DIFF(PD,PP,PU,XD,XP,XU)
      DIFF=((PD-PP)*(XP-XU)/(XD-XP)
     * +(PP-PU)*(XD-XP)/(XP-XU))/(XD-XU)
C     ***********************************************************************
C     *          SUBROUTINE FOR CALCULATION OF GRADIENTS                    *
C     ***********************************************************************
      RETURN
      END
```

APPENDIX D

```
C       FILE NAME:      COM000.FTN
C       ****************************************************************
C       *          PROGRAM FOR COMBINED CONVECTION SOLUTION            *
C       ****************************************************************
        INCLUDE 'COMMON.FTN'
        BYTE ALPHA(80)
        REAL NUL(M)
        COMMON/VORTIC/W1(M),W2(M),W3(M),RPW,RSDUW
        COMMON/STRFN/F1(M),F2(M),F3(M),RPF,RSDUF
        COMMON/TEM/T1(M),T2(M),T3(M),RPT,RSDUT
        COMMON/SAL/S1(M),S2(M),S3(M),RPS,RSDUS
        COMMON/VSQ/VSQ1(M),VSQ2(M),VSQ3(M),V2
        COMMON/SOR/SOR1(M),SOR2(M),SOR3(M),RPSOR
        COMMON/CONVE/AE(M),AW(M),AN(M),AS(M),AT(M)
        COMMON/DEN/RO1(M),RO2(M),RO3(M)
        COMMON/BW/BWE,BWW,BWEW,BWN(M),BWS(M),BWNS(M)
        COMMON/BF/BFE,BFW,BFEW,BFN(M),BFS(M),BFNS(M)
        COMMON/BT/BTE,BTW,BTEW,BTN(M),BTS(M),BTNS(M)
        COMMON/BS/BSE,BSW,BSEW,BSN(M),BSS(M),BSNS(M)
        COMMON/XY/Y(M),DDY(M),Y32,Y22,DY,DYY,X1,X2,X3
        COMMON/PROP/THECON,FUSION,DIFCL
        COMMON/VAR/JJ,JNM,JN,TINF,SALINF,VELINF
        DATA RSW,RSF,RST,RSS/4*0./
        DATA NUL/M*0./
        DATA V1/0./
        DATA NMAX/500/
        RSDUW=0.
        RSDUF=0.
        RSDUT=0.
        RSDUS=0.
        KKK=7*(21)+18
        TYPE *,' ENTER NAME OF DATA FILE'
        READ(5,857)ALPHA
857     FORMAT(80A1)
        ALPHA(80)=0
        OPEN(UNIT=1,TYPE='OLD',ACCESS='DIRECT',
```

```
     *  ASSOCIATEVARIABLE=III,FORM='UNFORMATTED',
     *  NAME=ALPHA)
        III=1
        READ(1'III)II,INM,IN,PR,SC,ZMUREF,VELINF,TINF,SALINF,
     *JJ,JNM,JN,THECON,FUSION,DIFCL,BWN,BWS,BWNS,BFN,BFS,BFNS,Y
        IN3=IN-3
        READ(1'III)DDY,BTN,BTS,BTNS,BSN,BSS,BSNS,Y32,Y22,DY,DYY
     *,RPW,RPF,RPT,RPS,RPSOR,CC
        TYPE*,' RPW,RPF,RPT,RPS,RPSOR,CC',RPW,RPF,RPT,RPS,RPSOR,CC
        ACCEPT*,RPW,RPF,RPT,RPS,RPSOR,CC
        WRITE(5,202)
        READ(5,201)NMAX
104     III=3
        READ(1'III)W1,F1,T1,S1,VSQ1,SOR1,RO1,BWE,BWW,BWEW
     *,BFE,BFW,BFEW,BTE,BTW,BTEW,BSE,BSW,BSEW,RW,RF,RT,RS
     *,X1,K
        WMAX=-2.
        FMAX=F1(JN)
        READ(1'III)W2,F2,T2,S2,VSQ2,SOR2,RO2,BWE,BWW,BWEW
     *,BFE,BFW,BFEW,BTE,BTW,BTEW,BSE,BSW,BSEW,RW,RF,RT,RS
     *,X2,K
202     FORMAT(' ENTER NMAX')
201     FORMAT(I5)
        I=II
        V1=0.
102     III=I+3
        READ(1'III)W3,F3,T3,S3,VSQ3,SOR3,RO3,BWE3,BWW3,BWEW3
     *,BFE3,BFW3,BFEW3,BTE3,BTW3,BTEW3,BSE3,BSW3,BSEW3,
     *RSDUW3,RSDUF3,RSDUT3,RSDUS3,X3,K
        K=K+1
        DX=(X3-X1)*2.
        J=JJ
6       JP=J+1
        JM=J-1
        DV=DX*DDY(J)
        STNW=F1(JP)
```

```
      STWME=F1(J)-F3(J)
      STSW=F1(JM)
      STNMS=F2(JP)-F2(JM)
      STSE=F3(JM)
      STNE=F3(JP)
      AW(J)=-(STNMS+STNW-STSW)/DV
      AE(J)=(STNMS+STNE-STSE)/DV
      AS(J)=-(STWME+STSW-STSE)/DV
      AN(J)=(STWME+STNW-STNE)/DV
      AT(J)=AE(J)+AW(J)+AN(J)+AS(J)
      IF(J.EQ.JNM) GO TO 62
      J=J+1
      GOTO 6
62    CONTINUE
      CALL EQN(JJ,JNM,W1,W2,W3,SOR2,BWE,BWW,BWN,BWS,WMAX,RPW,RSDUW,
     *I,IW,JW,IN3)
      J=JJ
4     ANUM=BFE*F3(J)+BFW*F1(J)
     * +BFN(J)*F2(J+1)+BFS(J)*F2(J-1)
     * +W2(J)*RO2(J)
      ADNM=BFEW+BFNS(J)
      IF(ADNM.EQ.0.)GOTO41
      CALL RESID(F2(J),ANUM,ADNM,FMAX,RPF,RSDUF)
41    IF(J.EQ.JNM)GOTO42
      J=J+1
      GOTO4
42    CONTINUE
      CALL EQN(JJ,JNM,T1,T2,T3,NUL,BTE,BTW,BTN,BTS,TINF,RPT,RSDUT,
     *I,IT,JT,IN3)
      CALL EQN(JJ,JNM,S1,S2,S3,NUL,BSE,BSW,BSN,BSS,SALINF,RPS
     *,RSDUS,I,IS,JS,IN3)
      DX=X2-X1
      KSAL=0
250   T2(1)=-0.003-0.0527*S2(1)-0.00004*(S2(1)**2.)
      DTDY=(Y32*(T2(2)-T2(1))-Y22*(T2(3)-T2(1)))/DY
      V2=THECON/RO2(1)/FUSION*DTDY
```

```
      SNEW=DIFCL*S2(2)/(V2*Y(2)+DIFCL)
      SNEW=S2(1)-(S2(1)-SNEW)*.5
      IF(KSAL.GT.51)GO TO 251
      IF(SNEW.EQ.S2(1))GO TO 251
      IF(S2(1).EQ.0.)GO TO 252
      IF(ABS(1.-SNEW/S2(1)).LT.CC)GO TO 251
252   S2(1)=SNEW
      KSAL=KSAL+1
      GO TO 250
251   S2(1)=SNEW
      IF(S2(1).LT.0.)S2(1)=0.
      F2(1)=F1(1)-(RO1(1)*V1+RO2(1)*V2)/2.*DX
      U2=DIFF(F2(3),F2(2),F2(1),Y(3),Y(2),Y(1))/RO2(2)
      W2(1)=(V2-V1)/DX-U2/Y(2)
      F2(JN)=F2(JNM)+VELINF*RO2(JN)*DYY
      DO10 J=1,JN
10    CALL DENSIT(S2(J),T2(J),RO2(J))
      VSQ2(1)=V2**2/2.
      DO200 J=2,JNM
      JP=J+1
      JM=J-1
      U=DIFF(F2(JP),F2(J),F2(JM),Y(JP),Y(J),Y(JM))/RO2(J)
      V=-DIFF(F3(J),F2(J),F1(J),X3,X2,X1)/RO2(J)
      VSQ2(J)=(U*U+V*V)/2.
200   CONTINUE
      J=JJ
5     JP=J+1
      JM=J-1
      Y1=Y(JM)
      Y2=Y(J)
      Y3=Y(JP)
      SS1=DIFF(VSQ3(J),VSQ2(J),VSQ1(J),X3,X2,X1)
     **DIFF(RO2(JP),RO2(J),RO2(JM),Y3,Y2,Y1)
      CALL ERRSNS(IER,IF1,IF2,IF3)
      IF(IER.NE.73) GOTO 2000
      TYPE*,I,J,VSQ3(J),VSQ2(J),VSQ1(J),X3,X2,X1
```

```
      TYPE*,RO2(JP),RO2(J),RO2(JM),Y3,Y2,Y1
2000  CONTINUE
      SR2=DIFF(RO3(J),RO2(J),RO1(J),X3,X2,X1)
      SS2=DIFF(VSQ2(JP),VSQ2(J),VSQ2(JM),Y3,Y2,Y1)*SR2
      SOROLD=SOR2(J)
      SOR2(J)=SOROLD+RPSOR*(SS1-SS2-9.81*SR2-SOROLD)
      IF(J.EQ.JNM)GO TO 52
      J=J+1
      GO TO 5
52    CONTINUE
100   III=I+2
      WRITE(1,'III)W2,F2,T2,S2,VSQ2,SOR2,RO2,BWE,BWW,
     *BWEW,BFE,BFW,BFEW,BTE,BTW,BTEW,BSE,BSW,BSEW,
     *RSDUW,RSDUF,RSDUT,RSDUS,X2,K
      IF(I.EQ.INM) GO TO 101
C     UPDATE**********************************************
      J=1
110   W1(J)=W2(J)
      W2(J)=W3(J)
      F1(J)=F2(J)
      F2(J)=F3(J)
      T1(J)=T2(J)
      T2(J)=T3(J)
      S1(J)=S2(J)
      S2(J)=S3(J)
      VSQ1(J)=VSQ2(J)
      VSQ2(J)=VSQ3(J)
      SOR1(J)=SOR2(J)
      SOR2(J)=SOR3(J)
      RO1(J)=RO2(J)
      RO2(J)=RO3(J)
      IF(J.EQ.JN)GO TO 72
      J=J+1
      GO TO 110
72    BWE=BWE3
      BWW=BWW3
```

```
      BWEW=BWEW3
      BFE=BFE3
      BFW=BFW3
      BFEW=BFEW3
      BTE=BTE3
      BTW=BTW3
      BTEW=BTEW3
      BSE=BSE3
      BSW=BSW3
      BSEW=BSEW3
      X1=X2
      X2=X3
      V1=V2
C RESIDUALS**********************************************
      RSW=AMAX1(RSW,RSDUW)
      RSF=AMAX1(RSF,RSDUF)
      RST=AMAX1(RST,RSDUT)
      RSS=AMAX1(RSS,RSDUS)
      RSDUW=0.
      RSDUF=0.
      RSDUT=0.
      RSDUS=0.
      I=I+1
      GOTO 102
 101  WRITE(1'III)W2,F2,T2,S2,VSQ2,SOR2,RO2,BWE3,BWW3,
     *BWEW3,BFE3,BFW3,BFEW3,BTE3,BTW3,BTEW3,BSE3,BSW3,
     *BSEW3,RSW,RSF,RST,RSS,X3,K
      WRITE(6,100)K,RSW,RSF,RST,RSS
100   FORMAT(I5,4E11.4)
      IF(AMAX1(RSW,RSF,RST,RSS).LT.CC.OR.K.EQ.NMAX)
     *GO TO 103
      RSW=0.
      RSF=0.
      RST=0.
      RSS=0.
      GO TO 104
```

```
103     CONTINUE
        CLOSE(UNIT=1)
        STOP
        END
        SUBROUTINE RESID(OLD,ANUM,ADNM,AMAX,RP,RSD)
        RS1=ANUM/ADNM-OLD
        OLD=OLD+RP*RS1
        RSD=AMAX1(RSD,ABS(RS1/AMAX))
        RETURN
        END
        SUBROUTINE DENSIT(S,T,D)
        SIGMA0=(-0.093+0.8148*S-0.000482*S**2+0.0000068*S**3)
        SIGT=-((T-3.98)**2)/503.570*(T+283.)/(T+67.26)
        AT=T/1000.*(4.7867-0.098185*T+0.0010843*T**2)
        BT=T/1000000.*(18.030-0.8164*T+0.01667*T**2)
        SIGMAT=SIGT+(SIGMA0+0.1324)*(1.-AT+BT*(SIGMA0-0.1324))
        D=SIGMAT+1000.
        RETURN
        END
        FUNCTION DIFF(PD,PP,PU,XD,XP,XU)
        DIFF=((PD-PP)*(XP-XU)/(XD-XP)
     * +(PP-PU)*(XD-XP)/(XP-XU))/(XD-XU)
C       ***********************************************************************
C       *     SUBROUTINE FOR CALCULATION OF GRADIENTS                         *
C       ***********************************************************************
      RETURN
      END
        INCLUDE 'EQN.FTN'
```

```
C       FILE NAME:      EQN.FTN
C       ***************************************************************
C       * SUBROUTINE FOR SPALDING'S SDS TERMS, REFERENCES [19,20] *
C       ***************************************************************
        SUBROUTINE EQN (JJ,JNM,PHI1,PHI2,PHI3,SOR,BE,BW,BN,BS,
     *PHIMAX,RP,RSD,I,IMAX,JMAX,IN3)
        INCLUDE 'COMMON.FTN'
        COMMON/CONVE/AE(M),AW(M),AN(M),AS(M),AT(M)
        DIMENSION PHI1(M),PHI2(M),PHI3(M),SOR(M),BN(M),BS(M)
        J=JJ
1       CE=0.5*(BE+ABS(AE(J))+ABS(BE-ABS(AE(J))))
        CW=0.5*(BW+ABS(AW(J))+ABS(BW-ABS(AW(J))))
        CN=0.5*(BN(J)+ABS(AN(J))+ABS(BN(J)-ABS(AN(J))))
        CS=0.5*(BS(J)+ABS(AS(J))+ABS(BS(J)-ABS(AS(J))))
        ANUM=(CE-AE(J))*PHI3(J)+(CW-AW(J))*PHI1(J)+(CN-AN(J))*PHI2(J+1)
     *+(CS-AS(J))*PHI2(J-1)+SOR(J)
        ADNM=CE+CW+CN+CS+AT(J)
        RS1=ANUM/ADNM-PHI2(J)
        PHI2(J)=PHI2(J)+RP*RS1
        RSS=RS1/PHIMAX
        IF(ABS(RSS).LE.ABS(RSD).OR.I.GE.IN3)GO TO 2
        IMAX=I
        JMAX=J
        RSD=RSS
2       J=J+1
        IF(J.GT.JNM)GO TO 5
        GO TO1
5       CONTINUE
        RETURN
        END
```